# Fatigue Tests of a Revised Exodermic Bridge Deck Design

Christopher Higgins
Assistant Professor of Civil Engineering

and

Heath Mitchell
Graduate Research Assistant

Report No.: 98-12

July 28, 1998

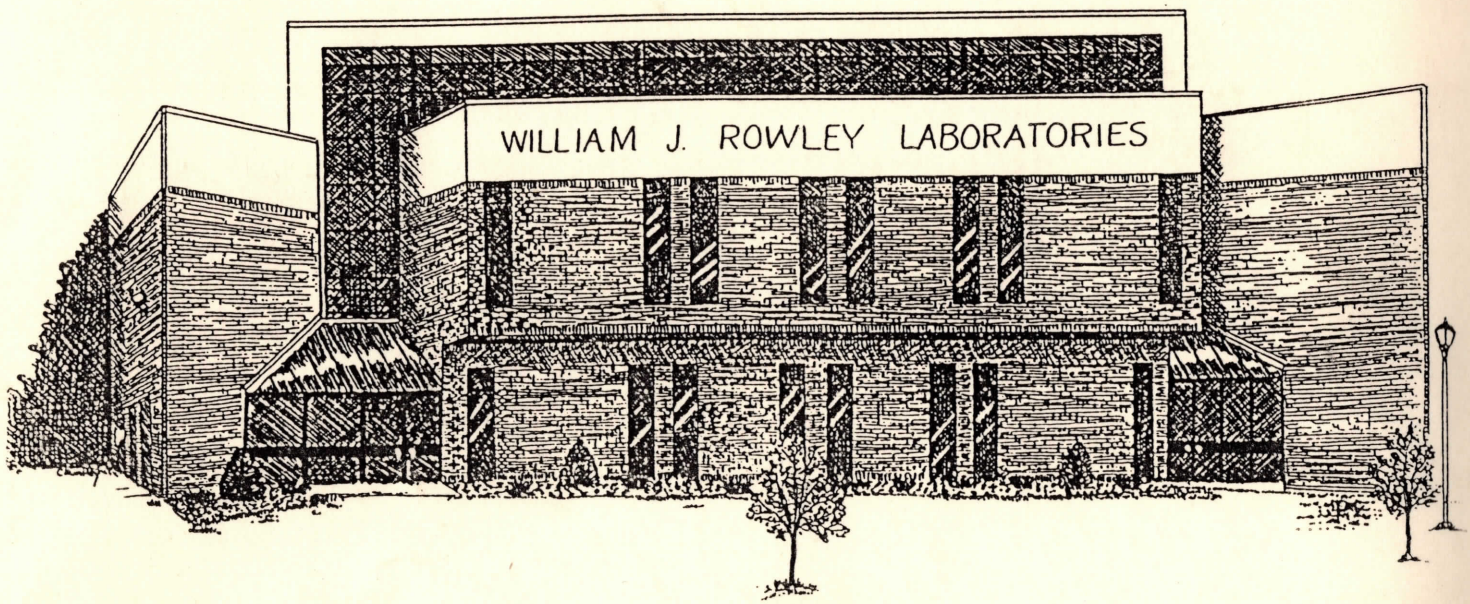

## Table of Contents

# 1.0 Introduction

## 1.1 Background

An Exodermic or "unfilled, composite steel grid" bridge deck (AASHTO LRFD 9.8.2.4) is a patented structural system that combines a fabricated steel grid and reinforced concrete slab. Previously, Exodermic decks used tertiary bars to develop composite action between the reinforced concrete slab and steel grid. Tertiary bars are rectangular bars to which ½ in. diameter vertical bars have been welded (typically at 12 in. centers), providing a shear transfer mechanism between the concrete slab and steel grid as shown in Fig. 1. These bars are typically welded into slots in the distribution bars of the base grid and extend 1 in. into the bottom of the concrete slab. While this system has performed well in the field and laboratory, a revised design has been developed to reduce manufacturing and erection costs.

The revised Exodermic design eliminates the tertiary bars used to develop composite action. Instead, composite action between the concrete deck and steel grid is produced by "concrete shear dowels" passing through holes located in the web of the main bearing bars and friction along the web embedded in the slab as shown in Fig. 2. The holes are punched in the webs of the main bearing bars and when concrete for the deck is cast, the fresh concrete fills the web holes.

## 1.2 Previous Research on the Original Exodermic Design

The first application of an Exodermic deck in the field was on the Driscoll Bridge on the Garden State Parkway in New Jersey in 1984. Another early project was on the Russell Road Bridge over the New York State Thruway in 1986 [Darlow and Bettigole, 1989]. Since 1985, the system has been widely used for both rehabilitation of existing structurally deficient decks as well as new construction [EBDI, 1996].

Experimental research has been conducted on Exodermic decks at both Lehigh University [Daniels and Slutter, 1985] and West Virginia University [Rao *et al.*, 1992]. Lehigh University conducted both static and fatigue tests on two 8 ft by 12 ft Exodermic decks. The panels contained 5 in. M Bar Type "H" Greulich I-beam main bars spaced 6 in. on-center. One panel employed a 2 in. concrete slab while the second employed a 3 in. slab. Both panels were simply supported and continuous over a center span. Static tests were performed by loading the panels at midspan with a maximum patch load of 20.8 kips on each span. The patch size was 24 in. by 10 in. Following static tests, approximately 2 million constant amplitude load cycles were applied to the panel with a 2 in. thick slab. Load amplitude varied from 2 to 20.8 kips. The panel with a 3 in. thick slab was subjected to approximately 3.3 million constant amplitude load cycles which varied from 2 to 20.8 kips. Test results indicated the decks exhibited infinite in-service fatigue life. After fatigue testing was completed at Lehigh, the two panels were shipped to West Virginia University for further testing.

West Virginia University conducted additional static tests on the Exodermic decks that had been previously tested under fatigue loading at Lehigh University. These decks were tested up to a maximum load of 90 kips without failure due to limitations of the loading frame. A 20 in. by 10 in. patch size was used during testing. Two additional Exodermic decks were also tested. These decks were 6 ft - 8 in. wide by 10 ft long and contained WT3x4.5 main bars spaced 10 in. on-center. The decks employed a 4 in. concrete slab with average concrete cylinder strengths of 5700 psi and 6400 psi. Several support conditions and loading orientations were investigated, and negative bending tests were conducted on the first specimen. The second specimen was subjected to a static load of 45 kips before fatigue testing. Fatigue tests were performed with 2 million constant amplitude load cycles which varied from 5 to 25 kips, followed by an additional 0.95 million constant amplitude load cycles which varied from 2 to 35 kips. Results indicated the panels compared well with orthotropic plate theory, the strength and stiffness of the deck is similar for the two directions of traffic, and exhibited no cracking after 2 million cycles at a stress range of 7.26 ksi.

## 1.3 Previous Research on the Revised Exodermic Design

Recent research has been conducted on the revised Exodermic deck design at Clarkson University [Higgins and Mitchell, 1997]. A simply supported prototype deck with an 8 ft span was tested to failure under monotonic static load. Overall dimensions of the panel were 9 ft long by 8 ft wide. Main bars were WT4x5 spaced 8 in. on-center. Distribution bars consisted of 1.5 in. by 0.25 in. rectangular bars spaced 6 in. on-center along the span.

The complete steel grid was hot-dip galvanized before the 4.5 in. thick concrete slab was cast. Composite action between the steel grid and concrete slab was achieved through the 0.75 in. diameter holes spaced 2 in. on-center in the web of the main bars and friction along the surface of the main bar webs which were embedded 1 in. into the concrete slab. Epoxy coated reinforcing bars were used in the concrete slab with #3 bars spaced 6 in. on-center in the transverse direction and #5 bars spaced 4 in. on-center in the longitudinal direction. The concrete contained a maximum coarse aggregate size of 3/8 in. and had a compressive strength of 3660 psi.

The deck was subjected to several small amplitude loading cycles before being loaded to failure. Test results indicated the prototype Exodermic bridge deck panel exhibited ductile behavior. The failure mode was punching shear of the concrete slab at the peak load of 123.5 kips. A residual load of 66 kips was supported by the deck after punching through the slab. The failure load was reasonably predicted using an existing code procedure for punching shear (ACI 318 Section 11.11.4). Composite action was maintained up to a load of approximately 80 kips. Above this load level, loss of shear transfer between the concrete slab and steel grid appeared gradual. Main bars did not equally participate in longitudinal load resistance and the deck exhibited significant two-way action. Measured stress ranges at the "shear holes" and welds between the main and distribution bars at the service load range were sufficiently low enough to provide an infinite expected fatigue life for the steel members.

## 1.4 Fatigue Test Objectives

Previously conducted static tests indicated good structural performance of the revised Exodermic deck design. However, no specific information was available regarding the fatigue resistance of this type of innovative shear transfer mechanism. To assess the behavior of composite members with the "concrete shear dowels" under repeated loading, fatigue tests were performed on a prototype deck specimen. The main objectives of the fatigue tests were:

1. Observe the behavior of a prototype deck with concrete shear dowels subjected to fatigue loading and identify significant changes in structural response caused by the repeated loading.
2. Assess the strength of the deck panel following fatigue loading.
3. Report test results.

This report presents findings of fatigue tests on a full-scale prototype Exodermic bridge deck panel employing an innovative shear transfer mechanism between the concrete slab and steel grid.

# 2.0 Description of Test Specimen

## 2.1 Introduction

A continuous two-span prototype Exodermic bridge deck was constructed in the Structural Engineering Research Laboratory at Clarkson University. The steel grid was fabricated by American Grid of Pittsburgh, Pennsylvania and delivered to Clarkson on February 10, 1998. The concrete slab was cast in the laboratory after instrumentation of reinforcing bars at selected locations. The test specimen is described and the instrumentation used to monitor structural behavior is presented in the following sections.

## 2.2 Test Specimen

The test specimen was a continuous two-span prototype Exodermic bridge deck with overall dimensions of 15 ft – 4 in. long by 8 ft wide as shown in Fig. 3. The deck was continuous over the center support and simply supported at the ends. At the center support, the deck was made integral with the center support beam using 0.75 in. diameter by 4 in. long headed shear studs welded to a 0.5 in. thick plate which was bolted to support beam as shown in Fig. 4. The width of this plate was 7.5 in. and represents the flange width of typical floor beams which would be used to support the deck on an actual bridge. Main bars were WT4x5 spaced 8 in. on-center as shown in Fig. 3. Distribution bars consisted of 1.5 in. by 0.25 in. rectangular bars spaced 6 in. on-center along the span. One-sided fillet welds were used to connect each of the distribution bars to the main bars

as shown in Fig. 5. The complete steel grid was hot-dip galvanized before the 4.5 in. thick concrete slab was cast.

Composite action between the steel grid and concrete slab was achieved through the 0.75 in. diameter holes spaced 2 in. on-center in the web of the main bars as shown in Fig. 5 and friction along the surface of the main bar webs which are embedded 1 in. into the concrete slab. When concrete for the deck was cast, fresh concrete filled the web holes in the main bars. After curing, these "concrete shear dowels" together with the embedded portion of the main bearing bars provide the shear transfer mechanism between the slab and steel grid. The actual grid tested was mistakenly fabricated with distribution bars located 0.1 in. higher than specified as shown in Figs. 6a and 6b. Due to this error (10%) a portion of each hole extended below the bottom of the slab and thus the size of the concrete dowels and area of web embedded in the slab was reduced from that specified. This error makes the test results conservative. It is noted that the actual grid to be used in service would have holes correctly located as shown in Fig. 5.

Hot-dip galvanized reinforcing bars were used in the concrete slab with #3 bars spaced 6 in. on-center in the transverse direction and #5 bars spaced 4 in. on-center in the longitudinal direction as shown in Fig. 7. Edges of the panel in the longitudinal direction were filled with additional concrete as shown in Fig. 8 to simulate continuity of adjacent deck panels on an actual bridge. The steel grid, reinforcing steel placement, and formwork are shown prior to casting the concrete slab in Fig. 9.

The concrete mix used for the slab was the New York State Department of Transportation "DP mix". The mix specification is shown in Appendix A. The concrete deck was cast in the Structural Engineering Research Laboratory at Clarkson University on February 27, 1998. A local, state-certified, ready-mix supplier provided concrete. Concrete was vibrated during placement using a mechanical vibrator to ensure adequate consolidation. The top surface of the slab was finished as smoothly as possible in order to facilitate observation of hairline cracks in the slab during testing. Following casting, the slab was covered with plastic and kept continuously moist. After curing for 7 days, the forms and covering were removed. Standard 4x8 in. cylinders were made at the time the slab was cast and tested at 7, 14, 21, and 28 days to monitor the compressive strength of the concrete as shown in Table 1. The compressive strength of the concrete at the start of testing was 5800 psi and was 6100 psi at 28 days. The cylinders were cured under the same environmental conditions as the concrete slab.

Several small hairline cracks were observed at the edges of the panel prior to testing. The cracks were randomly oriented and distributed and due to shrinkage of the concrete.

the slab are illustrated in Fig. 13. A summary of channel numbers, description, and conversion factors are contained in Appendix B.

Strain gages were used to determine local member stresses, lateral load distribution across the main bars, and internal member forces. At several locations, multiple sensors were used to determine the internal bending moment in the deck (Figs.11 and 13). At each of these locations, one clip gage and one strain gage were installed at the cross-section as shown in Fig. 14. Individual strain gages were placed on the bottom flange of the main bars under the load point to measure the relative contribution of each bar to load resistance (Channels GY1 to GY8 and BN1 to BN8 in Fig. 11). In addition to the main bars, strain gages were bonded to the #5 longitudinal reinforcing bars and #3 transverse reinforcing bars to determine internal slab stresses. All strain gages were bonded to hot-dip galvanized steel sections which required removal of the galvanized coating at gage locations. Sign conventions used for strain measurements are positive for tension and negative for compression.

Clip gages were bonded to the concrete surface to enable measurement of concrete strains. The gage length for each clip gage is 4 in. A clip gage was placed directly over the center support to determine when cracking first occurs in the concrete deck and to monitor the width of crack opening during fatigue testing. Two clip gages (Channels C1 and C2 in Fig. 13) were positioned between the center support and load points to determine the moment gradient and neutral axis locations in conjunction with strain gages

located on the main bars. Clip gage C4 in Fig. 13 was used to measure strain in the concrete slab perpendicular to the main bar direction.

Displacement transducers were used to measure displacements both along and across the test panel. At two locations, displacement transducers were used to measure relative deformation between the concrete slab and steel grid as shown in Fig. 15. Load applied to the test specimen was measured by an Eaton-Lebow 150 kip capacity load cell. The load cell was placed in series with the hydraulic actuator to monitor the force applied to the deck specimen. Data were acquired using a 16 bit PC-based IOtech Inc. DaqBoard Model 216A data acquisition board and three DBK15 expansion boards. A commercially available software program was used to control acquisition and data storage for later evaluation. During testing, data from all channels were continuously acquired at a sampling rate of 1 hz.

After completion of the fatigue tests, five additional strain gages were added to the webs of selected main bars as illustrated in Fig. 16a and 16b. The purpose of these strain gages was to permit identification of the neutral axis at various locations and determine if the steel grid and concrete slab remained composite. After adding these gages, static testing was again performed with a peak axle load of 41.6 kips applied to the specimen.

### 3.3 Fatigue Test Set-up

After casting the concrete slab, instrumentation was installed and a loading frame positioned around the specimen. The fatigue test set-up is shown schematically in Figs. 17 and 18. The panel was supported on three W12x90 floor beams spaced 7 ft – 2 in. apart. Each floor beam was supported on two W12x120 column sections spaced 4 ft on-center. These short column sections facilitated access to the underside of the specimen for regular inspections during fatigue testing. The center support was made integral with the deck using shear studs as described previously and the ends were simply supported on 2 in. diameter steel rollers as illustrated in Fig. 18. Steel shims were used to ensure uniform contact under the stems of each of the main bars at the roller supports. The east and west edges of the panel were unsupported.

The reaction frame consisted of two W12x120 tree columns with a W21x132 cross beam and was designed to provide sufficient stiffness and strength to ensure deformation of the test panel. A hydraulic actuator was mounted to the cross beam and applied force to a W14x99 spreader beam as shown in Fig. 19. The spreader beam acts like a truck axle to spread the applied load to two stiffened W10x45 loading patch beams. Load patch beams rested on 0.5 in. thick steel plates with plan dimensions 9.1 in. by 22.8 in. which correspond to a HS-20 tire patch with impact factor [AASHTO 3.30]. The stiffened W10x45 beams were used in conjunction with the steel plate to attempt to provide uniform loading over the whole surface of the patch. Directly under the steel plate a 0.5 in thick piece of neoprene was used to prevent stress concentrations due to imperfect contact

between the concrete slab and steel plate. The loading patch was oriented with the long dimension parallel to the main bars, to simulate a typical installation where the main bars are transverse to the direction of traffic.

Load was applied to the test specimen with a single 150 kip capacity hydraulic actuator. Tests were performed under load-control. The load cell attached to the hydraulic actuator provided feedback for actuator control. Hydraulic oil was supplied to the actuator by a 25 gpm, 3000 psi hydraulic supply, 40 gpm hydraulic service manifold, and 10 gpm servo-valve. The servo-valve was controlled using a closed-loop MTS 458-20 servo-hydraulic controller.

### 3.4 Fatigue Test Procedure

Prior to fatigue testing, the test panel was subjected to monotonic statically applied load. Cracking of the deck over the center support was monitored during testing. A maximum load of 42.4 kips was applied to the specimen during static loading. Following static testing, the specimen was subjected to fatigue loading. The fatigue load ranged from approximately 1 kip to 42.6 kips and was applied to the specimen at a frequency of 1 hz. This load range represents the axle load for an HS-20 truck with impact factor. A minimum load of 1 kip was selected so that the actuator, loading apparatus, and test specimen contact locations did not decompress as they would if the load were allowed to range from zero, which might have permitted unstable shifting of the load apparatus. Over 2 million load cycles were applied to the specimen.

At intervals of approximately 250,000 cycles, fatigue loading was suspended and the specimen subjected to static load. Again testing was conducted in load control with a peak axle load of 41.6 kips applied to the specimen. These tests were conducted to determine if the structural behavior was changing as a result of fatigue loading.

### 3.5 Static Test Results Before Fatigue Tests

The test specimen was subjected to several small amplitude load cycles before beginning fatigue loading. The loading history is shown in Fig. 20. The maximum applied load was 42.4 kips. Deck displacement was measured under the load patch and load-displacement response of the deck on the north and south spans for all the load cycles is shown in Fig. 21. The measured secant stiffness at the peak load was 970 kips/in for the north span and 1200 kips/in for the south span. As discussed in Chapter 4, the load patch over the north span was not uniformly loaded over the patch surface. Consequently, only half the intended patch area was loaded, concentrating the load on this span significantly. The initial stiffness for both spans was approximately 1700 kips/in and begins to soften at approximately 15 kips. Softening results from expected cracking of the concrete slab over the center support.

Concrete cracking was first observed at a load of 20 kips near the center of the deck directly over the midspan support. The hairline crack was located directly under clip gage C3 and was oriented perpendicular to the main bars. As the magnitude of load was

increased, the cracking spread laterally in the east-west direction and additional cracks formed parallel to the initial transverse crack. At the highest load, the cracks began to turn parallel to the main bars near the edges of the slab. The locations of cracks and progression of cracking are shown in Appendix C. Larger crack widths were observed at the north edge of the center support beam flange. The concentration of cracking at the north edge of the center support caused the north span to exhibit less stiffness than the south span. Cracks were hairline in nature following removal of the load.

Concrete strain measurements from the clip gages indicate the initiation of cracking over the center support at a load of 11 kips as shown in Fig. 22. As stated previously, cracks were not visible until a load of 20 kips. The measured concrete strain at the onset of cracking was approximately 125 με. ACI recommends a modulus of rupture value of $7.5\sqrt{f'_c}$ for deflection calculations and $6\sqrt{f'_c}$ for strength calculations, and the value can exhibit wide scatter [McGregor, 1992]. Applying the ACI recommended formula for modulus of elasticity [ACI 318-95] $E_c$=4.36 ksi, with the measured compressive strength at the time of testing (21 days) $f'_c$=5800 psi, the measured concrete strain value corresponds to a modulus of rupture of $7.1\sqrt{f'_c}$. This value is in the range of that recommended by ACI. As seen in Fig. 22, the cracks continue to widen as the load increases and do not fully close after the load is removed, as indicated by the residual deformation. If a single crack is assumed to cause the measured strain over the 4 in. gage length of clip gage C3, the crack width is estimated at 0.006 in. This estimate is

reasonable based on the observed crack widths. Later cracks that formed adjacent to the original parallel crack became wider than the first crack at larger load magnitudes. All other clip gages did not measure significant concrete strains.

Cracking was also observed from strain measurements of #5 reinforcing bars over the center support. Measured strains are shown in Figs. 23a to 23f for all instrumented #5 bars. As seen in these figures, the #5 bars over the support (P1, P2, P3, and P4) exhibited nonlinear behavior due to concrete cracking near the strain gage locations. Strains in the bars located closest to the center of the deck (P2 and P3) became nonlinear at approximately 12 kips. Adjacent bars became nonlinear at slightly higher loads of 14 kips (P1) and 16 kips (P4). The maximum strains in the center bars (P2 and P3) were similar with peak measured strain of approximately 420 με, corresponding to a stress of 12.2 ksi. Strains in adjacent bars were not equal, the west bar (P1) exhibited a peak strain of 310 με (9.0 ksi) and the east bar (P4) exhibited a peak strain of 210 με (6.1 ksi). This indicates larger cracks were located on the west side of the deck which was confirmed by visual observation of the crack pattern. All measured stresses indicated the reinforcing steel remains elastic.

Measured strains on #5 reinforcing bars at locations O3 and O6 were small and at higher load, the strains tend to become slightly negative indicating compression in the bars. Based on elastic beam analysis, the theoretical point of inflection is located 21.4 in. away from the center support. The small strain values measured by rebar gages O3 and O6 as

well as clip gages C1 and C2 indicate they are located close to a point of inflection. Due to the low measured strain values, the neutral axis could not be estimated at these locations.

Strains in several transverse #3 reinforcing bars were also measured as shown in Figs. 24a to 24f. Most of the measurements indicated small strains in these bars, except at locations O8 and P6. These reinforcing bars were located directly under the load patch and over the stem of a main bar. Measured strains in these reinforcing bars indicated cracking of the concrete slab along the stem of the main bar web for these locations at a load of approximately 14 kips. Fig. 24a indicates significantly more strain (and thus larger crack size) under the north load patch compared to the south patch. The maximum rebar stress was 7.5 ksi at location O8 compared to 3.2 ksi at location P6. Cracking along the stem of the T-section on the north span was verified when the deck was sawn into sections as described later in Chapter 4. The loading over only half the intended patch area as discussed in Chapter 4 exacerbated this cracking.

Strains were measured on the flanges of the main bars across the width of the deck to measure the relative contribution of each T-section to load resistance. Measured flange strains are shown in Figs. 25a and 25b for the south span. The relative contribution of each of the main bars to load resistance in the longitudinal direction at the peak load of 41.6 kips was determined by dividing each main bar strain by the sum of all the strains and are summarized in Table 2a. Bending strains in bars 2, 4, 9, and 11 were computed

by averaging the stress in the adjacent bars. As shown in Table 2a, the center T-sections contributed the largest proportion to load resistance. The strains were relatively symmetrical across the deck. Measured flange strains are shown in Figs. 26a and 26b for the north span. Flange stresses at midspan in each of the main bars are summarized in Table 2b at the peak load of 41.6 kips. As shown in this table, the east main bars have larger stresses than the west main bars in the north span. In particular bar #5 has higher stress than the adjacent bar #4. The cause of this imbalance was identified at the end of fatigue tests as described later in Chapter 4. The cumulative magnitudes of the stresses in the north and south spans indicated the load was equally shared between the spans.

Sensors were bonded to the concrete slab to measure displacement between the concrete and steel grid. During the first static test, only sensor BL7 recorded clean data during this test. Displacement between the slab and grid are shown in Fig. 27 for this location. The peak measured displacement was 0.0012 in. This measurement does not appear to indicate typical slip behavior, as the displacement returns to the origin upon unloading and later measurements indicated less deformation at this point. Both sensors BL2 and BL7 were adjusted after this test to provide more reliable data in the later fatigue tests of this specimen.

Relative response quantities for the initial static tests are shown in Figs. 28a to 28i, as the load varied from 0 to 41.6 kips on the final cycle. While adjusting the actuator at the start of the fatigue tests, a peak axle load of approximately 46 kips was accidently applied to

the deck when data were not recorded. This load caused additional concrete cracking and thus relative response quantities could not be directly compared between the initial static tests and static tests performed during fatigue loading. Therefore, identification of changes in structural response were made by comparing response at the start (250,000 cycles) and end of fatigue loading (2 million cycles) and Figs 28a to 28i are shown for completeness only.

### 3.6 Static Tests Results During Fatigue Tests

Following the initial static tests, the specimen was subjected to 2 million fatige cycles that varied from 1 kip to 42.6 kips. The specimen was inspected daily to note concrete crack extensions and identify any cracks in the steel grid. No cracking was observed in the steel grid members or welds. At intervals of approximately 250,000 cycles, fatigue testing was suspended and static tests were performed as shown in Table 3 with a peak axle load of 41.6 kips. The purpose of the interval static tests was to determine if the structural response was changing as a result of the fatigue loading.

Key response quantities are shown in Figs. 29a to 29j after 250,000 cycles and Figs. 30a to 30g after 2 million cycles. Strain distribution across the main bars are summarized for each cycle interval in Tables 4a and 4b for the south and north respectively. Peak response quantities at a load of 41.6 kips at each cycle interval are shown in Figs. 31a to 31j. As shown in these figures, most measured responses do not vary from the beginning to the end of the fatigue test. The notable exceptions were displacement of the north span

under the load point, strain in the transverse #3 reinforcing bars near the center of the panel (O8 and P6), and strain in the longitudinal #5 reinforcing bars over the center support (P2). It is anticipated that the uneven distribution of load under the north load patch, as discussed in Chapter 4 contributed to some of these changes.

The displacement of the north span under the load point increased by approximately 0.003 in. or 9% from 0.033 in. at 250,000 cycles to 0.036 in. at 2 million cycles as shown in Fig. 30a. The south span displacement response remained stable. There was a concentration of cracks along the north edge of the support beam flange as shown in Appendix C. These cracks and crack extensions combined with uneven distribution of the load under the north load patch (described in Chapter 4) are believed to be responsible for the minor softening of the north span. The softening is not believed to be a result of loss of composite action, as this phenomenon would cause a dramatic increase in displacement as well as an increase in main bar strains which was not observed.

Strains in the transverse #3 reinforcing bars under the load patch tended to increase during the fatigue tests indicating extension of cracks at these locations. At location O8 the rebar strain increased from 310 με at 250,000 cycles to 337 με at 2 million cycles (a 9% increase). At location P6 the rebar strain increased from 153 με 250,000 cycles to 190 με at 2 million cycles (a 24% increase). Even with the 24% increase in strain at the

south span, there was no significant change in the overall response or local member responses.

Some of the longitudinal #5 reinforcing bars over the center support exhibited small increases in strain during the fatigue tests. At location P2 the rebar strain increased from 275 με at 250,000 cycles to 288 με at 2 million cycles (a 5% increase). At location P6 the rebar strain increased from 83 με 250,000 cycles to 90 με at 2 million cycles (an 8% increase). The observed changes were due to crack extensions over the center support, which were also observed visually. Extensions of existing cracks were only observed up to 500,000 cycles and subsequently no significant crack extensions were visible.

Additional strain gages were placed on the webs of the main bars where flange gages were located following the last fatigue cycle. The purpose of these gages was to identify the neutral axis location. However, due to the punch-out in the web for the distribution bar at the web gage locations, there is a stress concentration at these locations. This causes larger measured web strain than would occur in a uniform strain field if the punch-out were not present. The web gages were helpful in qualitatively determining if the neutral axis had dramatically shifted downward due to loss of composite action. Typical measured web and flange strains at the main bars are shown in Fig. 32. These measurements indicated the lower portion of the web for main bars is in flexural tension and this can only be achieved if the deck has maintained significant composite behavior after the fatigue loading.

# 4.0 Visual Examination of Test Specimen After Fatigue Tests

## 4.1 Introduction

After 2 million cycles of repeated loading, the fatigue test was terminated without specimen failure or visible cracks in the steel grid members and welds. The surface of the concrete slab was inspected and the two span deck was cut into several pieces to permit visual assessment of the internal condition of the concrete shear dowels and steel-concrete interface.

## 4.2 Visual Inspection of Concrete Surface After Fatigue Tests

Following completion of fatigue loading, the fatigue test was terminated without failure or visible cracks in the steel grid members and welds. Loading fixtures were removed from the specimen and the surface of the slab was inspected. The south span exhibited symmetrical markings under the load patch from wear of the neoprene pad due to the repeated loading as shown in Fig. 33. However, the north span exhibited a nonsymmetrical pattern under the load patch as shown in Fig. 34. It was clear from this pattern that the applied load on the north span had not been evenly distributed over the whole surface of the patch. Instead, only half of the expected area was loaded. This uneven loading over the patch surface caused the load to be concentrated over main bar #5 and caused the unbalanced strain distribution across the main bars on the north span described in the previous section. The larger strain measured in the #3 transverse reinforcing bar at location O8 indicated cracking of the concrete slab parallel to the web

of the main bar. It is believed the strain in the #3 reinforcing bar on the north span under the load point was larger than that of the south span due to uneven loading of the patch surface.

### 4.3 Visual Inspection of Internal Condition of Shear Holes After Fatigue Tests

Following visual examination of the top surface of the concrete slab, a specialty contractor was hired to cut a portion of the deck into sections as shown in Fig. 35. The deck was cut with a large gasoline powered concrete saw which was equipped with a large diameter diamond blade capable of cutting through both the concrete slab and steel grid at the same time. Two transverse cuts were made across the deck and several cuts were made parallel to the main bars as shown in Fig. 36.

The internal condition of the concrete and steel interface was visually examined at each of the cut sections. The north span of the specimen was first cut away from the south span at cut #1, lifted off the supports, and positioned on the laboratory floor to permit additional cuts to be made. After the specimen was cut into sections, each of the surfaces was inspected to characterize the condition and bond of the concrete-steel interface.

No cracking or debonding of the concrete-steel interface was observed on cuts #1 and #2. However, some small cracks were observed along cut #3. Near the center of the span, diagonal, vertical, and horizontal cracks in the concrete were observed near the shear holes as illustrated in Figs. 37a and 37b. The observed crack patterns indicate a complex

state of stress in the slab. Cracks were typically not wide and no wear between the crack surfaces was noted. Bond between the concrete and steel, even in the presence of these cracks, appeared to be intact. The metal pans were removed in areas adjacent to the cracks to determine if additional cracks were visible or if the cracks were continuous along the span in the direction of the main bars. In general, the observed diagonal cracks could not be seen from the bottom of the slab and they did not appear continuous. Only one hairline crack could be identified from the bottom slab surface at an adjacent shear hole location on piece #B. In some instances it was difficult to determine if cracks were present due to a bead of silicon caulk along the pan-web interface which was used to prevent paste from flowing through this seam during placement of the concrete. The caulk obscured the interface between the concrete slab and main bar stem at the intersection making identification of cracks difficult.

A vertical crack was observed parallel to the west stem of main bar #7 as illustrated in Figs. 37a and 37b. The presence of this crack was anticipated based on strain gage measurements at location O8 and the uneven distribution of the pressure under the north patch described previously. The crack extended up from the bottom of the slab and terminated approximately at the mid-depth of the concrete slab. It was not possible to determine the overall length of the crack due to the presence of silicon caulk at the joint between the pan and main bar web.

# 5.0 Static Test of South Span After Fatigue Tests

## 5.1 Introduction

A final static test was performed on the south span portion of the two-span test specimen to evaluate the load carrying capacity of the deck following fatigue tests. The remaining portion of the deck specimen was loaded to the capacity of the hydraulic actuator. Several changes were made to the test set-up to conduct this final test. The instrumentation, test set-up, procedure, and results are presented in the following sections.

## 5.2 Instrumentation For Static Test of South Span After Fatigue Tests

Instrumentation for the prototype Exodermic bridge deck experiment consisted of 48 sensors, including strain gages, clip gages, displacement transducers, and a load cell. Instrumentation layout and channel identification for all displacement measurements are illustrated in Fig. 38. Instrumentation layout and channel identification for steel grid strain measurements are illustrated in Fig. 39. Instrumentation layout and channel identification for reinforcing steel strain measurements are illustrated in Fig. 40. Instrumentation layout and channel identification for clip gages bonded to the surface of the slab are illustrated in Fig. 41. A summary of channel numbers, description, and conversion factors are contained in Appendix B.

Data were acquired using a 16 bit PC-based IOtech Inc. DaqBoard Model 216A data acquisition board and four expansion boards. A commercially available software program was used to control acquisition and data storage for later evaluation. During testing, data from all channels were continuously acquired at a sampling rate of 2 hz.

### 5.3 Set-up for Static Test of South Span After Fatigue Tests

After removal of the north span, the south span was disconnected from the center support. The deck was made simply supported at the north and south edges by placing rollers at these locations. The same 7 ft. - 2 in. span was employed for this test as was used for the fatigue tests. An additional cross frame was erected to enable loading in the center of the deck. The reaction frame consisted of four W12x120 tree columns with two W21x132 cross beam as shown in Fig. 42 and 43. A W14x99 beam was bolted between the cross beams and the hydraulic actuator was mounted to this beam. A single tire patch was used to apply load to the center of the simply supported span. The same stiffened patch beam as described previously was used to load the deck. A different size shoe plate was used in conjunction with the stiffened patch beam to reflect the application of higher magnitude load. The shoe plate was 1 in. thick with plan dimensions of 10.2 by 25.5 in. This patch size corresponds to a HS-25 tire patch with impact factor [AASHTO 3.30]. A 0.5 in thick piece of neoprene was placed between the concrete slab and steel plate.

Load was applied to the test specimen with a single 150 kip capacity hydraulic actuator. Tests were performed under displacement-control. A displacement transducer attached to

the hydraulic actuator provided feedback for actuator control. The hydraulic and control system was the same as described previously.

## 5.4 Procedure for Static Test of South Span After Fatigue Tests

Two load patch orientations were studied in the service load range to determine the effect on behavior. The first test was performed with the long dimension of the patch perpendicular to the main bars. This represents the condition where traffic flows in the direction of the main bars. The peak load applied during this test was 22 kips. After investigating this configuration, the long dimension of the patch was reoriented transverse to the main bars. This configuration was typical of the orientation used during the previous fatigue tests. The specimen was loaded several times in the service load range and then loaded to the maximum force capacity of the hydraulic actuator.

## 5.5 Static Test Results of South Span After Fatigue Tests

The panel was subjected to three small amplitude load cycles (peak load of 21 kips, 22 kips and 21 kips, respectively) with the patch orientation transverse to the main bars (simulating the case where traffic is moving in the direction of the main bars). The load-midspan deflection response is shown in Fig. 44. The initial stiffness was 481 kips/in and the secant stiffness was 446 kips/in. No new cracks or extension of existing cracks were observed.

The test specimen was then subjected to two 21 kip load cycles before application of the maximum load on the final cycle. The load-midspan deformation response of the panel for the first two cycles and the final cycle up to the service level load is shown in Fig. 45. The initial stiffness was 472 kips/in and the secant stiffness was 431 kips/in. A comparison of load-midspan deformation responses for the two patch orientations is shown in Fig. 46. The deck response was similar for both patch orientations.

The relative contribution of each main bars at a load of 20 kips for the parallel and transverse patch orientations is summarized in Table 5. The values were computed by dividing the strain in each main bar by the sum of the strains in all main bars. Strains for bars 2, 4, 9 and 11 were computed by averaging the values of adjacent bars. As shown in the table, load distribution is similar for both patch orientations.

Structural response was further investigated at the service load level for the patch orientation parallel to the main bars. Strains at two instrumented cross-sections are shown in Figs. 47 and 48. Strains were linear in the concrete slab and main bars and the web gages exhibited flexural tensile strain, indicating composite action between the steel grid and concrete slab. Web strain in Fig. 47 is higher than flange strain at this location. This is unexpected for the given support conditions, but likely due to the location of the web gage near the distribution bar punch-out, which produces a non-uniform strain field. The neutral axis location was calculated for these two cross-sections assuming fully composite behavior by using the strain measurements for the top of the concrete and the

bottom flange of the main bar. The theoretical neutral axis is located 3.13 in. from the top surface of the concrete and was found using a modular ratio of 6.3 and an effective slab width of 8 in. The measured neutral axis at location C5 is 3.25 in. from the surface of the concrete as shown in Fig. 49, which compares reasonably well with the theoretical value. The measured neutral axis at location C1 is shown in Fig. 50. The neutral axis at this point is approximately 3.6 in. from the surface of the concrete and does not compare as well with the theoretical value.

Loading continued for a final cycle from the service load level to the 144 kip capacity of the actuator without failure of the deck. North, south and average midspan support displacements as are shown in Fig. 51. The north support exhibits stiffer behavior and is likely due to the effects of the simulated stringer flange plate and shear studs composite with the deck. Figure 52 shows the as-measured and corrected load-midspan displacement behavior. The "measured" curve shows cumulative system displacement, including support deformations while the "corrected" curve represents just the deck displacement after the average support displacement was removed. The secant stiffnesses for the "measured" and "corrected" curves are 264 kips/in. and 291 kips/in., respectively.

Relative deformation between the concrete and main bars at locations BL7, BL8 and BL11 is shown in Fig. 53. The response at BL 11, which is located at the end of the deck, shows virtually no relative displacement indicating no loss of composite action at the support. The relative displacements observed at locations BL7 and BL7 are attributed to

bending of the deck as well as some possible localized slip. Relative displacement between adjacent main bar webs at location GN4 is shown in Fig. 54. This displacement is attributed to weak direction bending of the deck and spreading of the main bars which would be anticipated for an orthotropic deck plate.

Flange strain and stress at midspan in main bars #5-#8 are shown in Fig. 55. Relative contribution of each of the main bars to load resistance at each load step during the final cycle is summarized in Table 6. The values in this table were calculated using data from 6 in. north of midspan and represent the strain in each bar divided by the sum of the strain in all bars. Strain in bars 2, 4, 9, and 11 represent the average of adjacent bars. At the service load level the outside bars each carry approximately 5% of the load and the center bars each carry about 12% of the load. However, as load increased, the outer bars contribute less and the central bars carry additional load. This redistribution takes place at higher load levels due to concrete cracking, which reduces the ability of the deck to distribute the load laterally between main bars. Additionally, main bar #7 appears to pick-up load at a higher rate than main bar #6 as the load increased. At the final load step, main bar #7 is carrying nearly 18% of the load whereas bar #6 is only carrying 14%.

The integrity of the shear transfer mechanism was evaluated using data from two instrumented cross-sections. At location C1, the compressive strain in the concrete decreased as the load increased, as shown in Fig. 56, whereas the longitudinal reinforcing steel, GY8, increases in compressive strain and appears to change slope at the same time

as the main bar flange, GY6. This indicates some degree of strain incompatibility, however these sensors were located in a region that may contain cracks from the previous fatigue test and the concrete cracks in this area at higher load levels as shown in Appendix C. This observed response indicated complex behavior and formation of alternative load paths at higher load levels due to concrete cracking and possible localized slip between the grid and slab. At location C5, all three measured strains appear to increase at a constant rate with the applied load, as shown in Fig. 57. If composite action at this section were lost, strain measurements on the main bar web should begin to change direction as seen in previous tests of an Exodermic deck with concrete shear dowels [Higgins and Mitchell, 1997]. This behavior was not observed as the web and flange strains increase proportionally, indicating composite action.

Strain in the #3 transverse reinforcing steel is shown in Fig. 58. The maximum strain occurs at P6 beneath the load patch and is above yield strain of the steel (2070 με). At P5 there appears to be nearly zero strain as shown in Fig. 59, together with the concrete strain at the slab surface at location C2.

At each load step the deck was inspected for cracks in the concrete. Clip gages were also positioned on the concrete surface to detect cracks. Measured concrete strains are shown in Fig. 60. Significant crack growth appears at location C6 at approximately 110 kips while not until approximately 140 kips at location C3. This is supported by the observed crack pattern on the concrete surface as shown in Appendix C.

## 6.0 Future Research

The "concrete shear dowel" design of the embedded main bearing bars of the steel grid employed by the revised Exodermic bridge deck design is a new method for developing composite action between a concrete slab and steel grid. Based on experimental findings of the prototype Exodermic test panel, suggestions for future research include:

1. Simple static push-through tests, consisting of an individual steel section with concrete slab, could be performed to directly assess the behavior of the "concrete shear dowels". Different web hole diameters, configurations, and hole spacing, as well as the effects of concrete strength and aggregate size can be investigated. These tests would facilitate development of analytical models for the shear transfer mechanism. These models would provide additional flexibility to future designers of Exodermic bridge decks and permit selection of optimal hole layout, grid main bar spacing, etc.
2. Cracking observed at the shear hole locations directly under the load patch did not appear to have a deleterious effect on the behavior of the deck specimen, however alternative hole configurations and reinforcements could be investigated to reduce or eliminate this cracking.
3. The behavior of the Exodermic deck is complex and simple beam tests could be performed to permit direct two-dimensional characterization of the shear transfer mechanism and facilitate development of engineering models for the shear transfer connection. Various moment and shear interactions could be investigated

as well as different elastic neutral axis locations. Simple beam fatigue tests could also be performed and compared with similar specimens employing traditional shear studs to directly compare the fatigue behaviors.

4. Behavior of the revised Exodermic design under different combinations of shear and moment as well as negative moment should be investigated if future designs differ significantly from that tested. Additional studies should be undertaken if the design proportions differ significantly from that tested.

## 7.0 Summary of Observations and Conclusions

A full-scale two-span prototype Exodermic bridge deck has been subjected to over 2 million fatigue cycles at a load range of 41.6 kips in the Structural Engineering Research Laboratory at Clarkson University. Static tests were performed every 250,000 cycles during the fatigue test to determine if the structural response changed. Following fatigue tests, portions of the deck were cut into sections to assess the condition of the steel-concrete interface. The remaining portion of the specimen was converted into a single span deck and tested to the maximum capacity of the hydraulic actuator without failure. Based on experimental testing, the following observations and conclusions are presented:

1. All measured strains in the grid and embedded reinforcement were in the elastic range at the service axle load of 41.6 kips.
2. Measured strains in the main bars did not significantly change during fatigue testing, indicating no significant loss of composite action between the steel grid and concrete slab at these locations.
3. Steel grid members did not exhibit cracking after fatigue loading of 2 million cycles.
4. The final static test was performed without failure of the specimen up to the 143 kip capacity of the hydraulic actuator.
5. Clip gage instrumentation indicated concrete cracking over the center support at an axle load of approximately 11 kips, though these were not visible until 20 kips. No significant extensions of concrete cracks were observed after 500,000 cycles.

6. After fatigue testing, it was discovered that the load on the north patch was unevenly distributed. Only half of the anticipated area was loaded which may have resulted in additional cracking of the slab under the north patch.
7. Concrete cracking along the stem of main bar #7 under the load patch was indicated by strain gage measurements on the #3 transverse reinforcement at an axle load of approximately 14 kips. The north span exhibited higher strains due to uneven pressure distribution under the load patch. Extension of these cracks during fatigue loading was indicated by increases in measured strains in the #3 transverse reinforcement under the load patch. Cracks, anticipated in the south span from strain measurements of the #3 transverse reinforcing steel, did not appear to have a deleterious effect on the behavior of the single span specimen during the final static test, up to the 143 kip capacity of the hydraulic actuator.
8. Displacement response of the south span did not significantly change due to the fatigue loading. The north span displacement response increased by 0.003 in. after 2 million fatigue cycles.
9. Saw-cutting of the specimen identified small concrete cracks in the shear transfer area between the steel grid and slab in the north span. These cracks appeared isolated to the region under the load patch and were located near the center main bars. Bond between the grid and concrete slab appeared to be intact even in the presence of the cracks.
10. If the observed concrete cracking were to propagate throughout the slab, composite action could be diminished. For the test conditions, the cracking was

localized and would not have been identified from global response measurements of the structure.

11. The observed condition of the specimen at saw cut locations indicates that future testing can be performed on single span specimens when evaluating the performance of the concrete dowels.
12. Patch orientation did not appear to significantly change the response of the specimen in the service load range.
13. There was no clear indication of loss of composite behavior between the steel grid and concrete slab during the final static test.
14. During the final static test, the deck exhibited significant two-way action.

## Acknowledgments

Exodermic Bridge Deck Inc. of Lakeville, Connecticut provided financial support for this research and the assistance of Mr. Robert A. Bettigole is acknowledged. Materials for the steel grid portion of the test specimen were provided by American Grid Inc., of Pittsburgh, Pennsylvania.

## References


American Association of State Highway and Transportation Officials (AASHTO). (1994). "AASHTO-LRFD Bridge Design Specifications," AASHTO, Washington, DC.

American Association of State Highway and Transportation Officials (AASHTO). (1989). "Standard Specifications for Highway Bridges," AASHTO Executive Office, Washington, DC.

American Concrete Institute (ACI). (1995). ACI 318-95 "Building Code Requirements for Structural Concrete," American Concrete Institute, Detroit MI.

Daniels, J. H., and Slutter, R. G. (1985). "Behavior of Modular Unfilled Composite Steel Grid Bridge Deck Panels," Fritz Engineering Laboratory Report No. 200.84.795.1, Lehigh University, Bethlehem, PA.

Darlow, M. S. and Bettigole, N. H. (1989). "Instrumentation and Testing of Bridge Rehabilitated with Exodermic Deck," *ASCE Journal of Structural Engineering*, ASCE, 115(10), 2461-2480.

Exodermic Bridge Deck Inc. (1996). "Exodermic Bridge Deck," Product Literature, EBDI, Lakeville, CT.

GangaRao, H. V.S., Raju, P. R., and Ramesh, K. (1992). "Concrete Filled Steel Grid Bridge Decks," Report No. FHWA-WV-86, West Virginia University, Morgantown, WV.

Higgins, C. and Mitchell, H. (1997) "Tests of a Revised Exodermic Bridge Deck Design," Report No. 97-16, Clarkson University.

McGregor, J. G. (1992) Reinforced Concrete Mechanics and Design, Prentice Hall, New York.

| Cylinder Age | $f'_c$ (psi) |
|---|---|
| 7 Day | 4300 |
| 14 Day | 5100 |
| 21 Day (Start of Fatigue) | 5900 |
| 28 Day | 6100 |
| Single Span Static Test | 6600 |

Table 1 - Concrete cylinder compressive strengths.

| | BN #8 T #1 | Interpolate T #2 | BN #7 T #3 | Interpolate T #4 | BN #6 T #5 | BN #5 T #6 | BN #4 T #7 | BN #3 T #8 | Interpolate T #9 | BN #2 T #10 | Interpolate T #11 | BN #1 T #12 |
|---|---|---|---|---|---|---|---|---|---|---|---|---|
| 0 Cycles | 4.1% | 4.8% | 5.4% | 8.1% | 10.8% | 15.2% | 14.4% | 11.1% | 9.0% | 7.0% | 5.6% | 4.2% |

Table 2a -Relative contribution of main bars to load resistance during initial static load on south span.

| | GY #8 T #1 | Interpolate T #2 | GY #7 T #3 | Interpolate T #4 | GY #6 T #5 | GY #5 T #6 | GY #4 T #7 | GY #3 T #8 | Interpolate T #9 | GY #2 T #10 | Interpolate T #11 | GY #1 T #12 |
|---|---|---|---|---|---|---|---|---|---|---|---|---|
| 0 Cycles | 3.5% | 3.6% | 3.8% | 7.8% | 11.8% | 12.7% | 15.6% | 13.0% | 11.1% | 9.2% | 5.7% | 2.2% |

Table 2b -Relative contribution of main bars to load resistance during initial static load on north span.

| Cycle Increment | Actual Cummulative Cycles | Nominal Cummulative Cycles |
|---|---|---|
| 0 | 0 | 0 |
| 259598 | 259,598 | 250,000 |
| 241979 | 501,577 | 500,000 |
| 256042 | 757,619 | 750,000 |
| 252801 | 1,010,420 | 1,000,000 |
| 248383 | 1,258,803 | 1,250,000 |
| 260563 | 1,519,366 | 1,500,000 |
| 247784 | 1,767,150 | 1,750,000 |
| 253645 | 2,020,795 | 2,000,000 |

Table 3 - Number of fatigue cycles when static tests were conducted.

| Cycle Number | BN #8 T #1 | Interpolate T #2 | BN #7 T #3 | Interpolate T #4 | BN #6 T #5 | BN #5 T #6 | BN #4 T #7 | BN #3 T #8 | Interpolate T #9 | BN #2 T #10 | Interpolate T #11 | BN #1 T #12 |
|---|---|---|---|---|---|---|---|---|---|---|---|---|
| 250K | 3.2% | 4.4% | 5.6% | 8.4% | 11.2% | 15.7% | 15.0% | 11.6% | 9.2% | 6.8% | 5.3% | 3.7% |
| 500K | 2.8% | 4.1% | 5.3% | 8.4% | 11.5% | 15.9% | 15.5% | 12.0% | 9.3% | 6.5% | 5.0% | 3.6% |
| 750K | 2.9% | 4.1% | 5.4% | 8.4% | 11.5% | 15.9% | 15.6% | 12.2% | 9.4% | 6.6% | 4.9% | 3.2% |
| 1Mil. | 2.8% | 4.1% | 5.5% | 8.4% | 11.3% | 15.7% | 15.3% | 12.0% | 9.3% | 6.6% | 5.2% | 3.7% |
| 1.25 Mil. | 3.0% | 4.1% | 5.2% | 8.3% | 11.3% | 15.5% | 15.2% | 11.9% | 9.4% | 6.9% | 5.4% | 3.9% |
| 1.5 Mil. | 2.5% | 3.8% | 5.2% | 8.4% | 11.6% | 16.0% | 15.7% | 12.3% | 9.4% | 6.6% | 5.0% | 3.4% |
| 1.75 Mil. | 2.4% | 3.8% | 5.2% | 8.4% | 11.6% | 16.0% | 15.7% | 12.3% | 9.5% | 6.7% | 5.1% | 3.5% |
| 2 Mil. | 2.6% | 3.9% | 5.1% | 8.2% | 11.3% | 15.7% | 15.4% | 12.1% | 9.4% | 6.7% | 5.4% | 4.1% |

Table 4a - Relative contribution of main bars to load resistance during fatigue test on south span.

| Cycle Number | GY #8 T #1 | Interpolate T #2 | GY #7 T #3 | Interpolate T #4 | GY #6 T #5 | GY #5 T #6 | GY #4 T #7 | GY #3 T #8 | Interpolate T #9 | GY #2 T #10 | Interpolate T #11 | GY #1 T #12 |
|---|---|---|---|---|---|---|---|---|---|---|---|---|
| 250K | 3.0% | 3.6% | 4.3% | 8.1% | 11.8% | 13.9% | 15.7% | 13.4% | 10.6% | 7.8% | 5.2% | 2.6% |
| 500K | 2.7% | 3.5% | 4.4% | 8.1% | 11.9% | 14.3% | 16.0% | 13.6% | 10.6% | 7.5% | 5.0% | 2.5% |
| 750K | 2.8% | 3.6% | 4.5% | 8.2% | 11.9% | 14.2% | 15.9% | 13.6% | 10.5% | 7.4% | 4.9% | 2.5% |
| 1Mil. | 2.8% | 3.6% | 4.4% | 8.2% | 11.9% | 13.8% | 15.7% | 13.7% | 10.7% | 7.8% | 5.1% | 2.4% |
| 1.25 Mil. | 2.6% | 3.4% | 4.3% | 8.2% | 12.0% | 14.1% | 15.9% | 13.6% | 10.6% | 7.7% | 5.1% | 2.5% |
| 1.5 Mil. | 2.5% | 3.5% | 4.5% | 8.2% | 12.0% | 14.5% | 16.2% | 13.9% | 10.5% | 7.1% | 4.7% | 2.3% |
| 1.75 Mil. | 2.3% | 3.4% | 4.5% | 8.3% | 12.2% | 14.5% | 16.2% | 13.9% | 10.5% | 7.2% | 4.7% | 2.2% |
| 2 Mil. | 2.6% | 3.5% | 4.4% | 8.3% | 12.2% | 14.2% | 16.0% | 13.8% | 10.6% | 7.4% | 4.8% | 2.2% |

Table 4b - Relative contribution of main bars to load resistance during fatigue test on north span.

| Load Orientation | Main Bar #1 (BR8) | Main Bar #2 | Main Bar #3 (BR7) | Main Bar #4 | Main Bar #5 (BR6) | Main Bar #6 (BR5) | Main Bar #7 (BR4) | Main Bar #8 (BR3) | Main Bar #9 | Main Bar #10 (BR2) | Main Bar #11 | Main Bar #12 (BR1) |
|---|---|---|---|---|---|---|---|---|---|---|---|---|
| Parallel | 4.9% | 6.1% | 7.4% | 9.6% | 11.8% | 12.1% | 12.0% | 10.5% | 8.5% | 6.6% | 5.7% | 4.8% |
| Transverse | 4.5% | 5.7% | 7.0% | 9.2% | 11.5% | 12.7% | 12.7% | 10.9% | 8.8% | 6.6% | 5.7% | 4.7% |

Table 5 - Relative contribution of main bars to load resistance for single span static test and different patch orientations relative to the main bar direction (20 kip load).

| Load (kips) | Main Bar #1 (BR8) | Main Bar #2 | Main Bar #3 (BR7) | Main Bar #4 | Main Bar #5 (BR6) | Main Bar #6 (BR5) | Main Bar #7 (BR4) | Main Bar #8 (BR3) | Main Bar #9 | Main Bar #10 (BR2) | Main Bar #11 | Main Bar #12 (BR1) |
|---|---|---|---|---|---|---|---|---|---|---|---|---|
| 20 | 4.9% | 6.1% | 7.4% | 9.6% | 11.8% | 12.1% | 12.0% | 10.5% | 8.5% | 6.6% | 5.7% | 4.8% |
| 49 | 4.4% | 5.7% | 7.1% | 9.6% | 12.1% | 13.2% | 12.7% | 10.8% | 8.6% | 6.4% | 5.2% | 4.1% |
| 74 | 3.8% | 5.3% | 6.9% | 9.5% | 12.2% | 13.4% | 14.7% | 11.0% | 8.6% | 6.1% | 4.9% | 3.6% |
| 99 | 3.3% | 5.0% | 6.7% | 9.5% | 12.3% | 13.4% | 16.1% | 11.3% | 8.7% | 6.0% | 4.6% | 3.2% |
| 125 | 2.9% | 4.8% | 6.7% | 9.5% | 12.4% | 13.1% | 16.9% | 11.5% | 8.8% | 6.1% | 4.4% | 2.8% |
| 144 | 2.8% | 4.7% | 6.7% | 9.1% | 11.6% | 13.9% | 17.7% | 11.8% | 8.9% | 6.0% | 4.3% | 2.6% |

Table 6 - Relative contribution of main bars to load resistance for single span static test at various load levels.

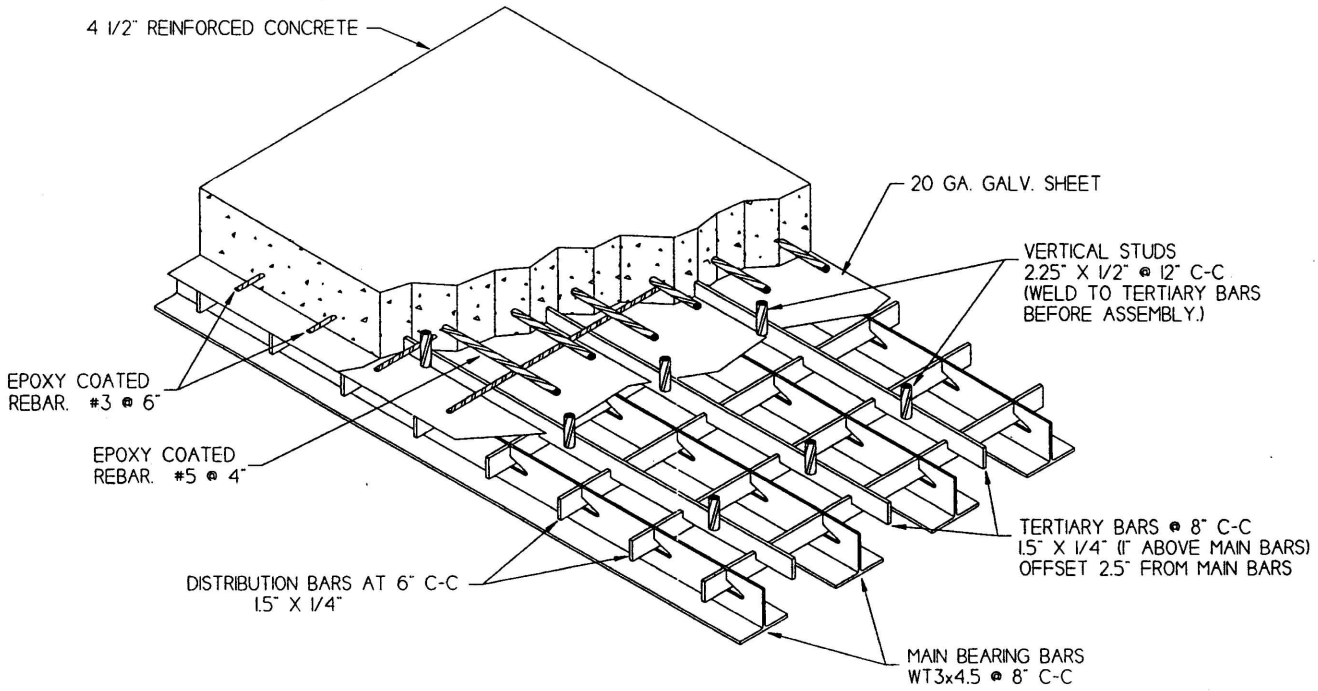


Fig. 1 - Example of existing Exodermic bridge deck design [EBDI, 1996].

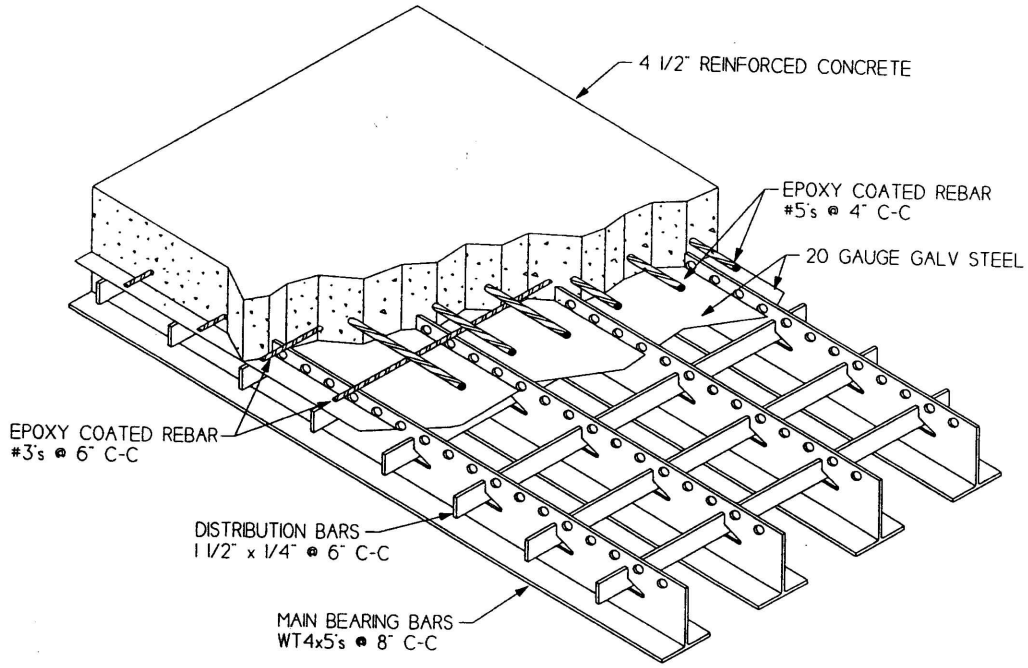


Fig. 2 - Example of modified Exodermic bridge deck design with "shear holes" located in web of main bars [EBDI, 1997].

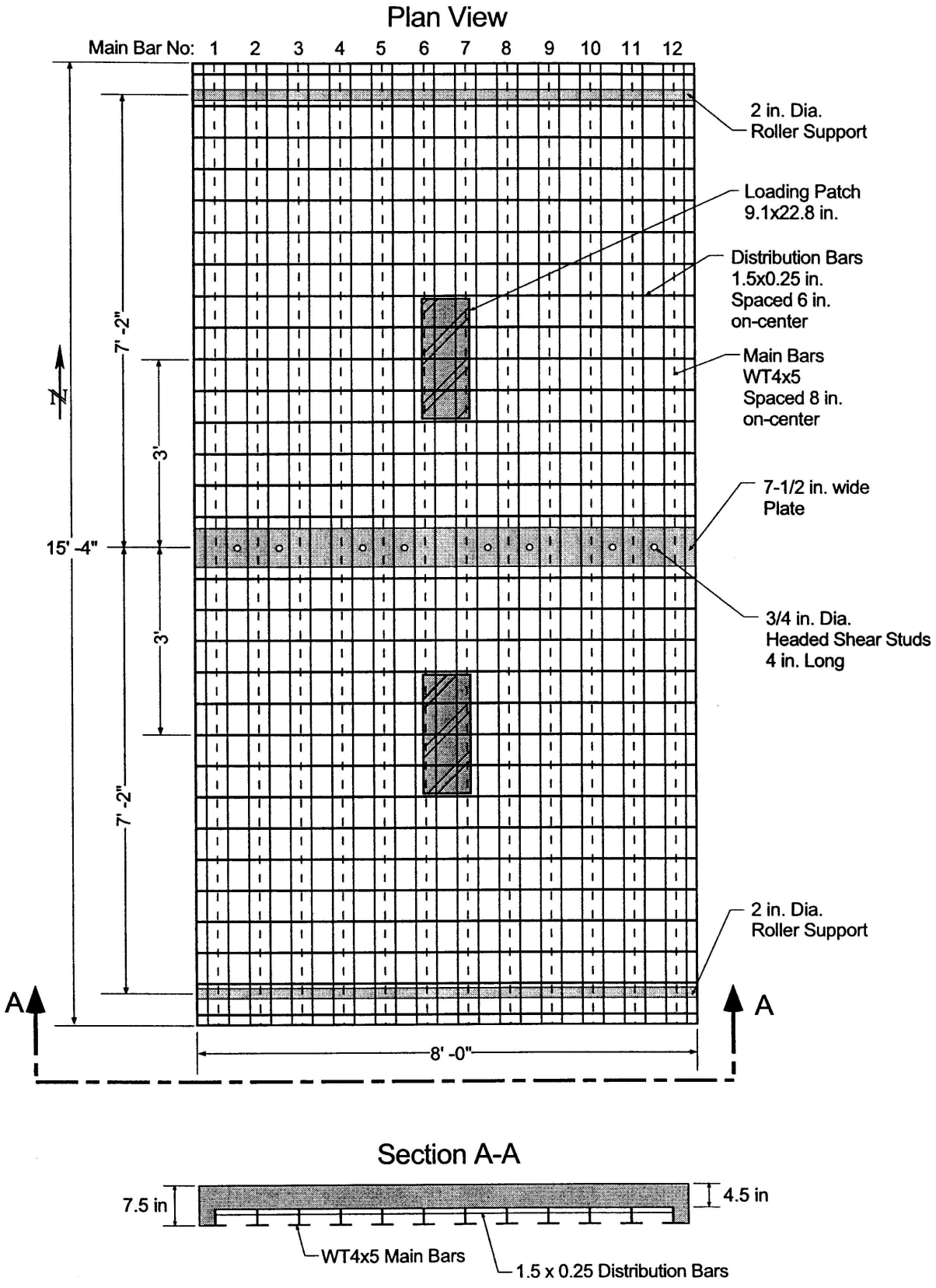


Fig. 3 - Overall dimensions and layout of prototype Exodermic bridge deck specimen.

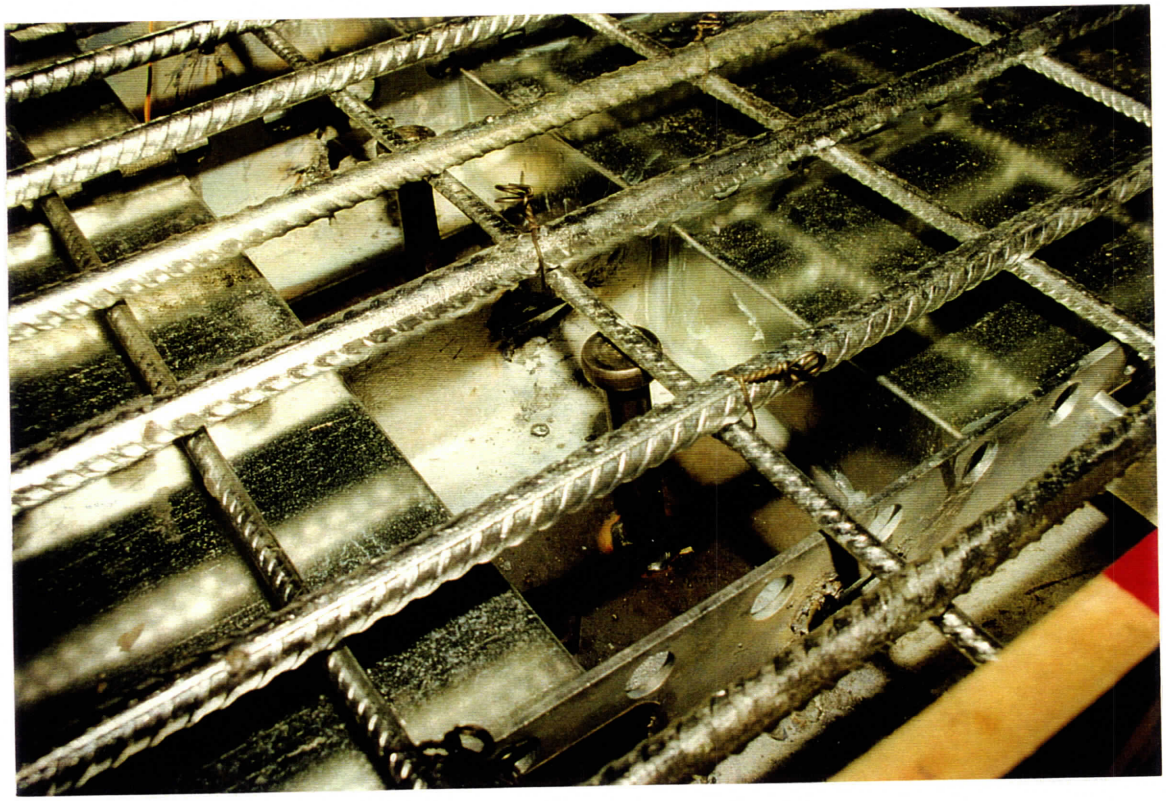

Fig. 4 - Center support detail.

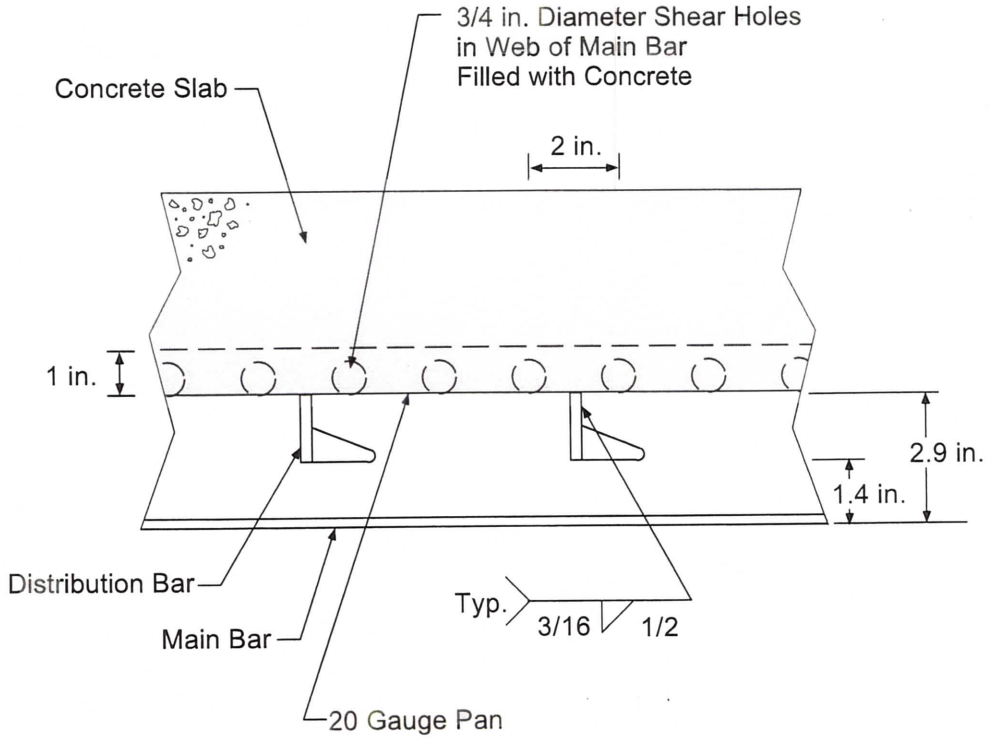


Fig. 5 - As specified main and distribution bar detail.

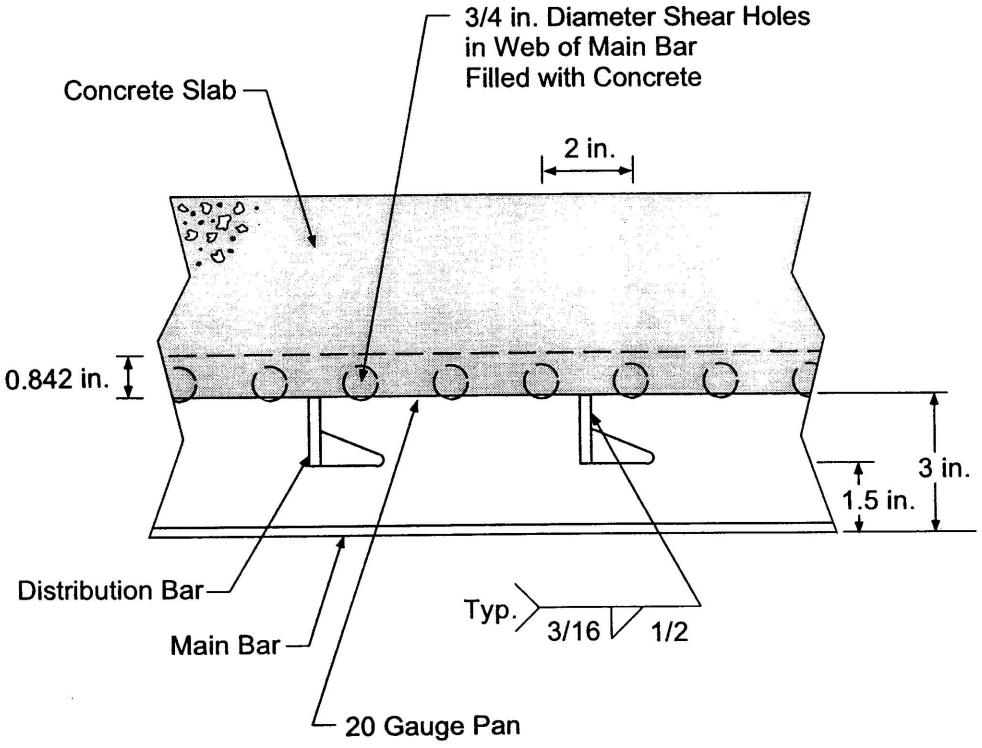


Fig. 6a - As fabricated main and distribution bar detail.

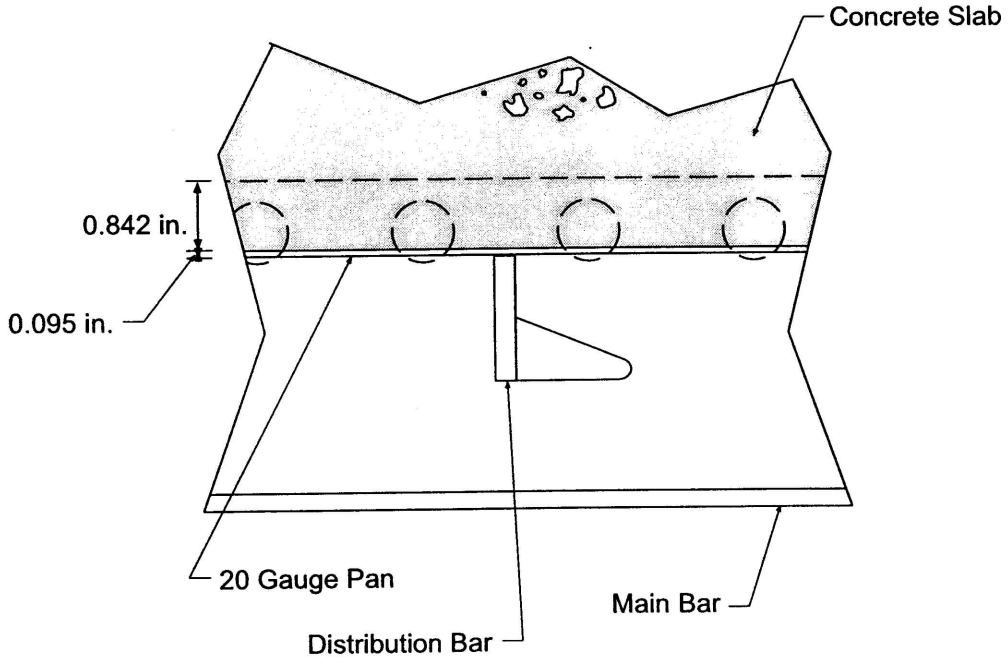


Fig. 6b - Close-up view of as fabricated main and distribution bar detail.

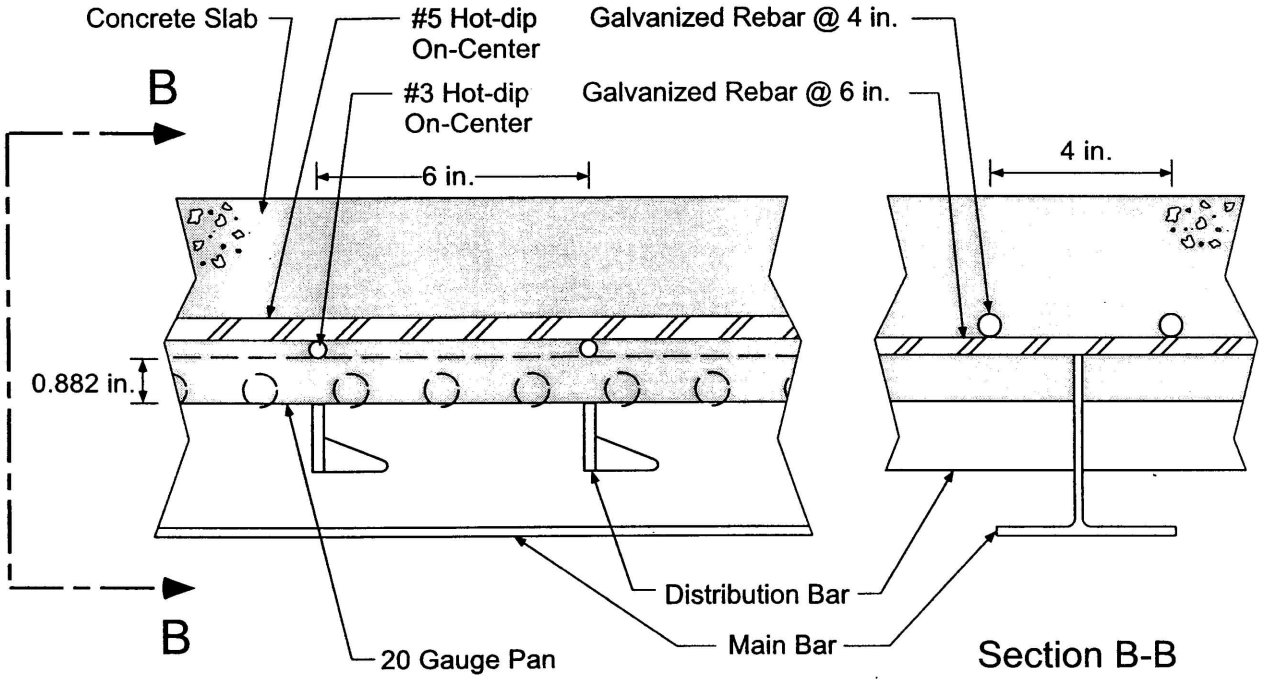


Fig. 7 - Concrete slab reinforcing steel layout.

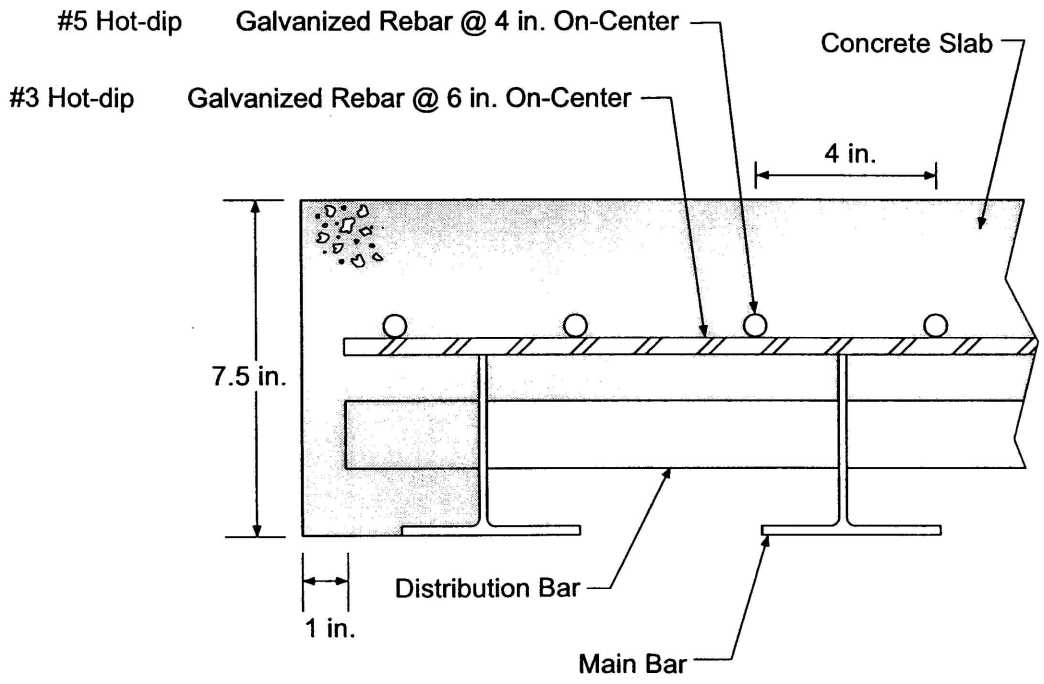


Fig. 8 - Detail at the unsupported edge of the test panel.

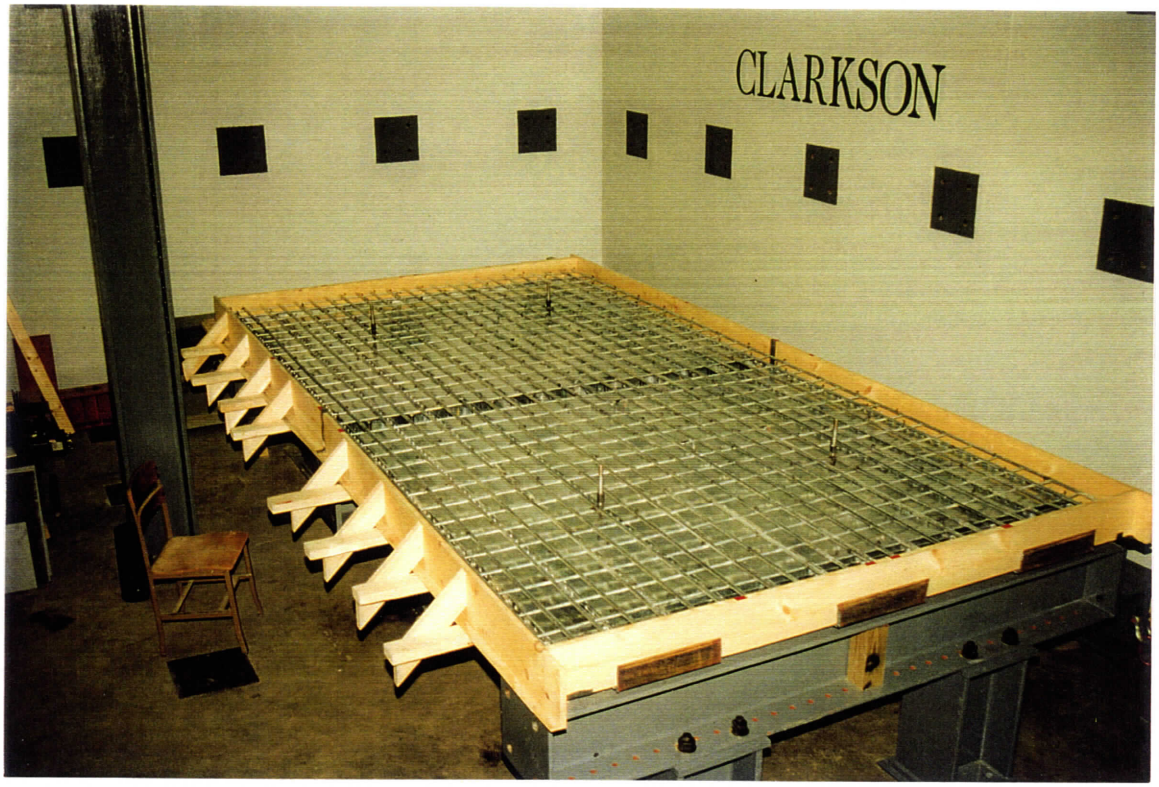


Fig. 9 - Steel grid, reinforcing steel and formwork prior to casting of concrete.

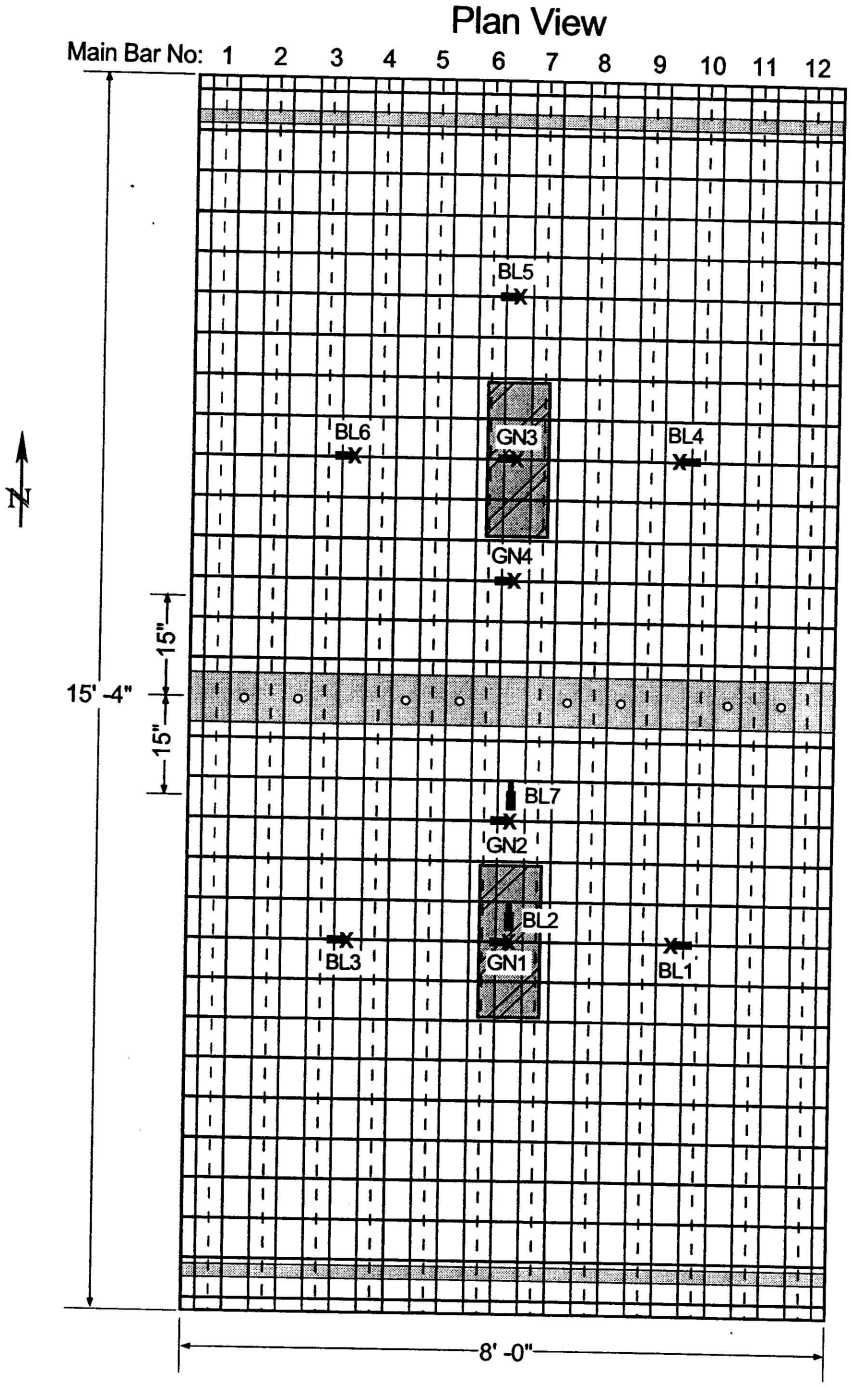


Legend

Displacement transducer. Rectangle indicates connection to T-section.

Slip gage bonded to underside of concrete slab used to measure relative deformation at adjacent distribution bar.

Fig. 10 - Displacement transducer locations.

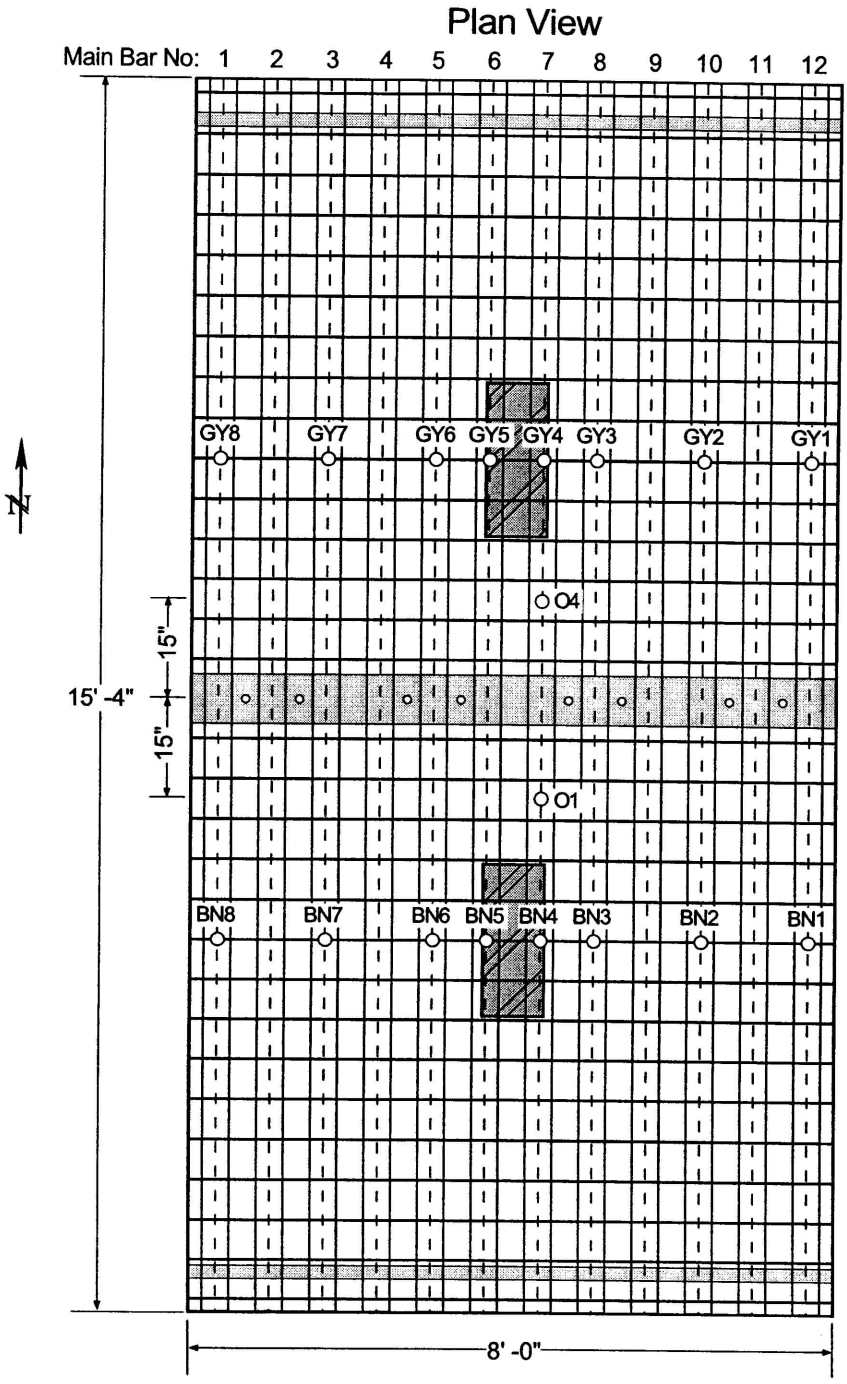


Fig. 11 - Strain gage locations on steel grid.

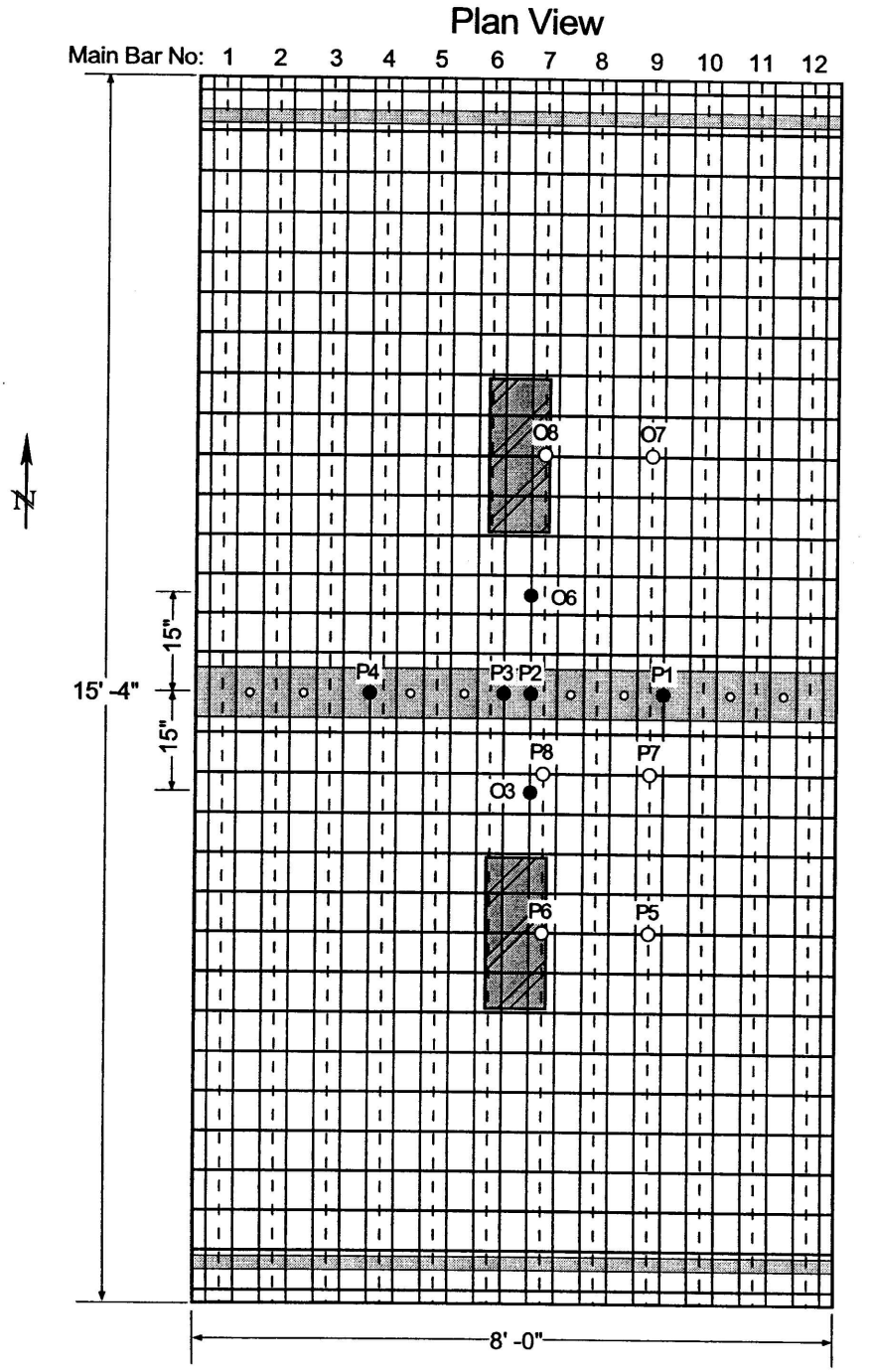


Legend

- Strain gage on embedded #5 reinforcing steel.
- o Strain gage on embedded #3 reinforcing steel.

Fig. 12 - Strain gage locations on reinforcing steel.

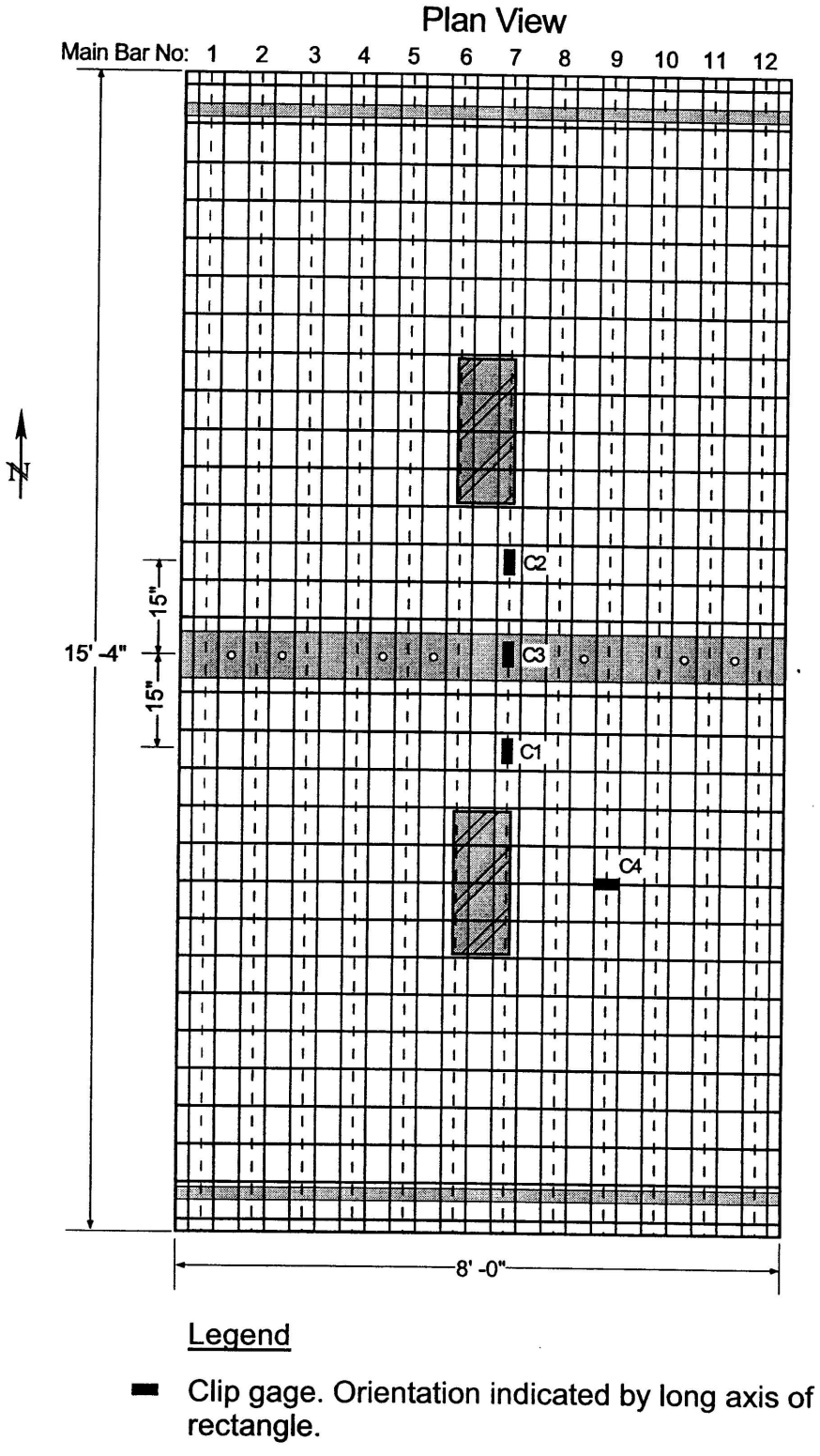


Fig. 13 - Clip gage locations.

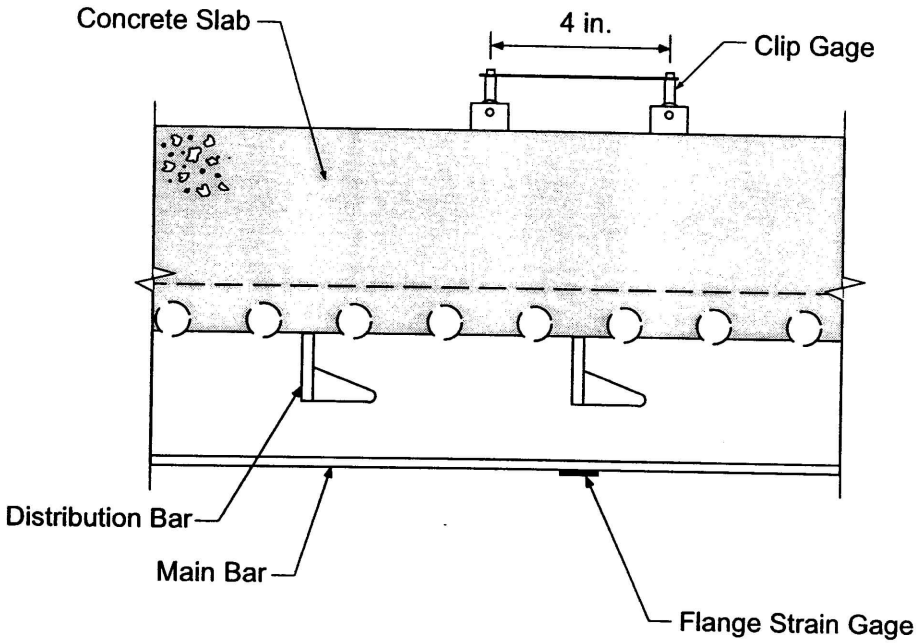


Fig. 14 - Instrumented locations with strain gages on the bottom flange of the main bars and clip gage on the concrete slab.

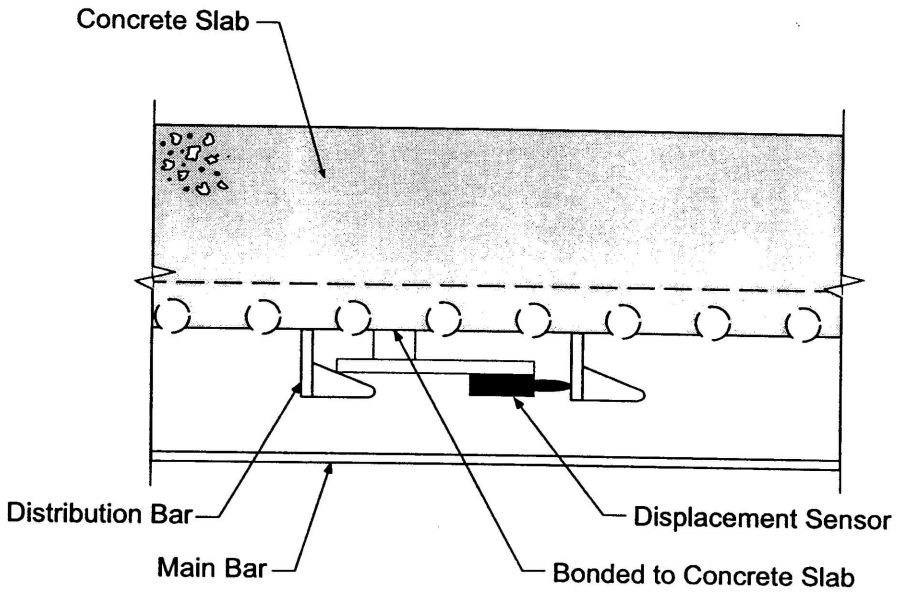


Fig. 15 – Detail of displacement transducer used to measure relative deformation between steel grid and concrete slab.

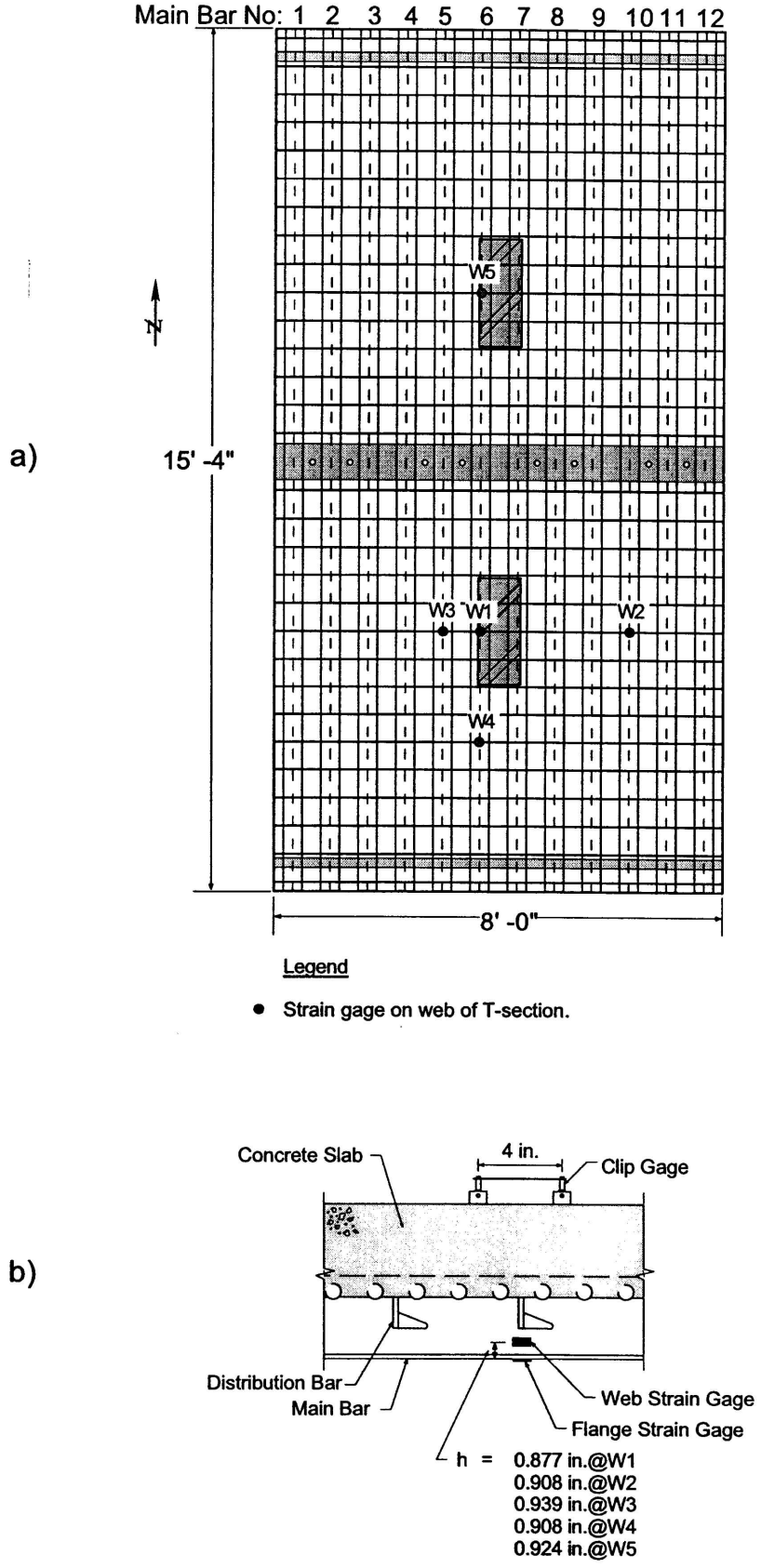


Fig. 16 - Additional web strain gage locations (a) and instrumented cross-section detail (b).

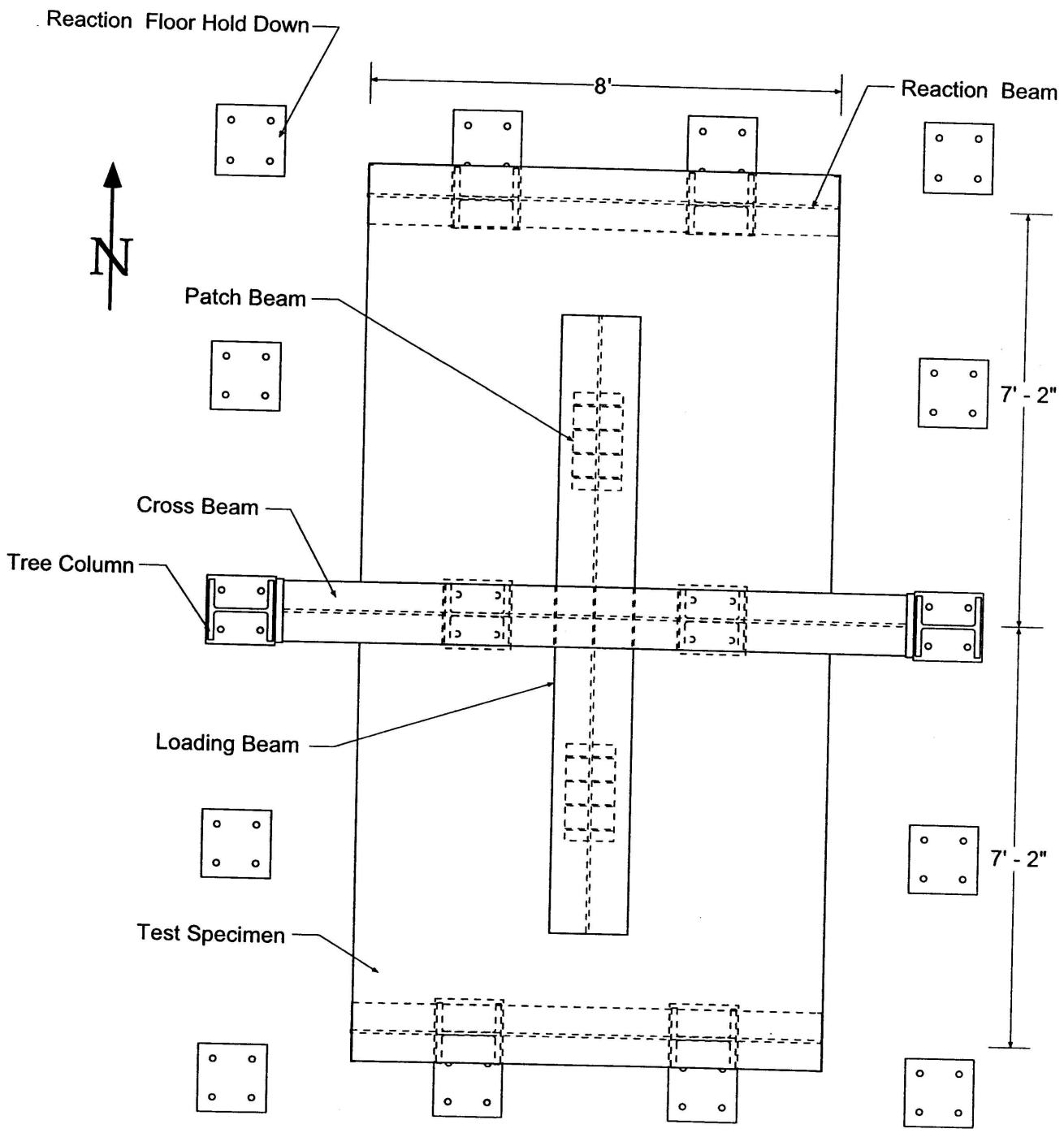


Fig. 17 - Plan view of test set-up.

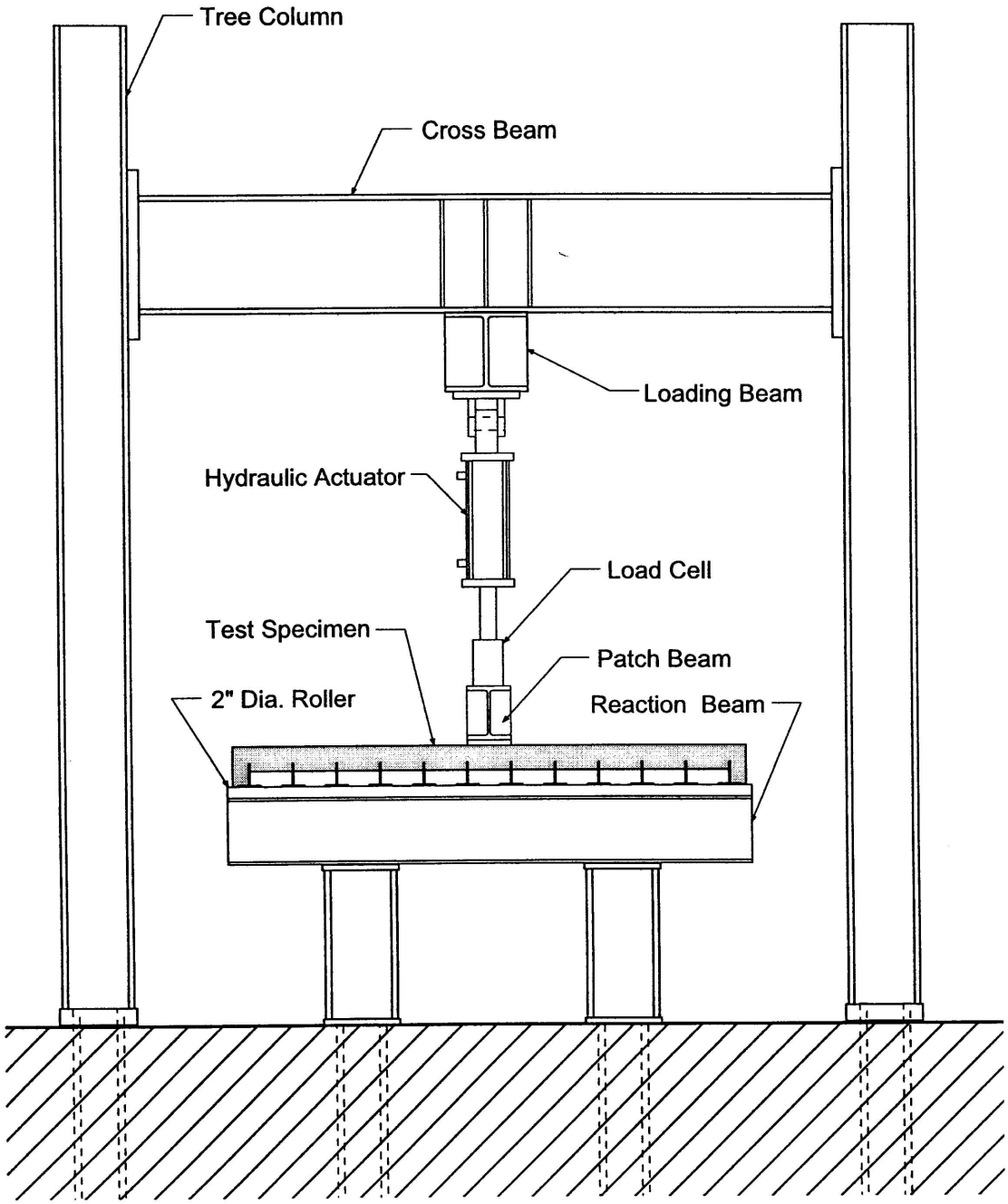


Fig. 18 - Elevation view of test set-up.

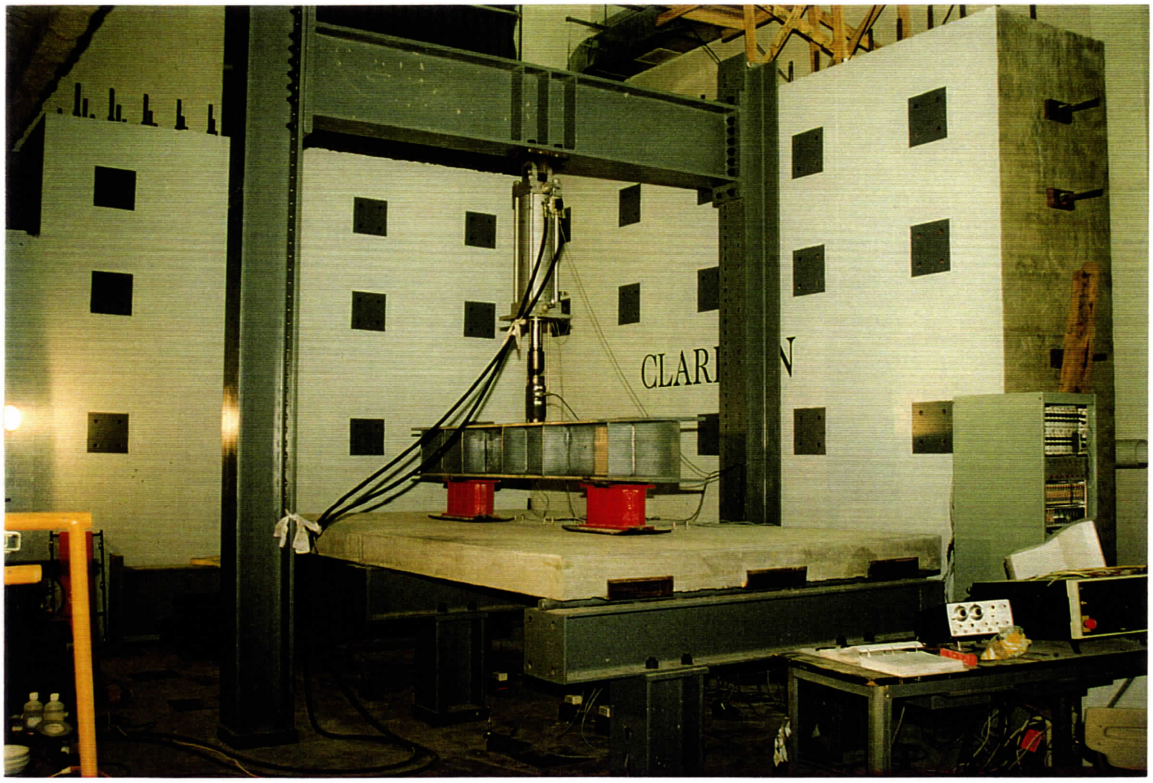

Fig. 19 - Overall test set-up.

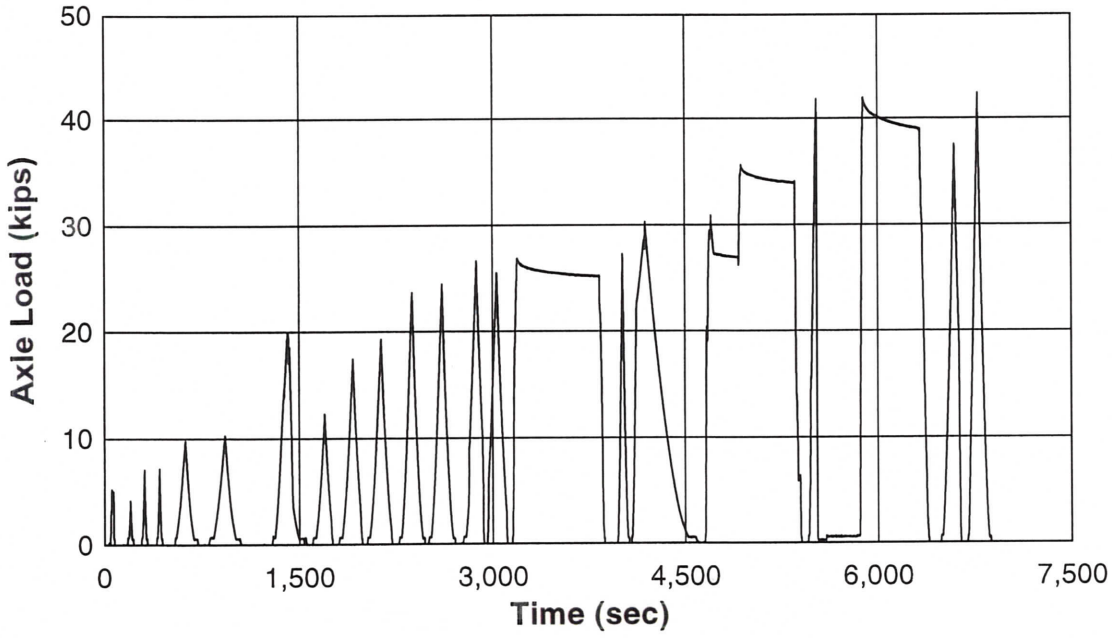


Fig. 20 - Static loading history prior to fatigue testing.

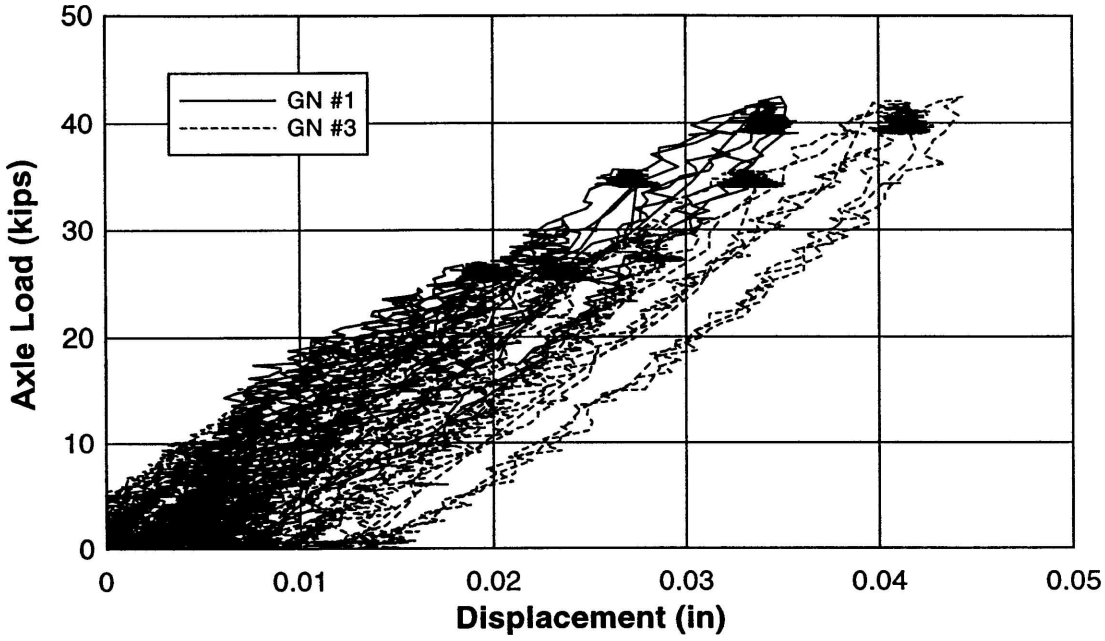


Fig. 21 - Displacement response at load point for all initial static load cycles.

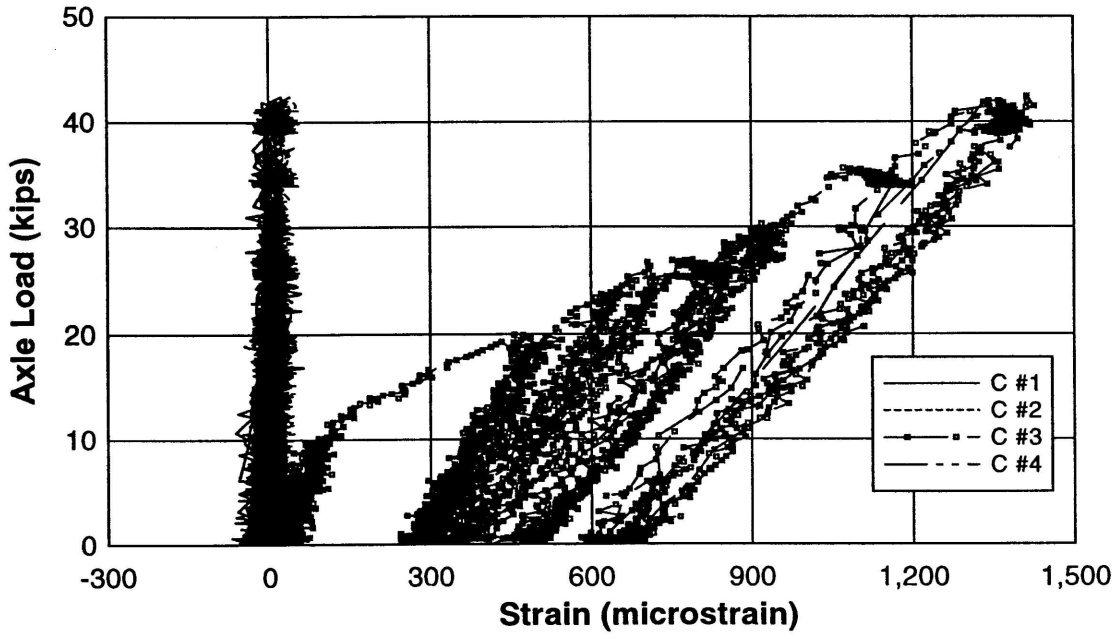


Fig. 22 - Concrete strain measurements for all initial static load cycles.

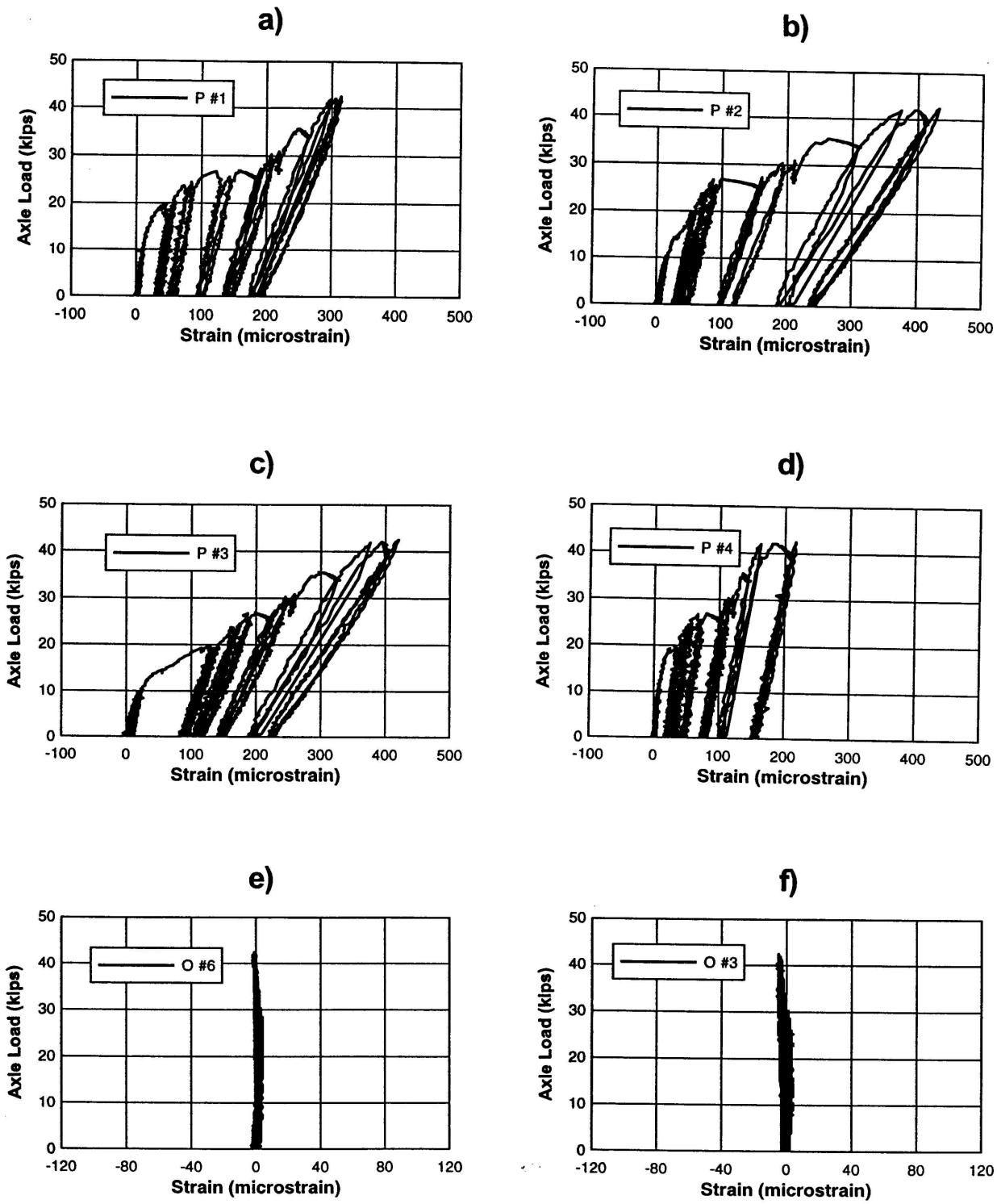


Fig. 23 (a-f) - Individual #5 reinforcing bar strain measurements for all initial static load cycles.

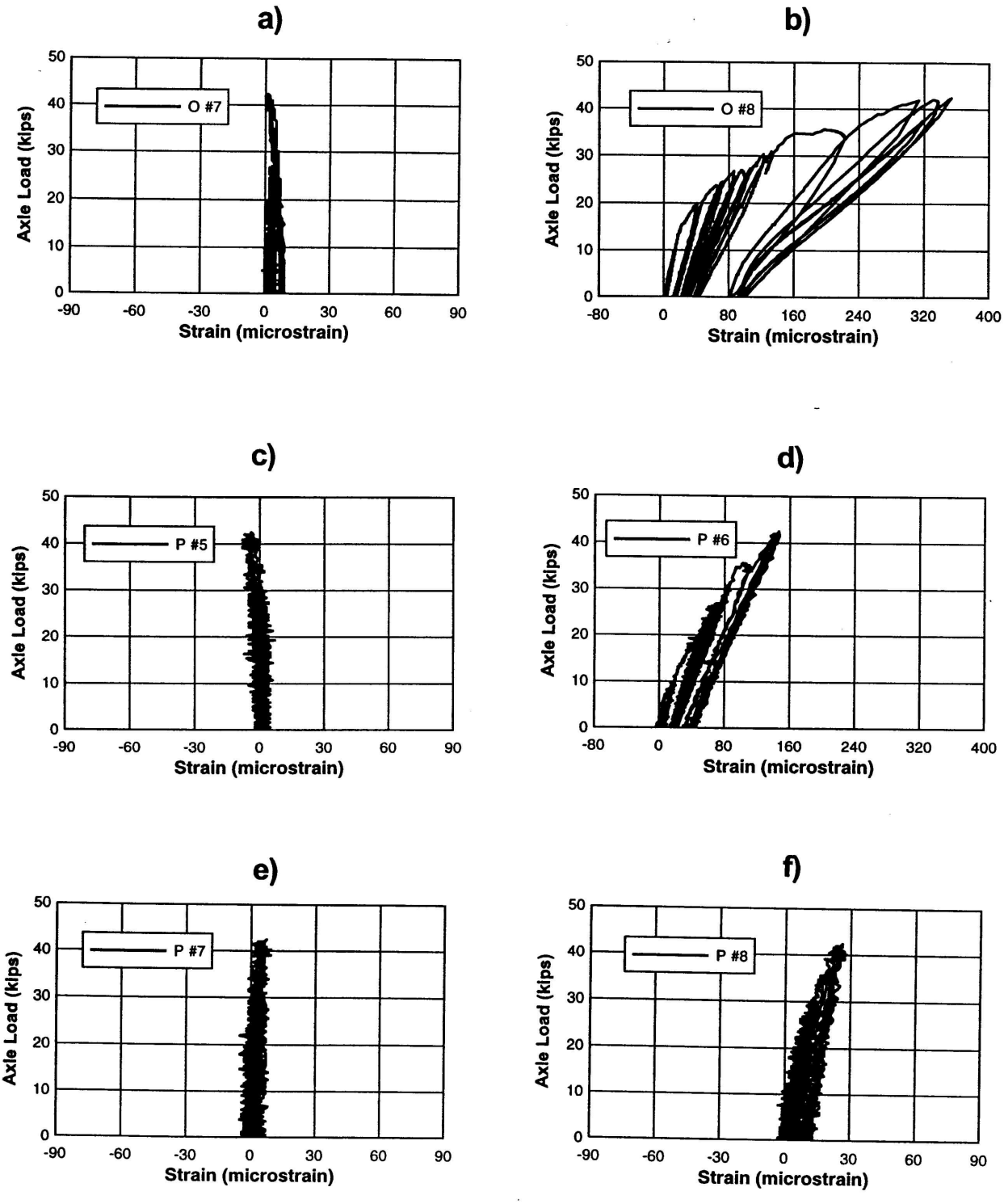


Fig. 24 (a-f) - Individual #3 reinforcing bar strain measurements for all initial static load cycles.

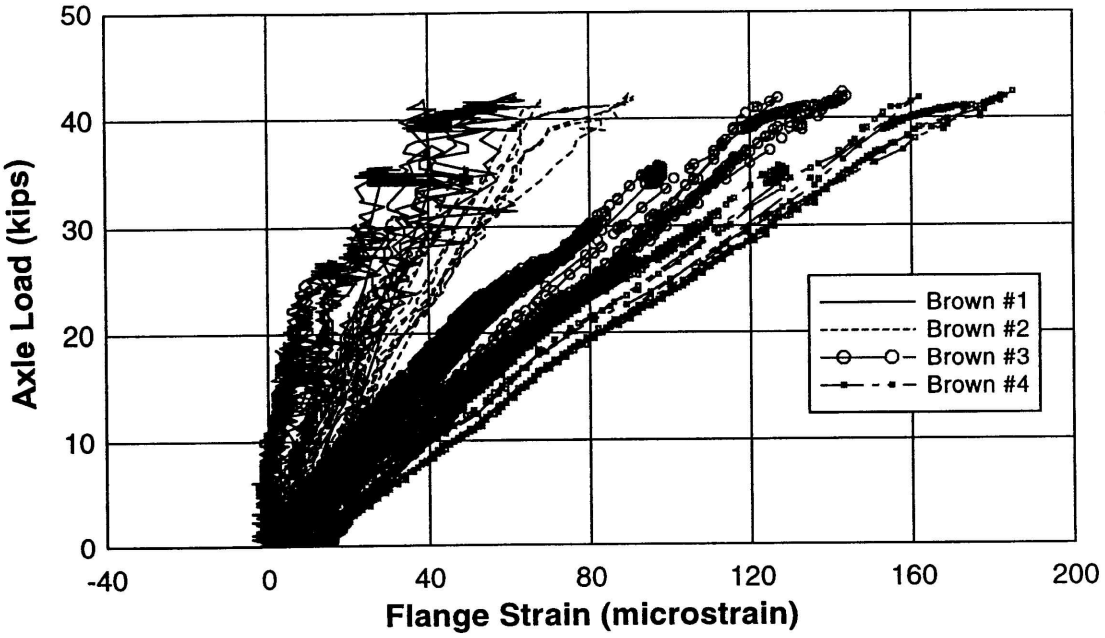


Fig. 25a – South span flange strain in main bars #1, #3, #5 and #6 for all initial static load cycles.

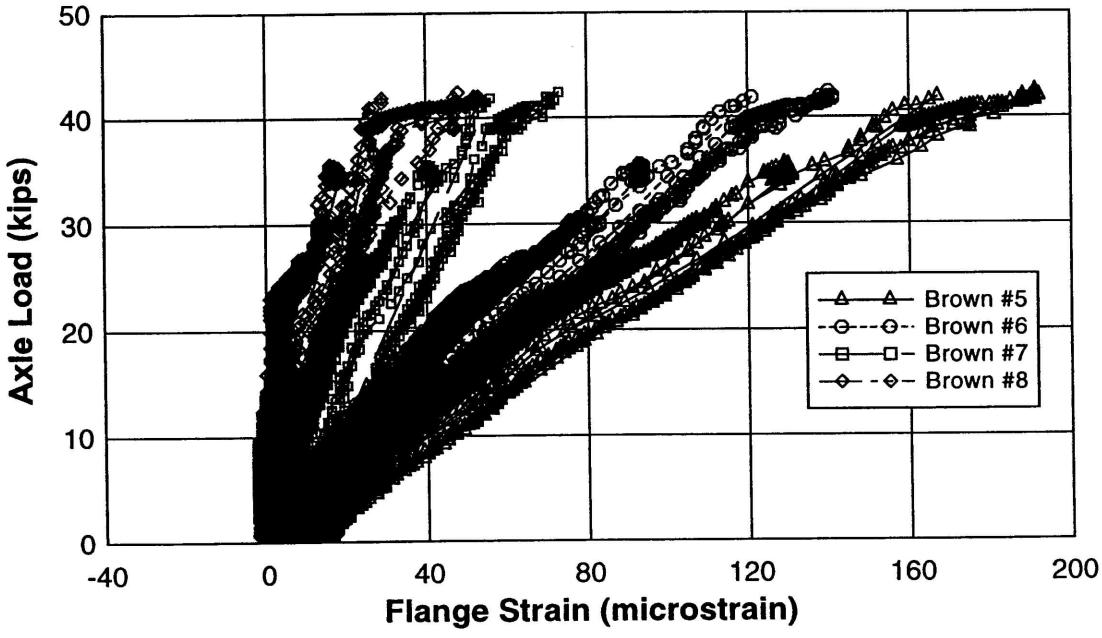


Fig. 25b – South span flange strain in main bars #7, #8, #10 and #12 for all initial static load cycles.

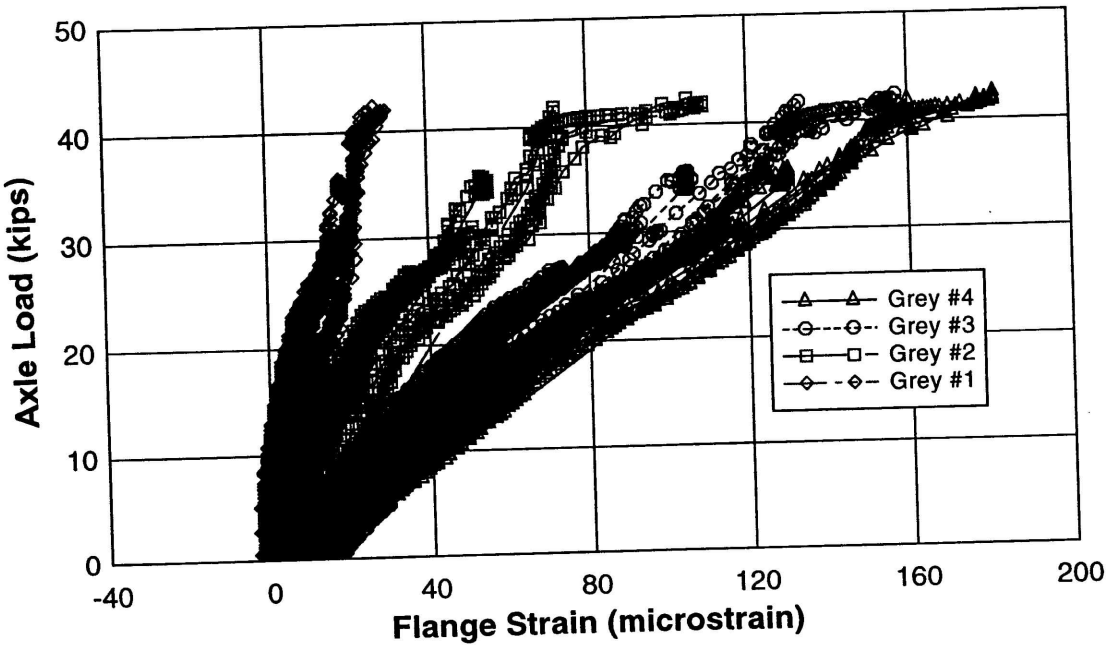


Fig. 26a – North span flange strain in main bars #1, #3, #5 and #6 for all initial static load cycles.

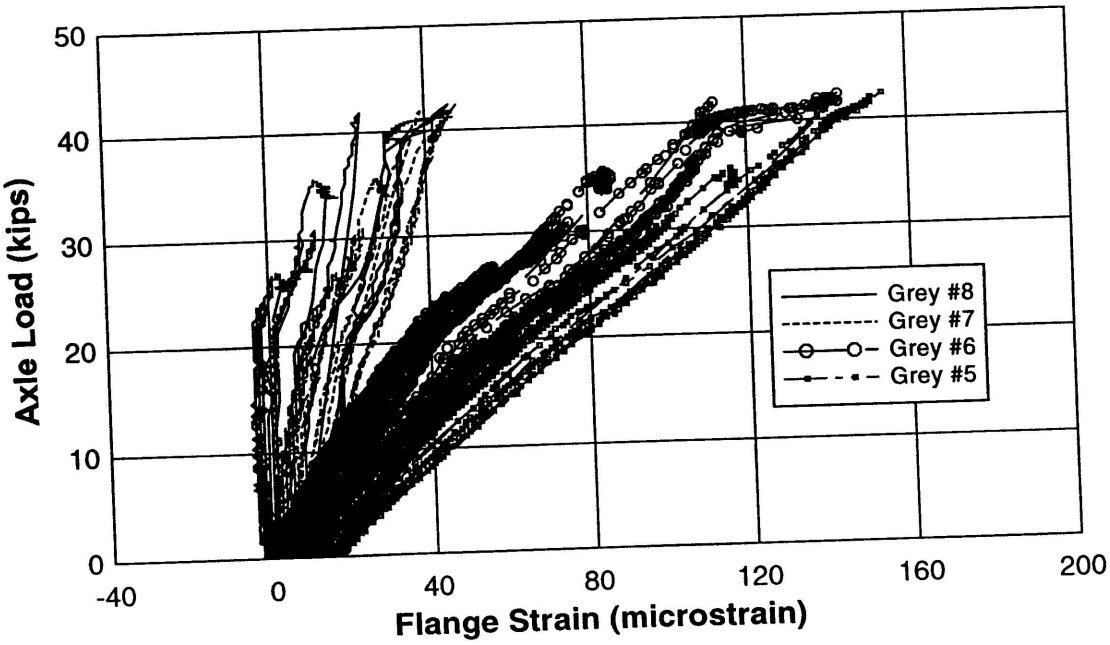


Fig. 26b – North span flange strain in main bars #7, #8, #10 and #12 for all initial static load cycles.

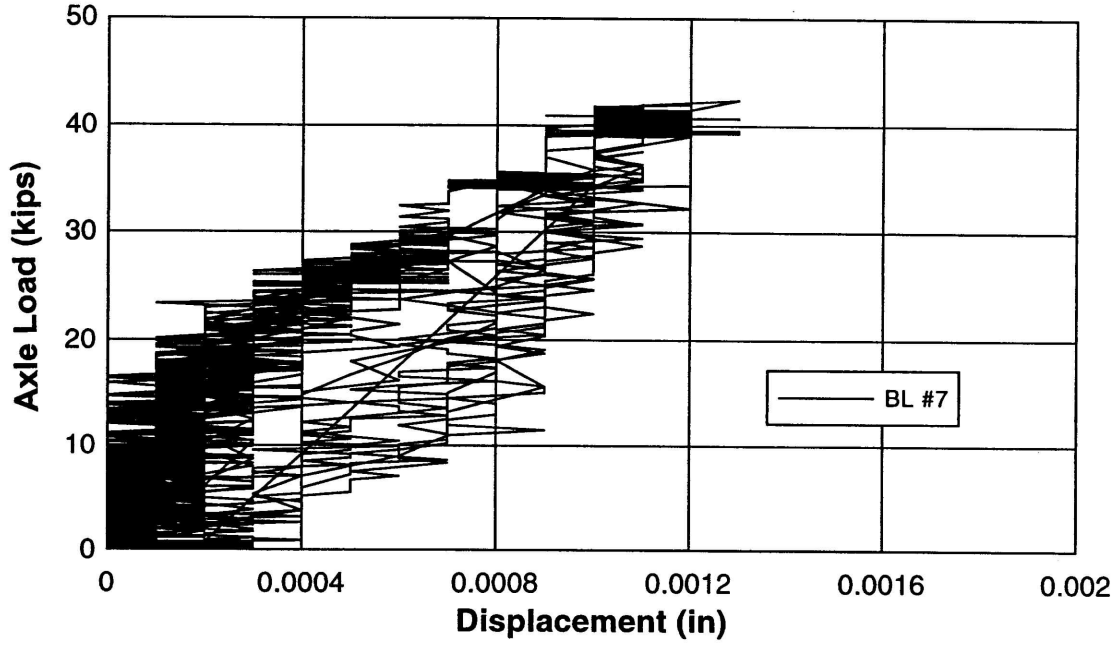


Fig. 27 – Relative displacement between concrete and steel grid for all initial static load cycles.

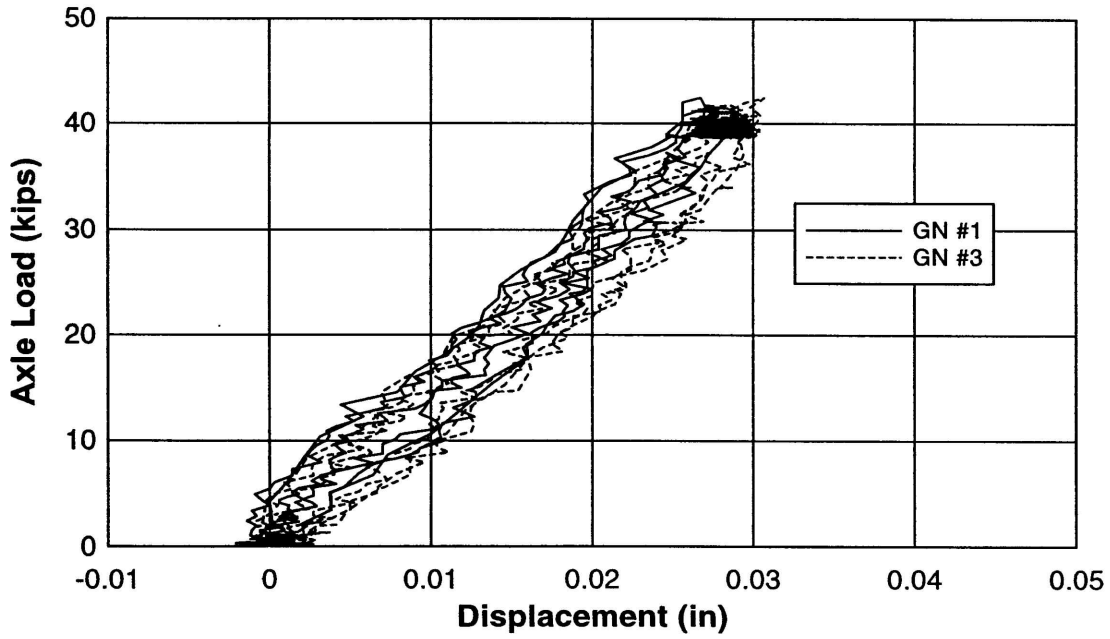


Fig. 28a – Relative displacement response for static load cycles to maximum load of 41.6 kips.

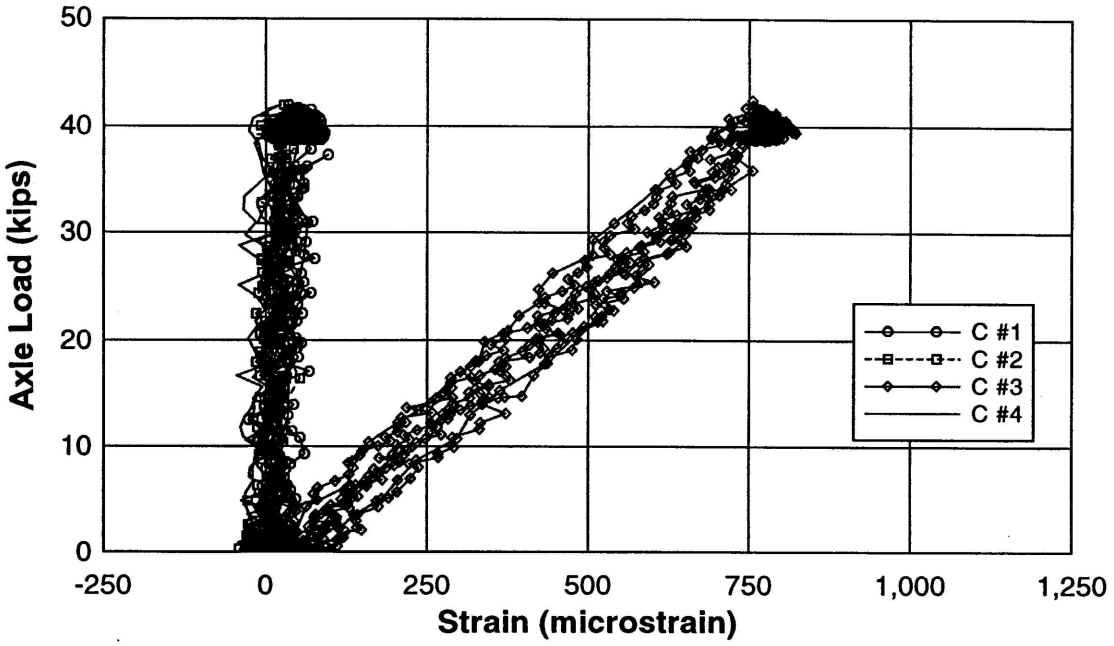


Fig. 28b – Relative concrete strain measurements for static load cycles to maximum load of 41.6 kips.

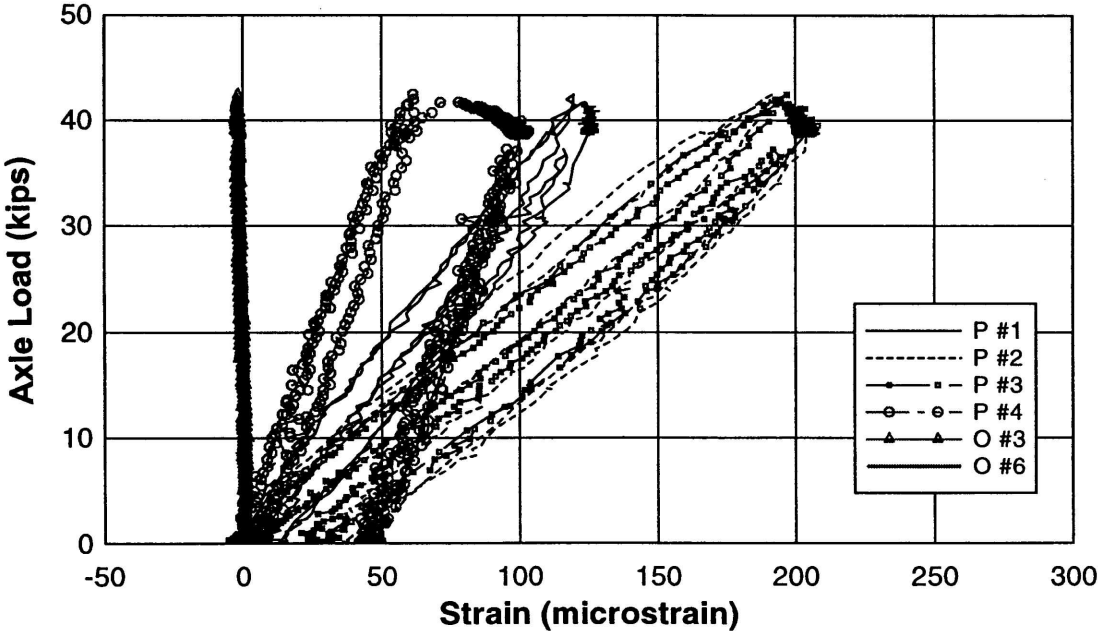


Fig. 28c – Relative #5 reinforcing bar strain measurements for static load cycles to maximum load of 41.6 kips.

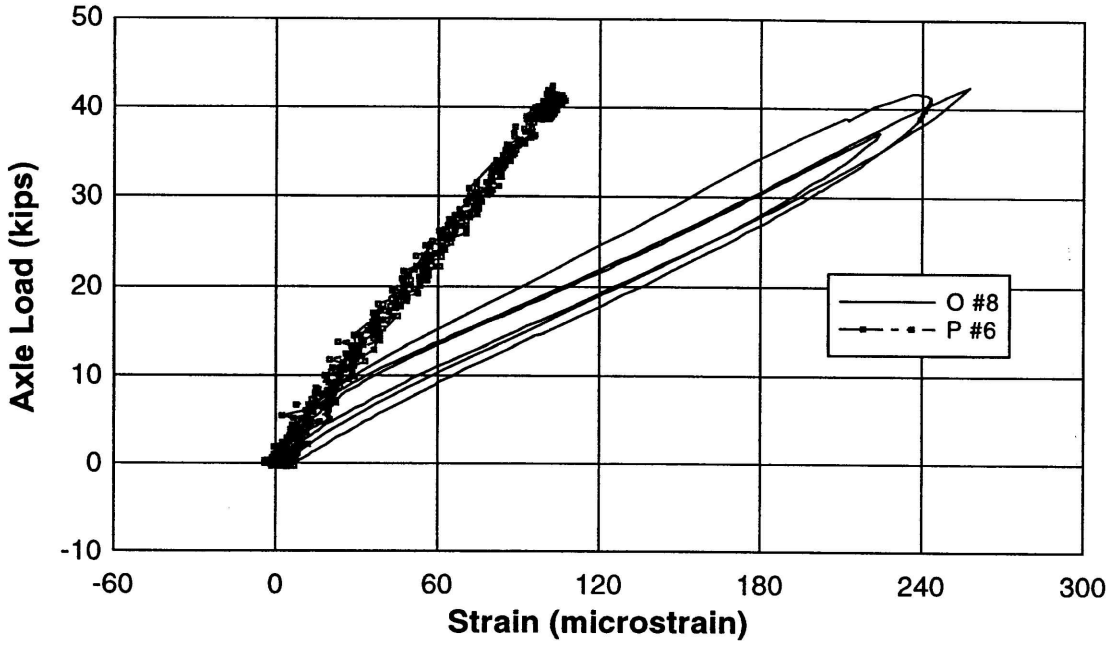


Fig. 28d – Relative #3 reinforcing bar strain measurements under load patch for static load cycles to maximum load of 41.6 kips.

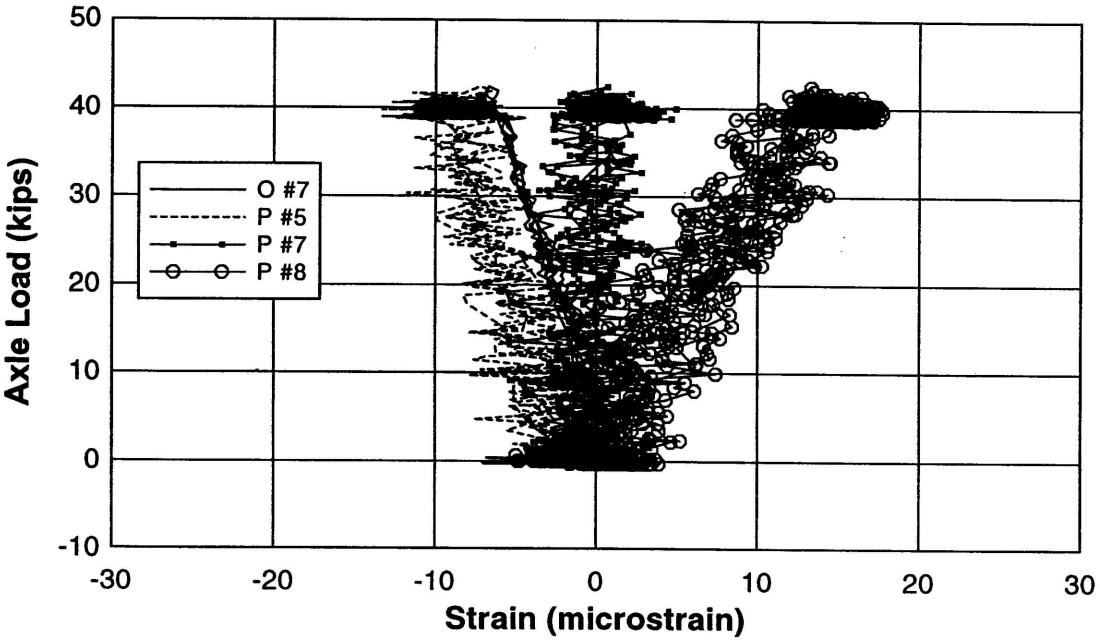


Fig. 28e – All other #3 reinforcing bar relative strain measurements for static load cycles to maximum load of 41.6 kips.

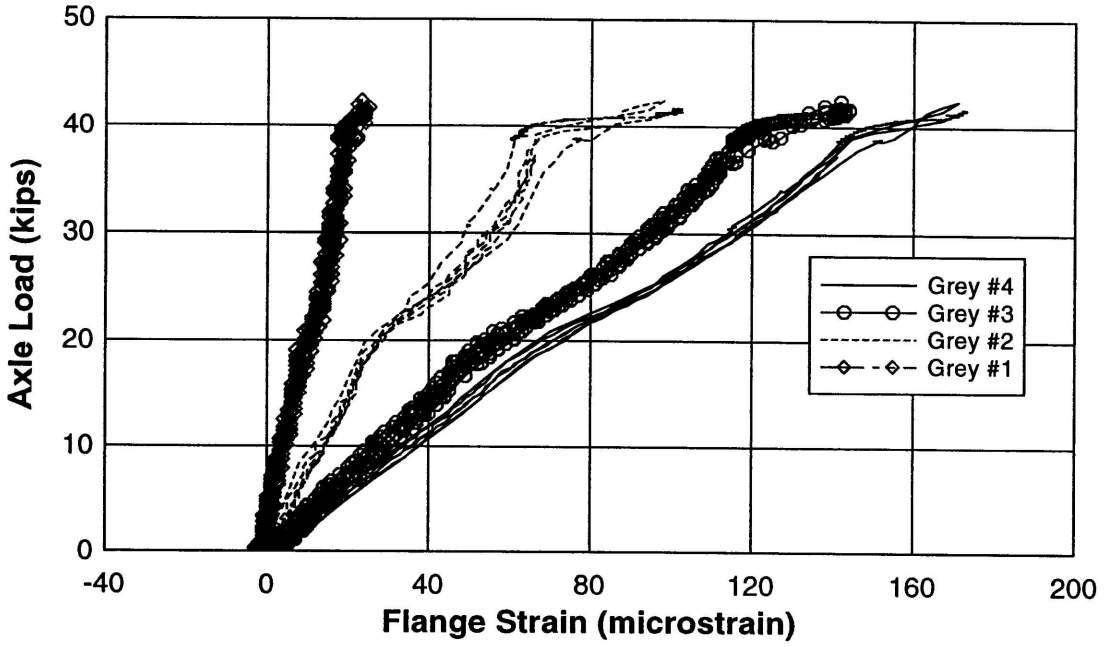


Fig. 28f – Relative north span flange strain in main bars #1, #3, #5 and #6 for static load cycles to maximum load of 41.6 kips.

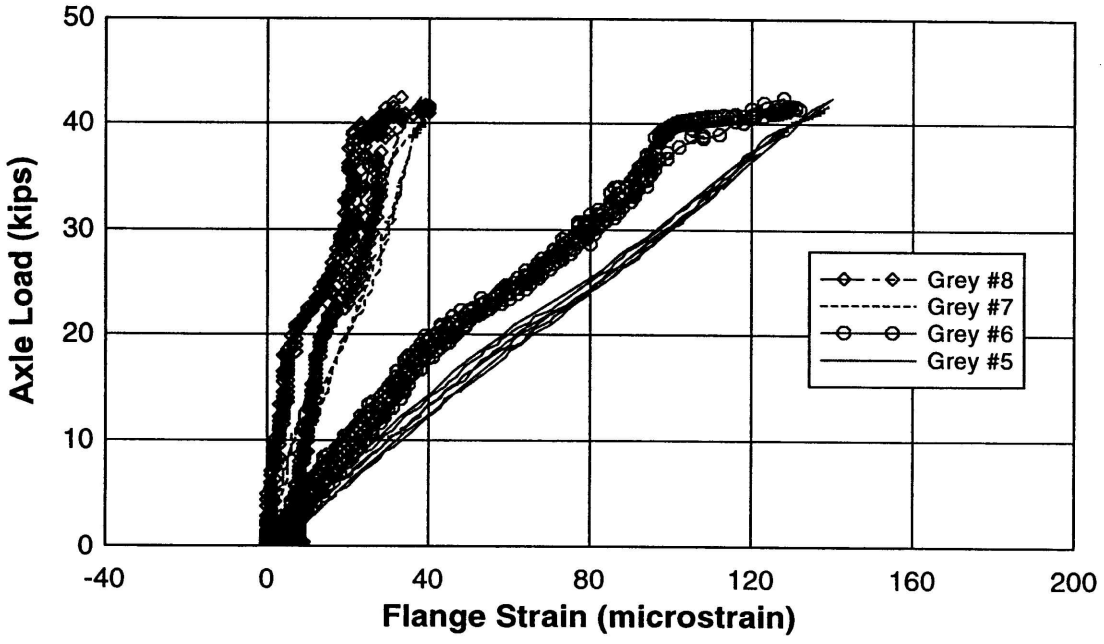


Fig. 28g – Relative north span flange strain in main bars #7, #8, #10 and #12 for static load cycles to maximum load of 41.6 kips.

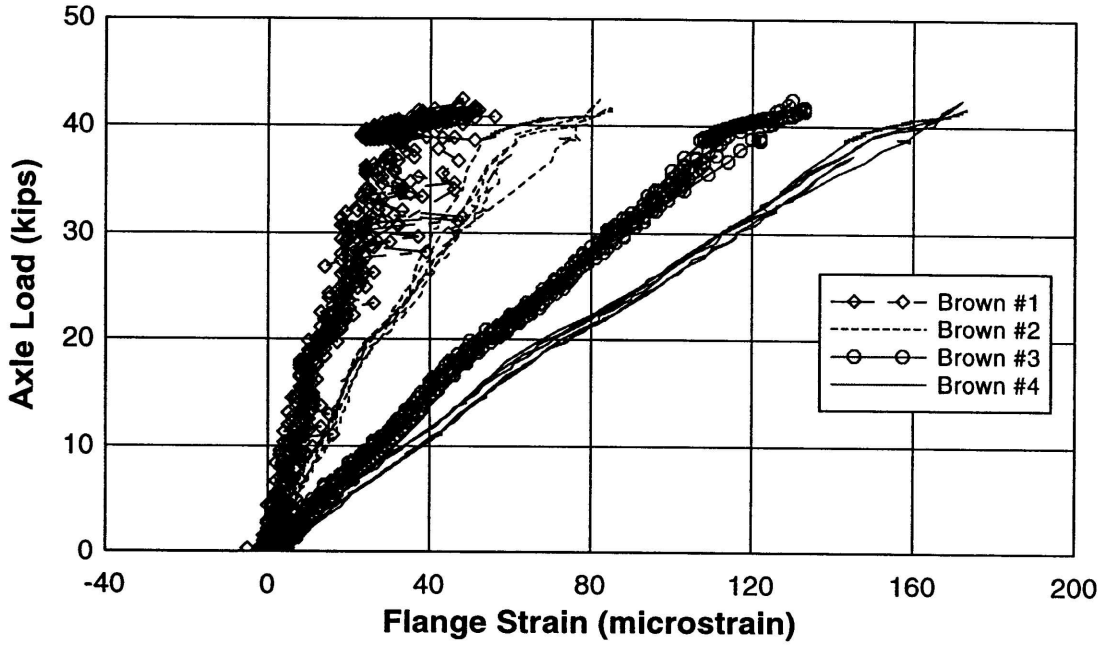


Fig. 28h – Relative south span flange strain in main bars #1, #3, #5 and #6 for static load cycles to maximum load of 41.6 kips.

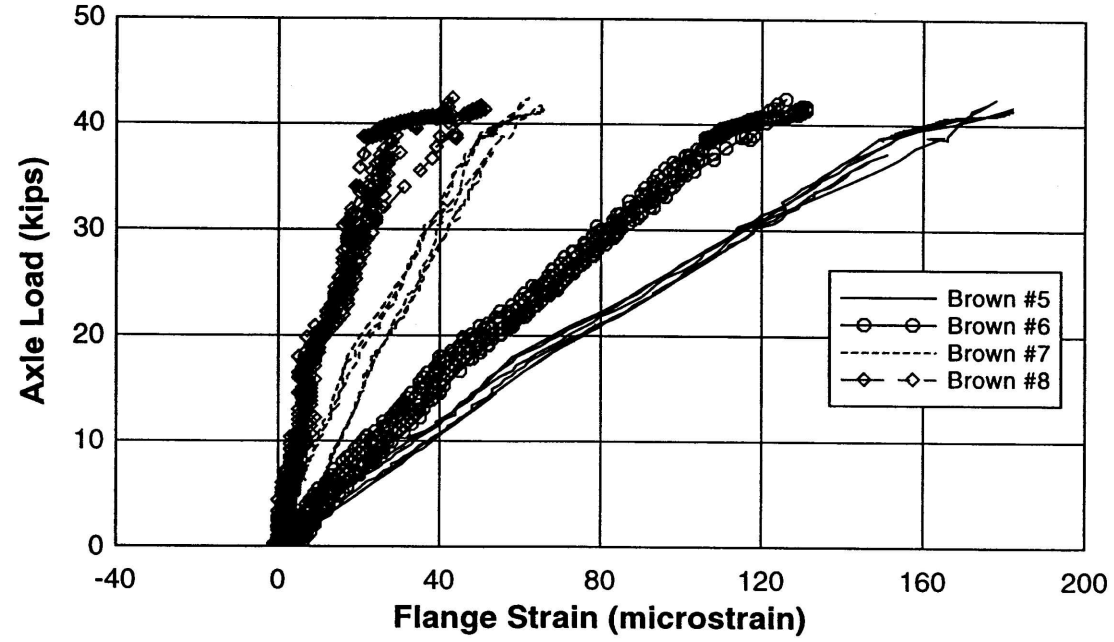


Fig. 28i – Relative south span flange strain in main bars #7, #8, #10 and #12 for static load cycles to maximum load of 41.6 kips.

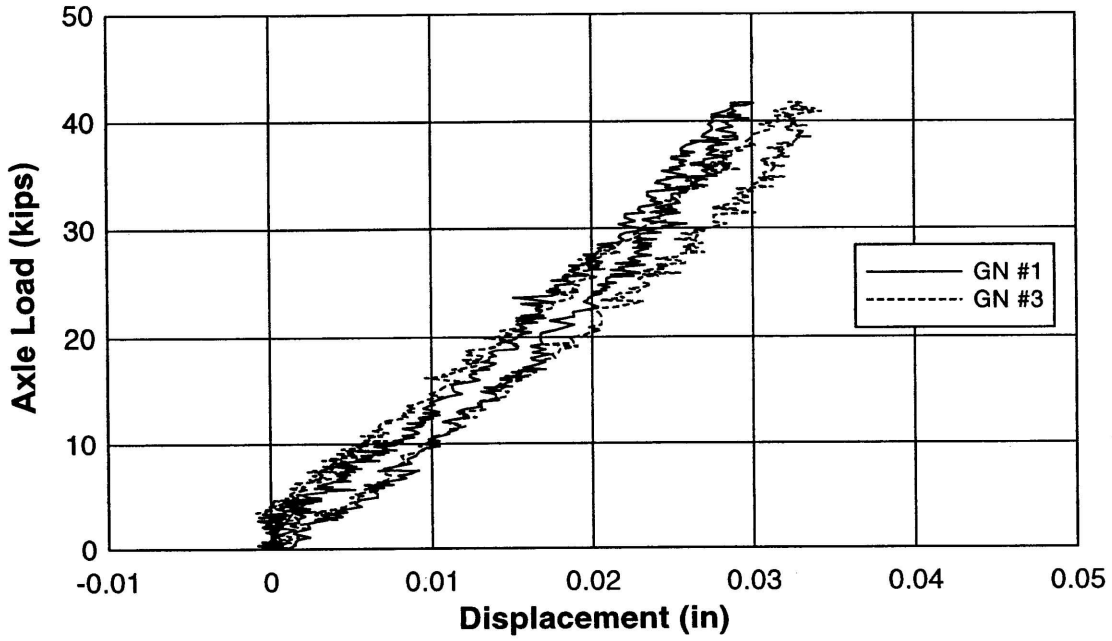


Fig. 29a - Relative displacement response after 250,000 fatigue cycles.

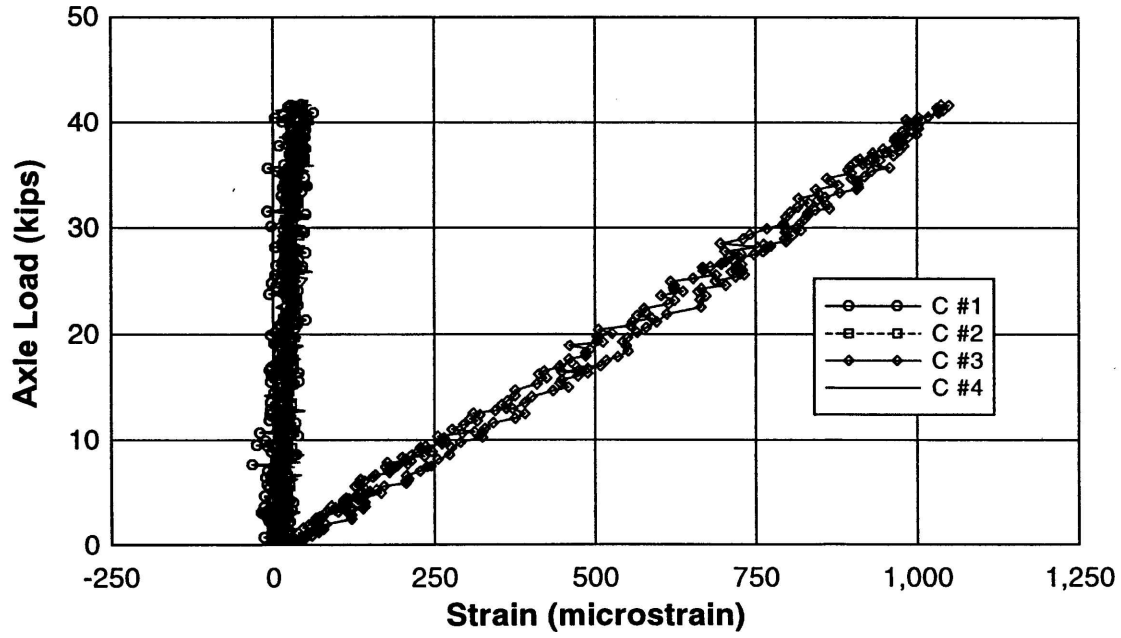


Fig. 29b – Relative concrete strain measurements after 250,000 fatigue cycles. Gages are located in the negative moment region and measure tension. C2 measures crack width (maximum width = 0.004 in., based on 4 in. gage length).

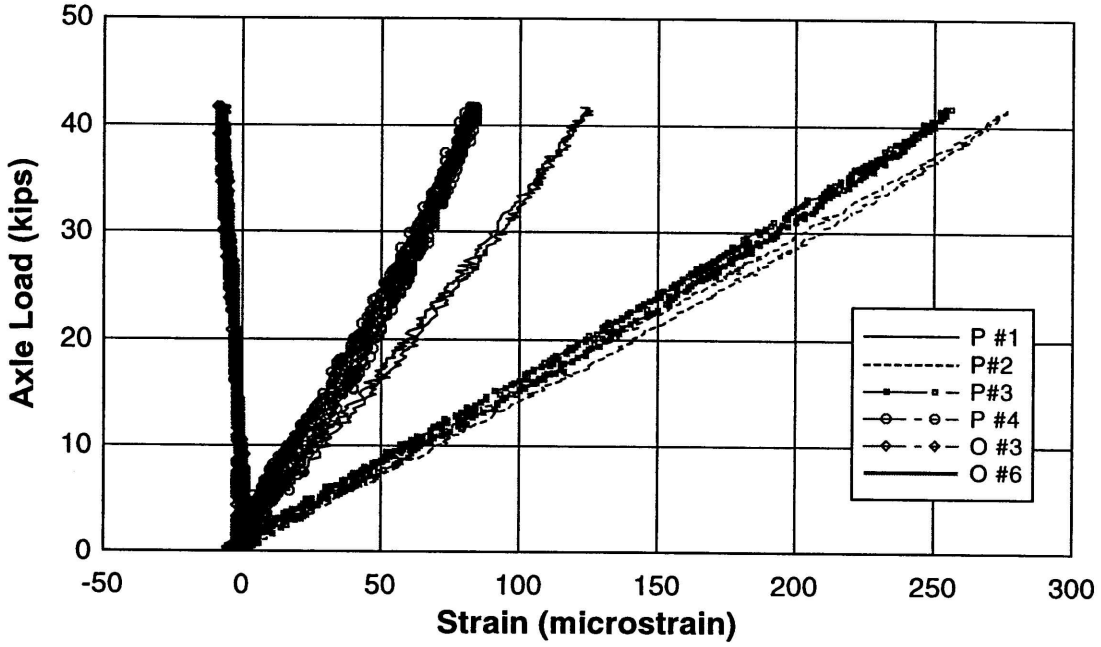


Fig. 29c - Relative #5 reinforcing bar strain measurements after 250,000 fatigue cycles.

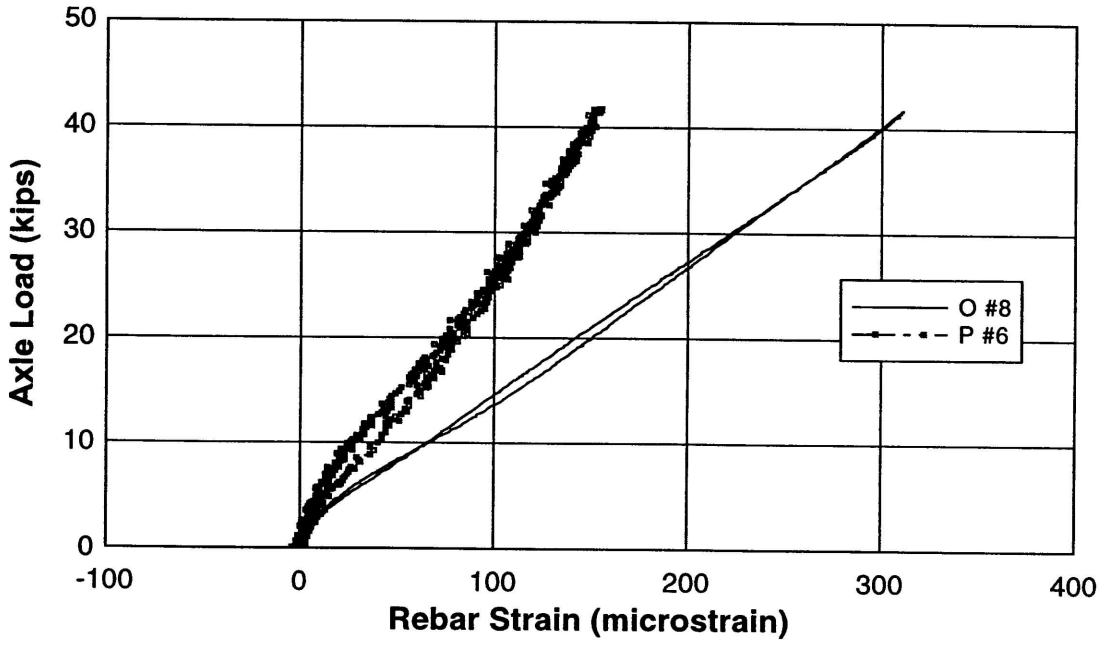


Fig. 29d – Relative #3 reinforcing bar strain measurements under load patch after 250,000 fatigue cycles.

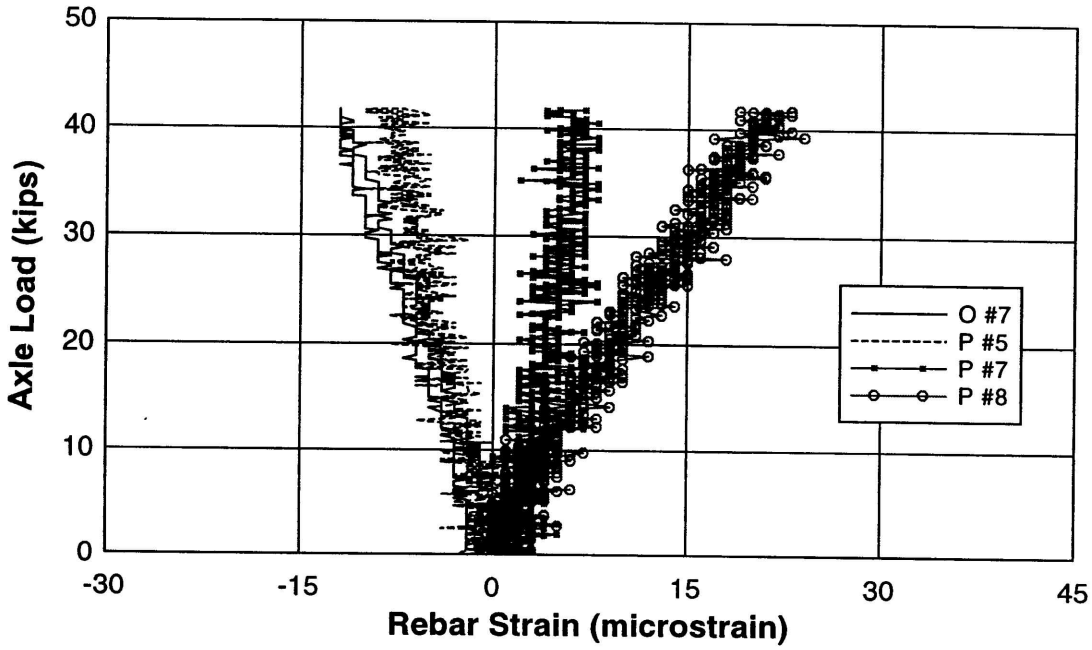


Fig. 29e – All other #3 reinforcing bar relative strain measurements after 250,000 fatigue cycles.

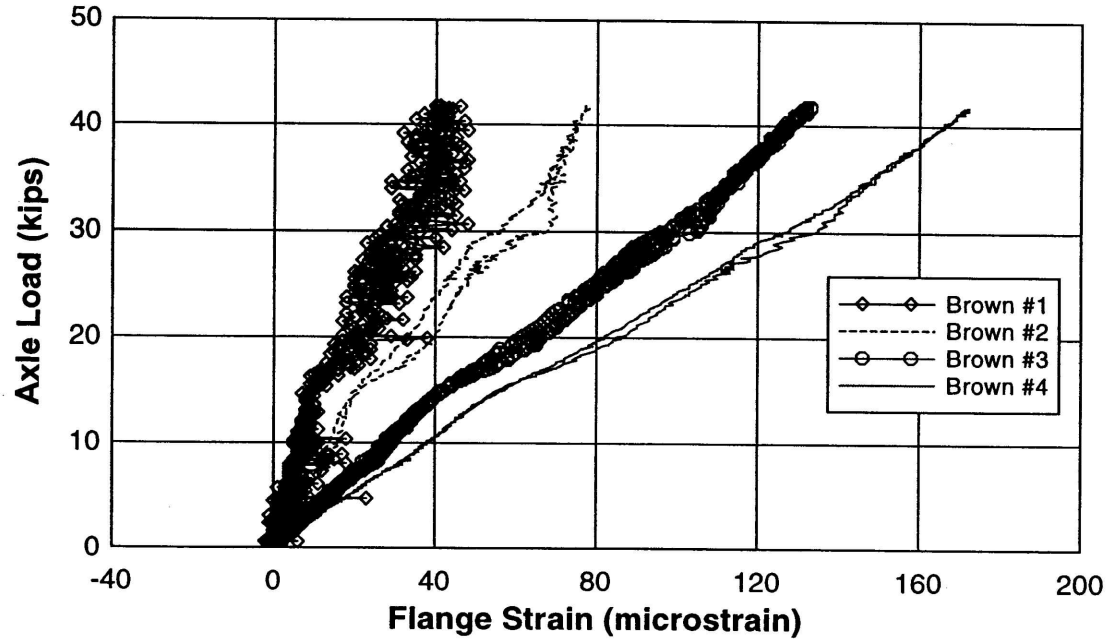


Fig. 29f – Relative north span flange strain in main bars #1, #3, #5 and #6 after 250,000 fatigue cycles.

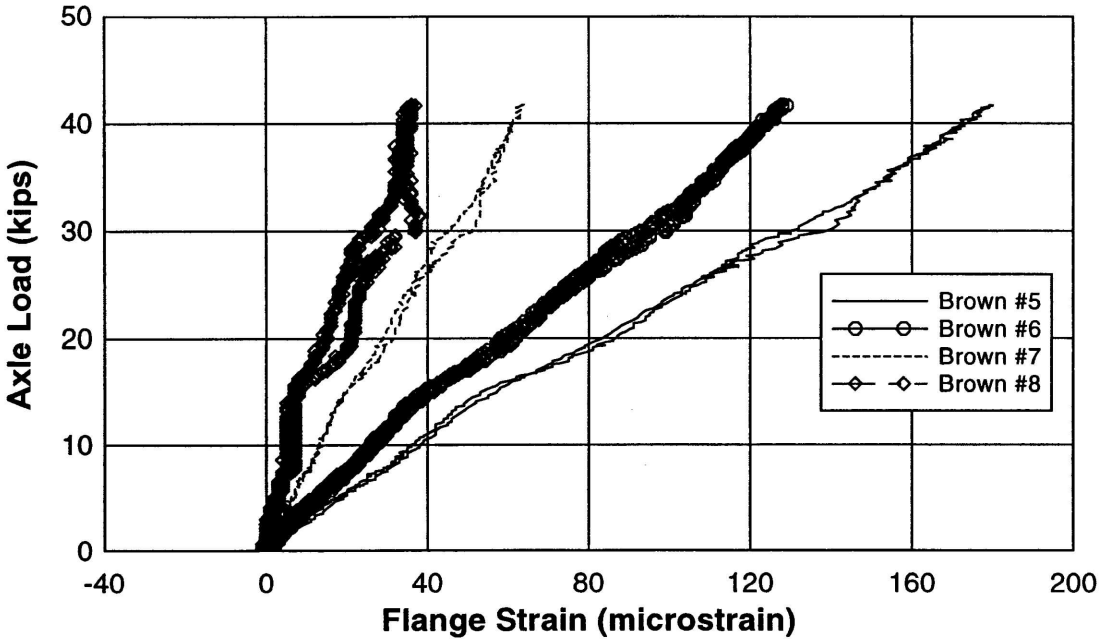


Fig. 29g – Relative north span flange strain in main bars #7, #8, #10 and #12 after 250,000 fatigue cycles.

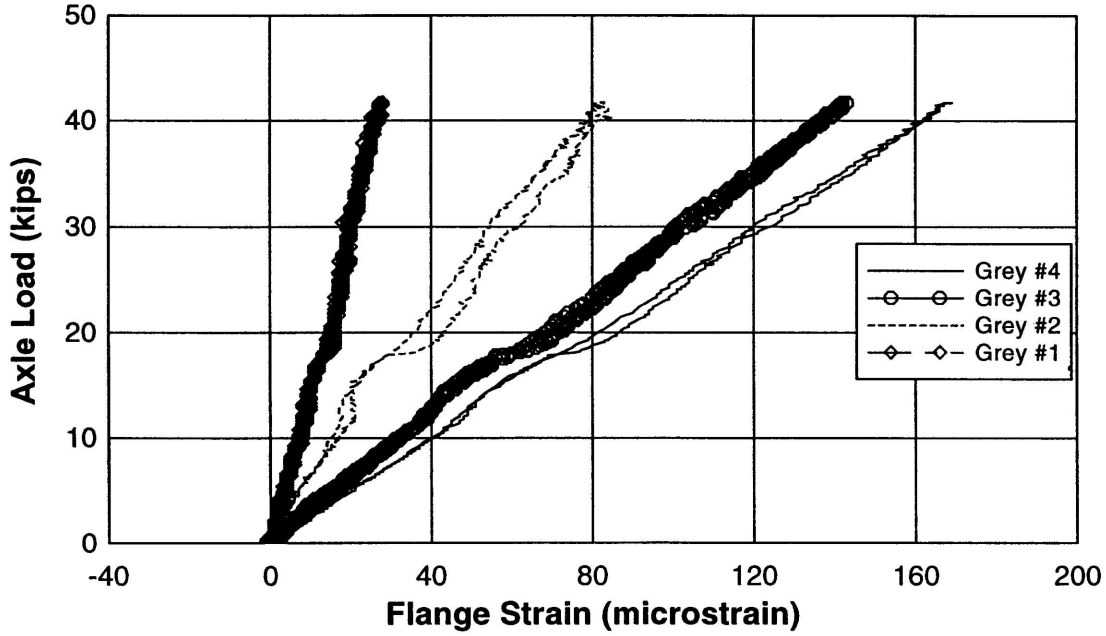


Fig. 29h – Relative south span flange strain in main bars #1, #3, #5 and #6 after 250,000 fatigue cycles.

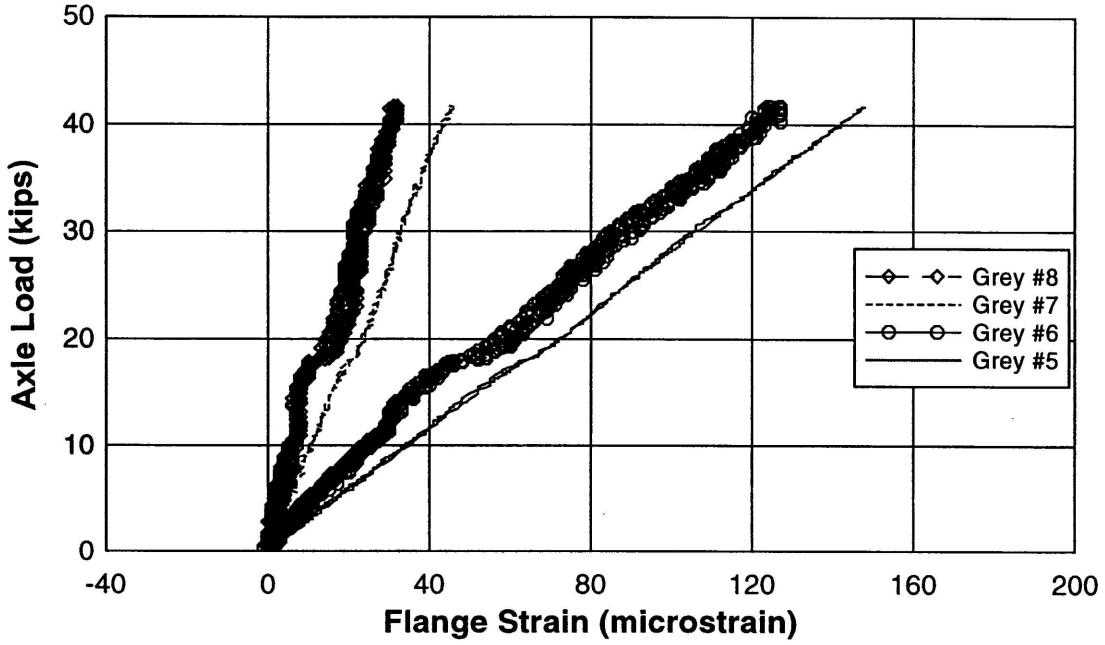


Fig. 29i – Relative south span flange strain in main bars #7, #8, #10 and #12 after 250,000 fatigue cycles

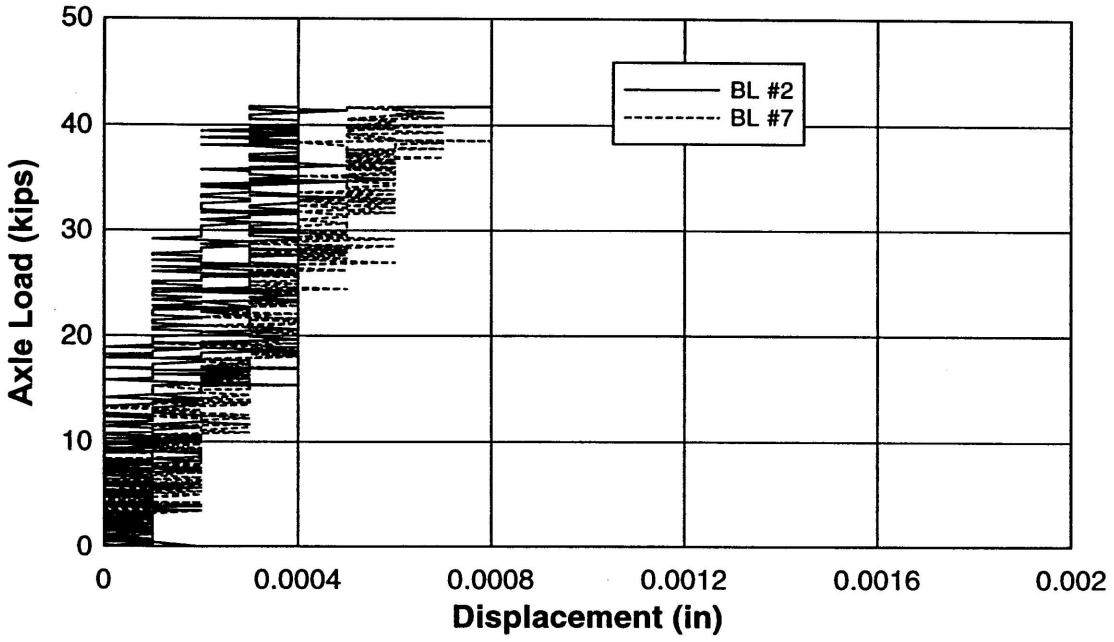


Fig. 29j – Relative displacement between steel grid and concrete slab after 250,000 fatigue cycles.

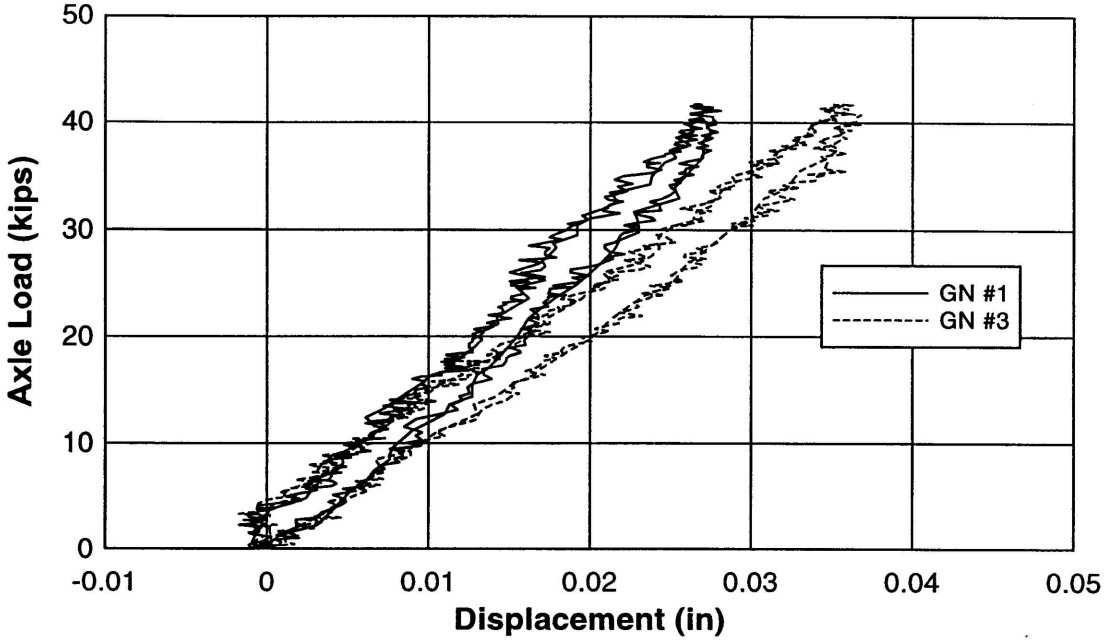


Fig. 30a - Relative displacement response after 2 million fatigue cycles.

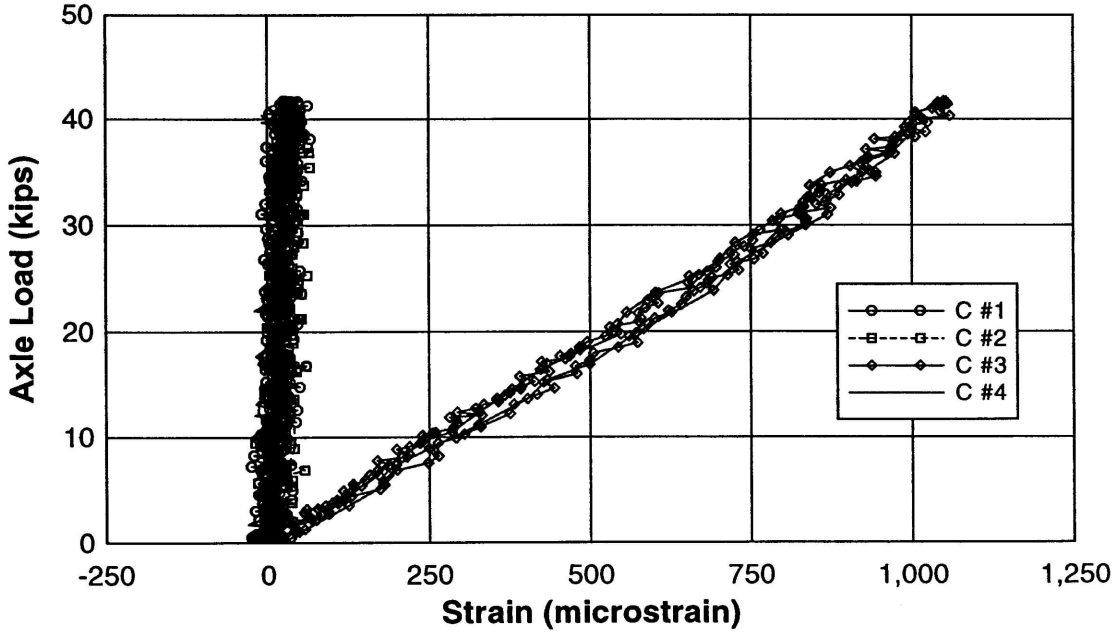


Fig. 30b – Relative concrete strain measurements after 2 million fatigue cycles.

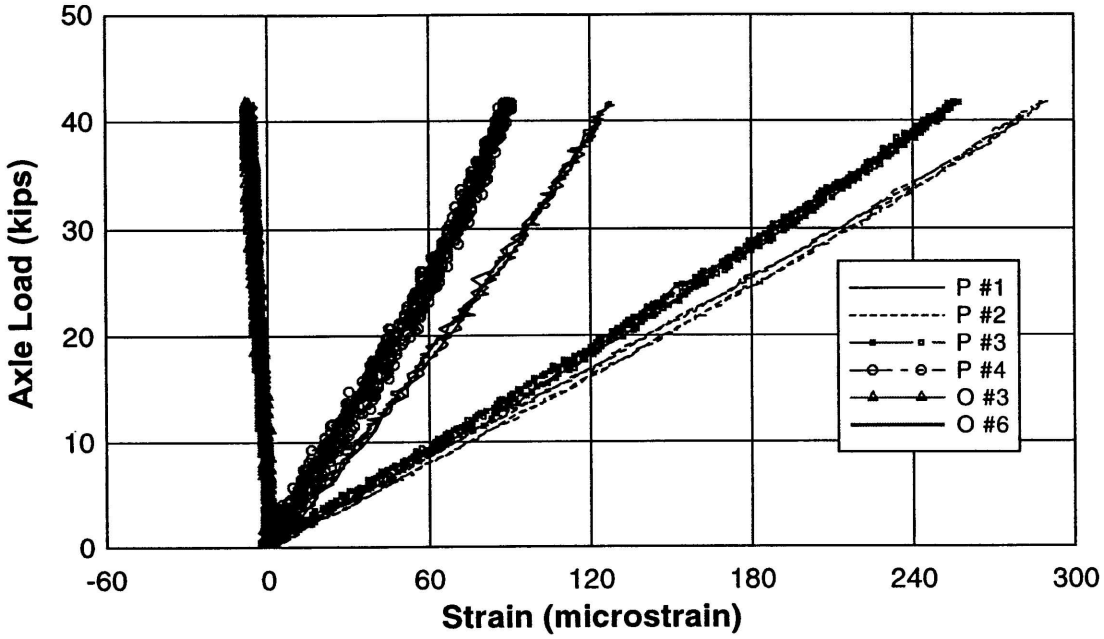


Fig. 30c - Relative #5 reinforcing bar strain measurements after 2 million fatigue cycles.

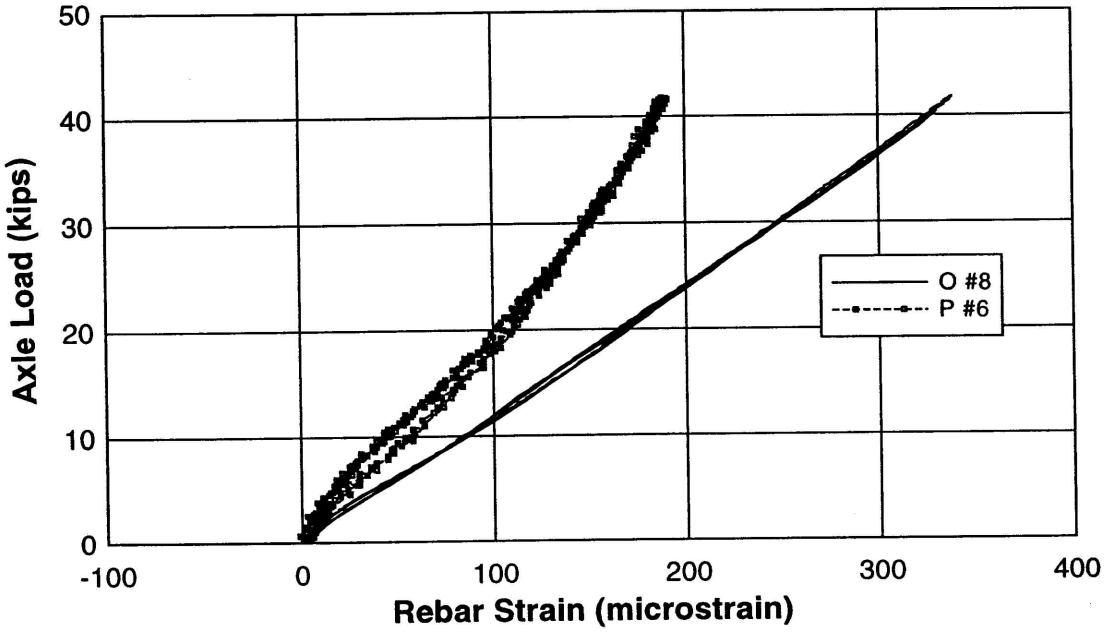


Fig. 30d – Relative #3 reinforcing bar strain measurements under load patch after 2 million fatigue cycles.

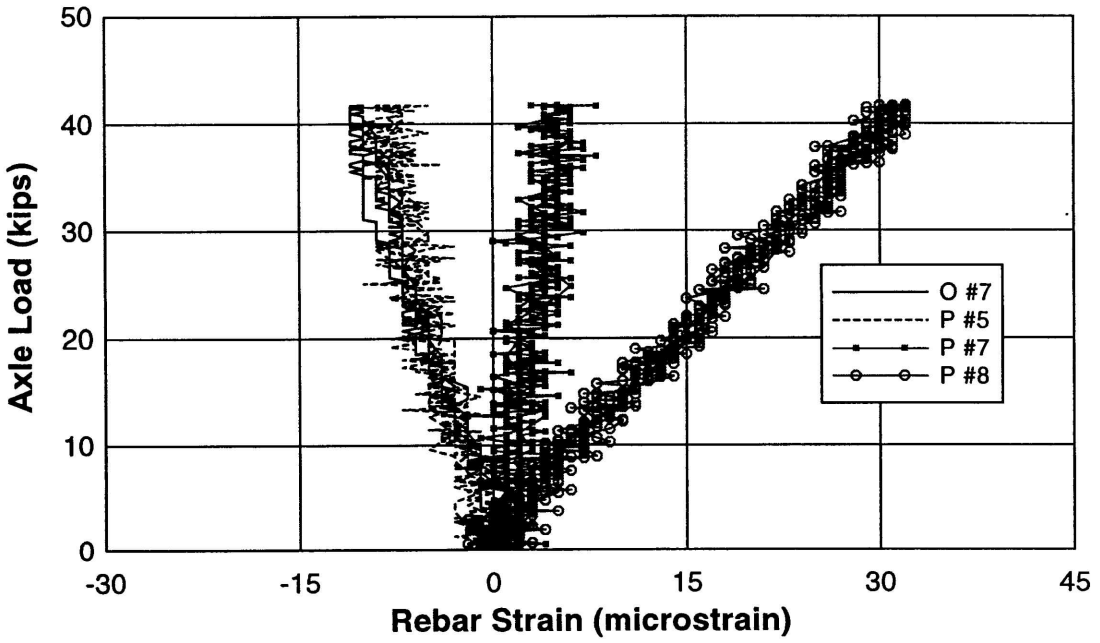


Fig. 30e – All other #3 reinforcing bar relative strain measurements after 2 million fatigue cycles.

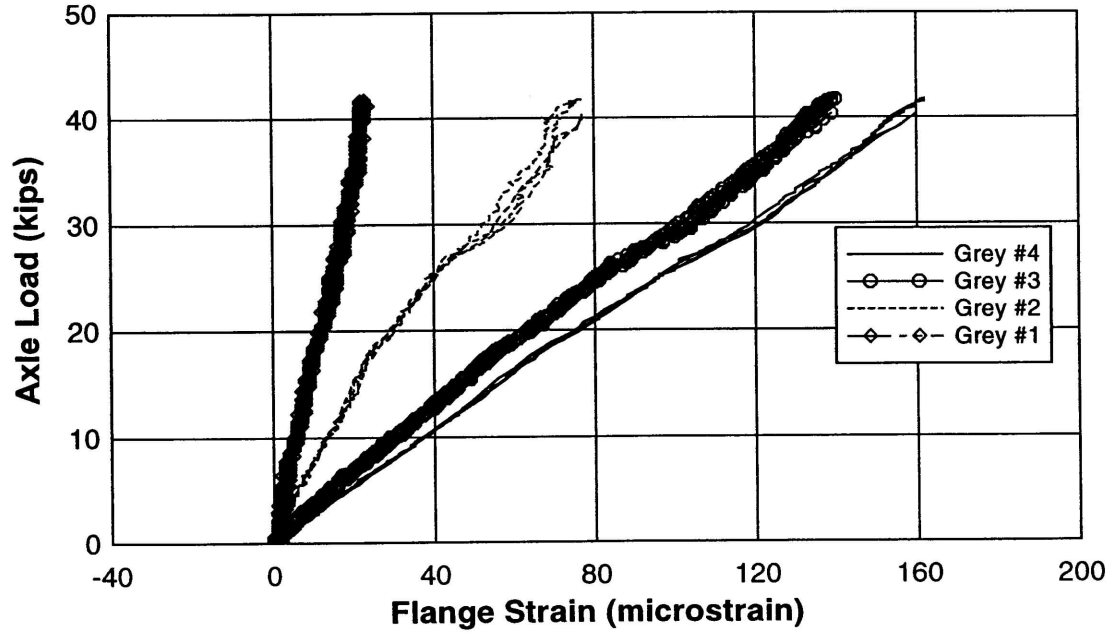


Fig. 30f – Relative north span flange strain in main bars #1, #3, #5 and #6 after 2 million fatigue cycles.

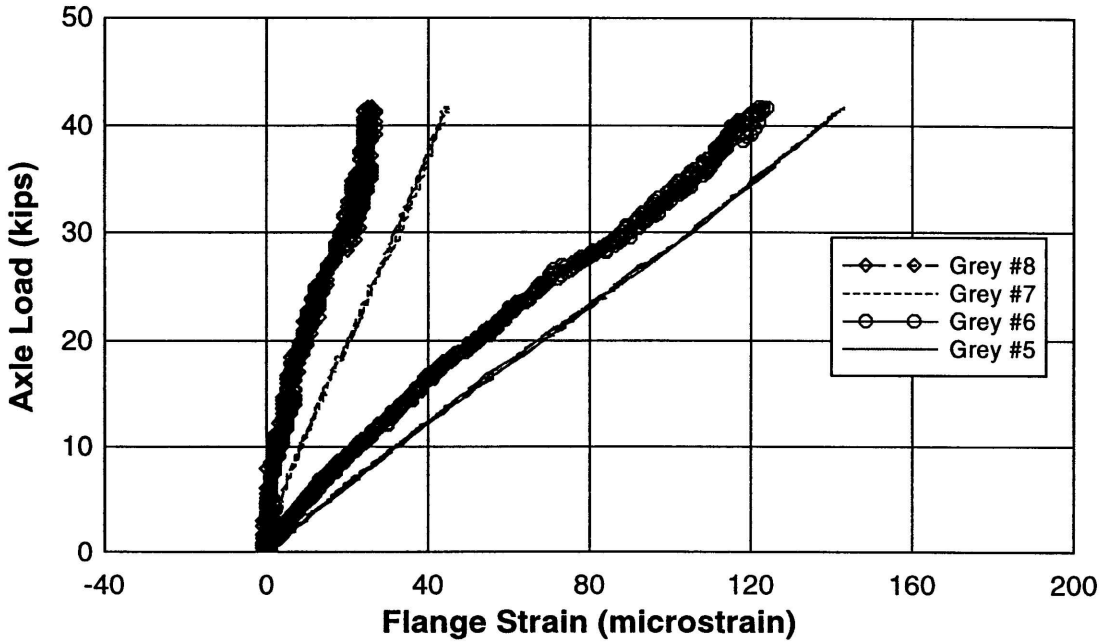


Fig. 30g – Relative north span flange strain in main bars #7, #8, #10 and #12 after 2 million fatigue cycles.

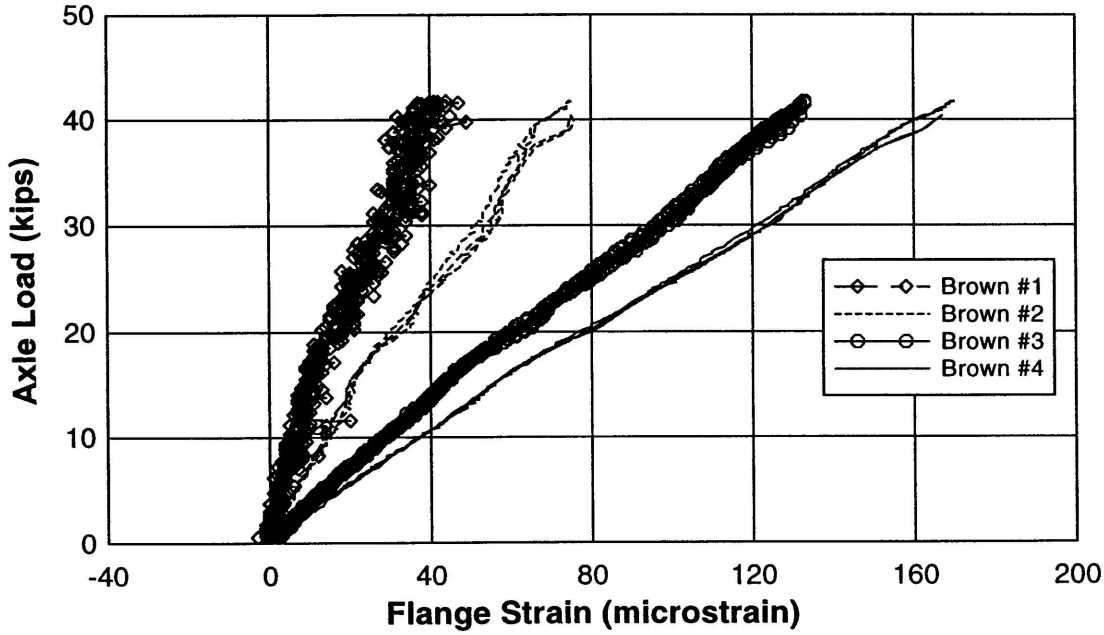


Fig. 30h – Relative south span flange strain in main bars #1, #3, #5 and #6 after 2 million fatigue cycles.

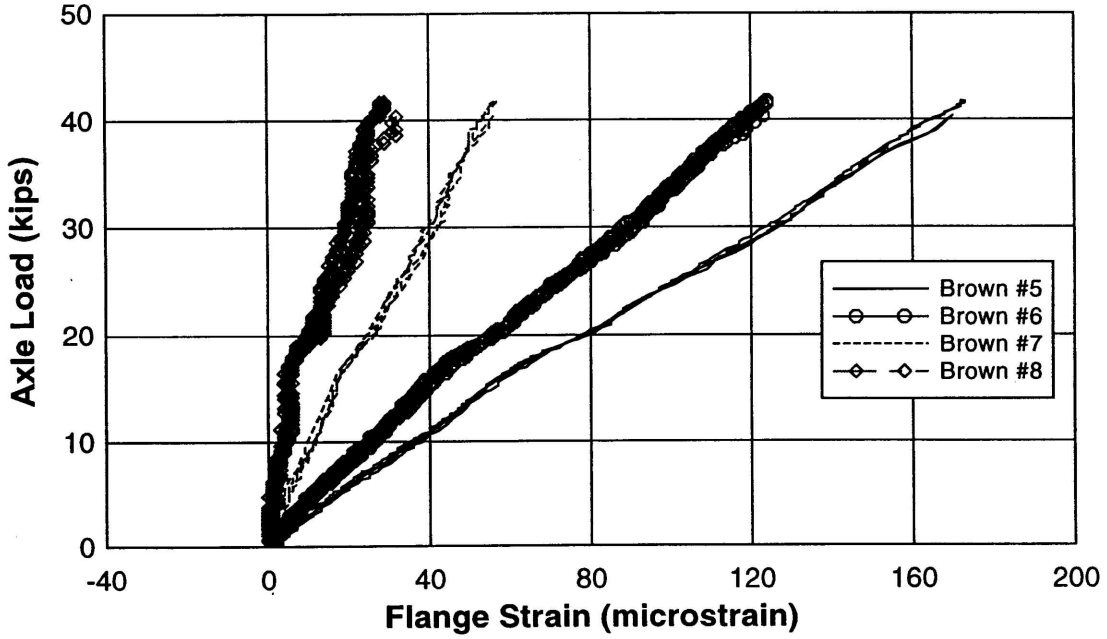


Fig. 30i – Relative south span flange strain in main bars #7, #8, #10 and #12 after 2 million fatigue cycles.

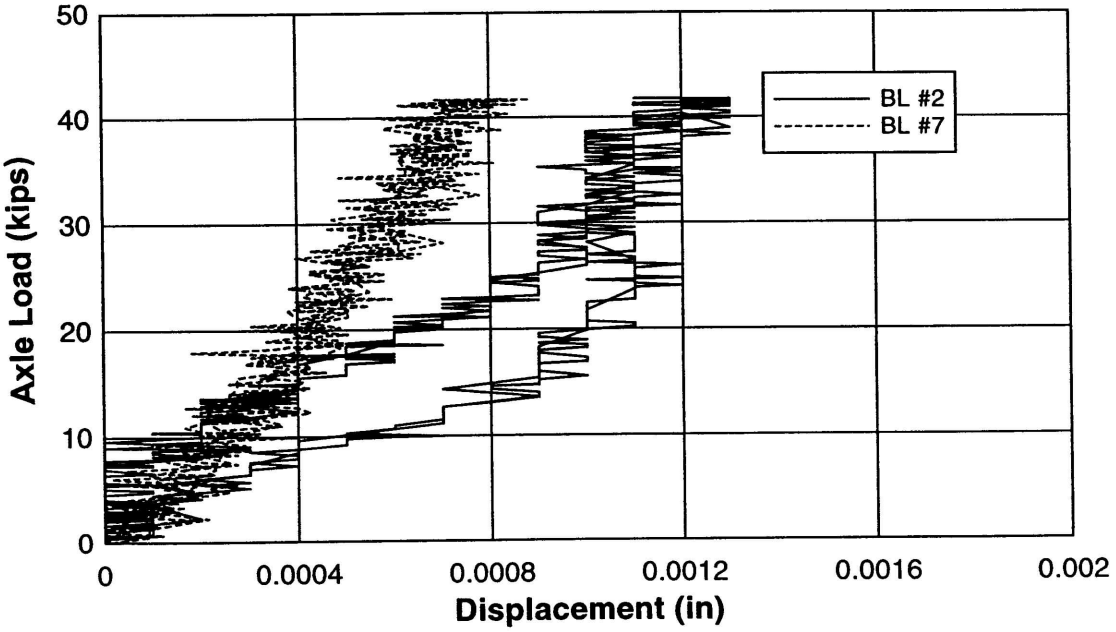


Fig. 30j – Relative displacement between steel grid and concrete slab after 250,000 fatigue cycles.

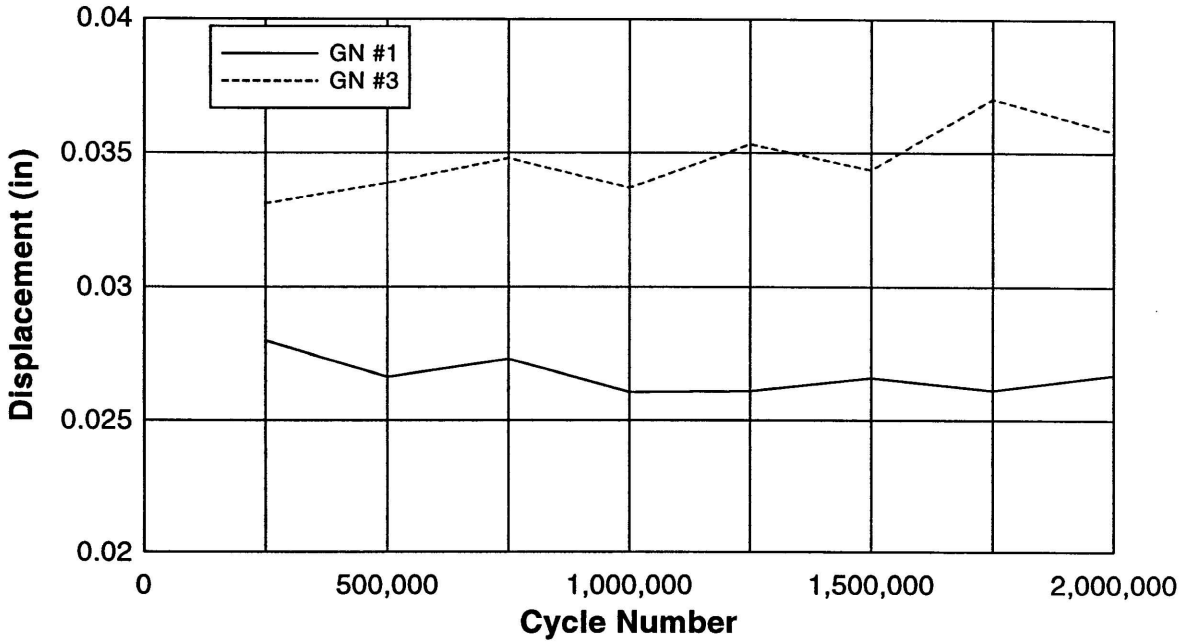


Fig. 31a – Midspan displacement at 41.6 kips at each static test interval during fatigue test.

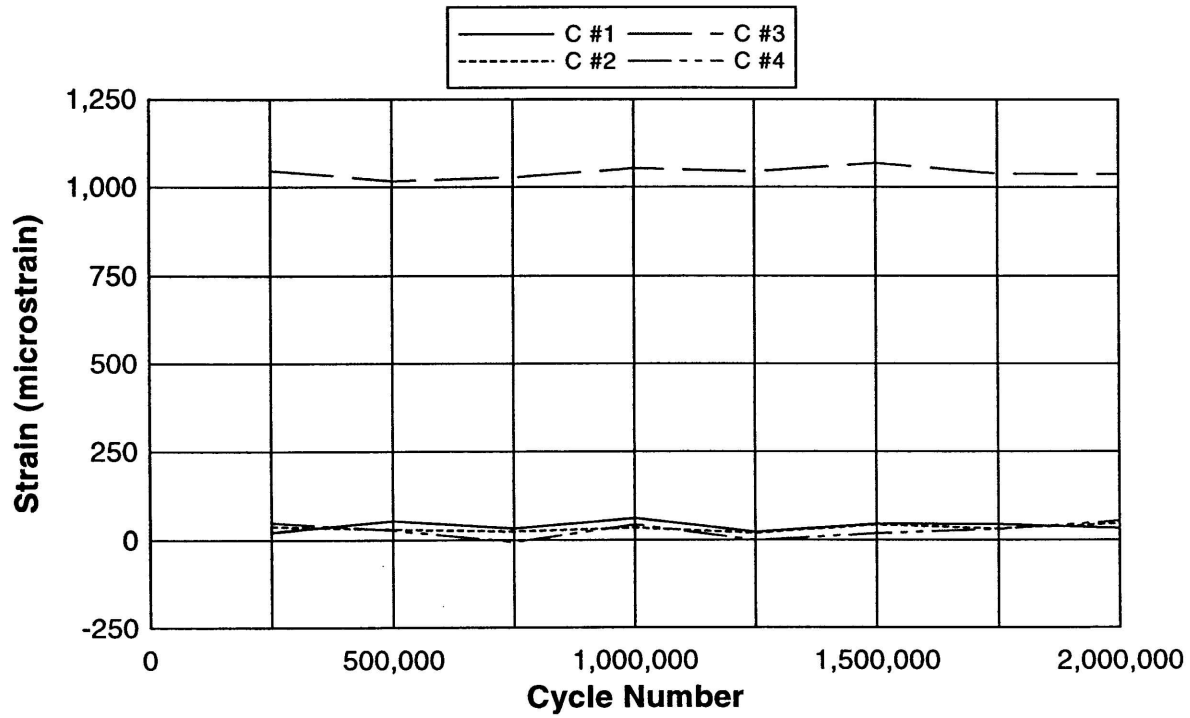


Fig. 31b – Concrete strain measurements at 41.6 kips at each static test interval during fatigue test.

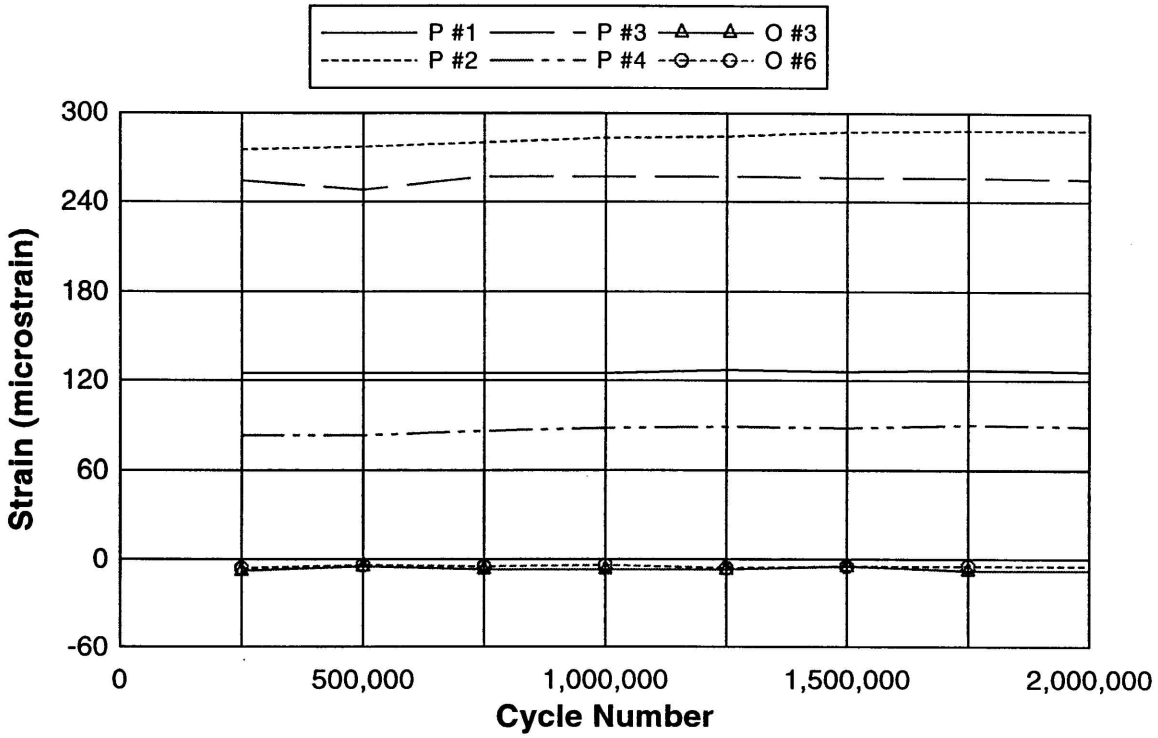


Fig. 31c – #5 reinforcing bar strain measurements at 41.6 kips at each static test interval during fatigue test.

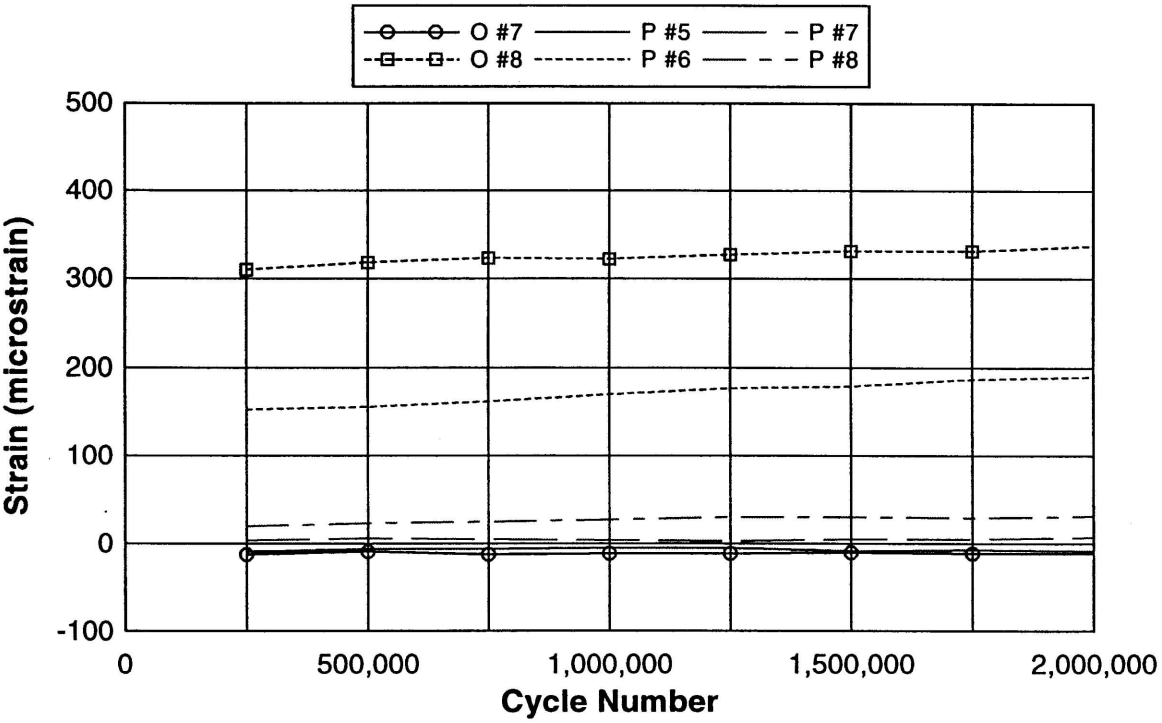


Fig. 31d – #3 reinforcing bar strain measurements at 41.6 kips at each static test interval during fatigue test.

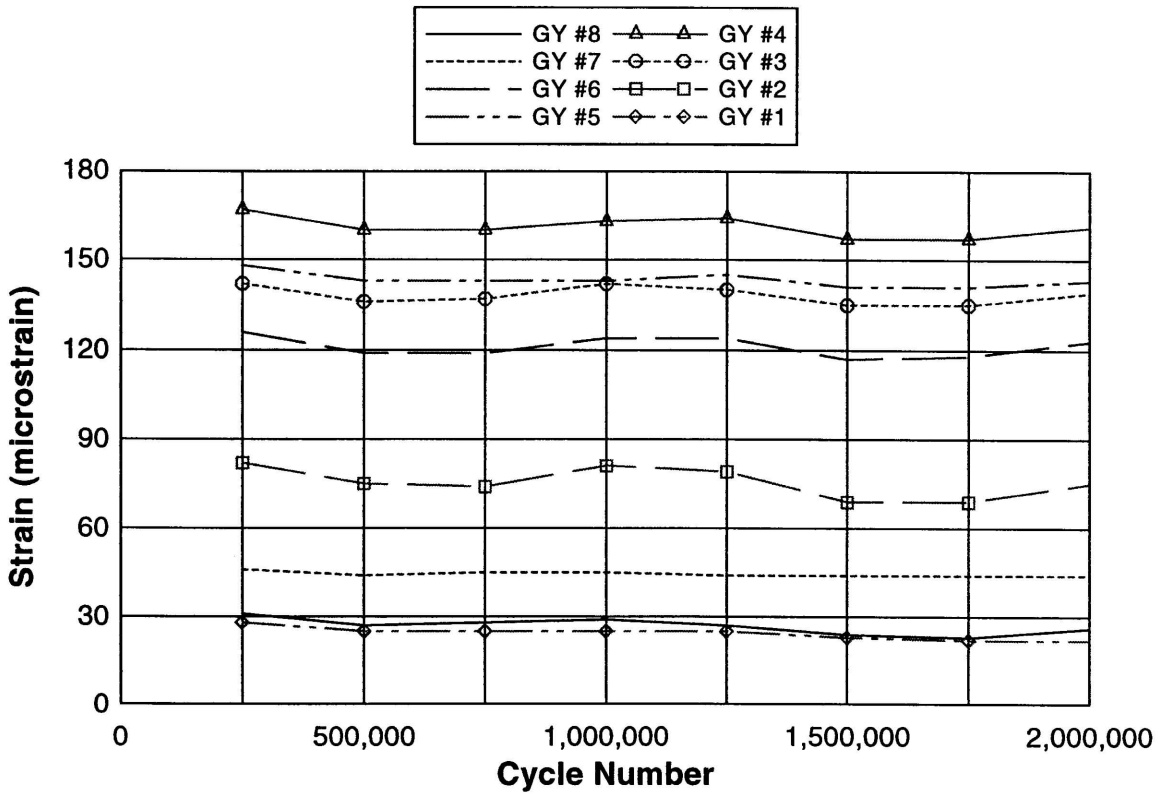


Fig. 31e – North span flange strain in main bars at 41.6 kips at each static test interval during fatigue test.

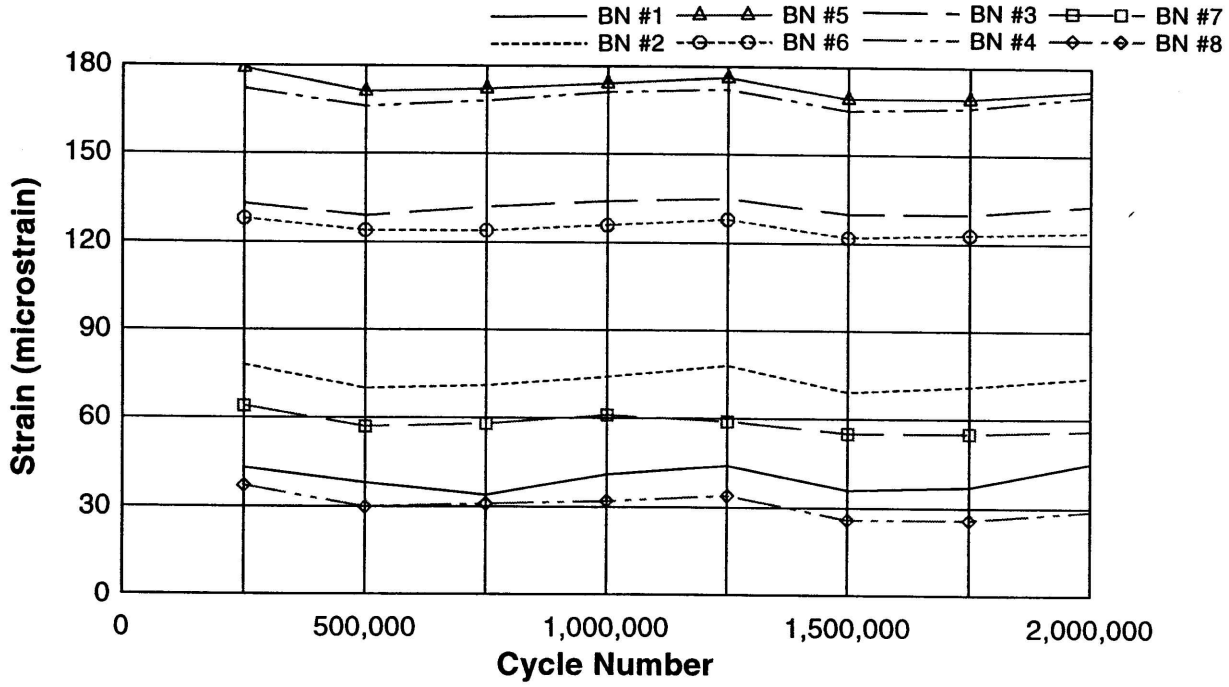


Fig. 31f – South span flange strain in main bars at 41.6 kips at each static test interval during fatigue test.

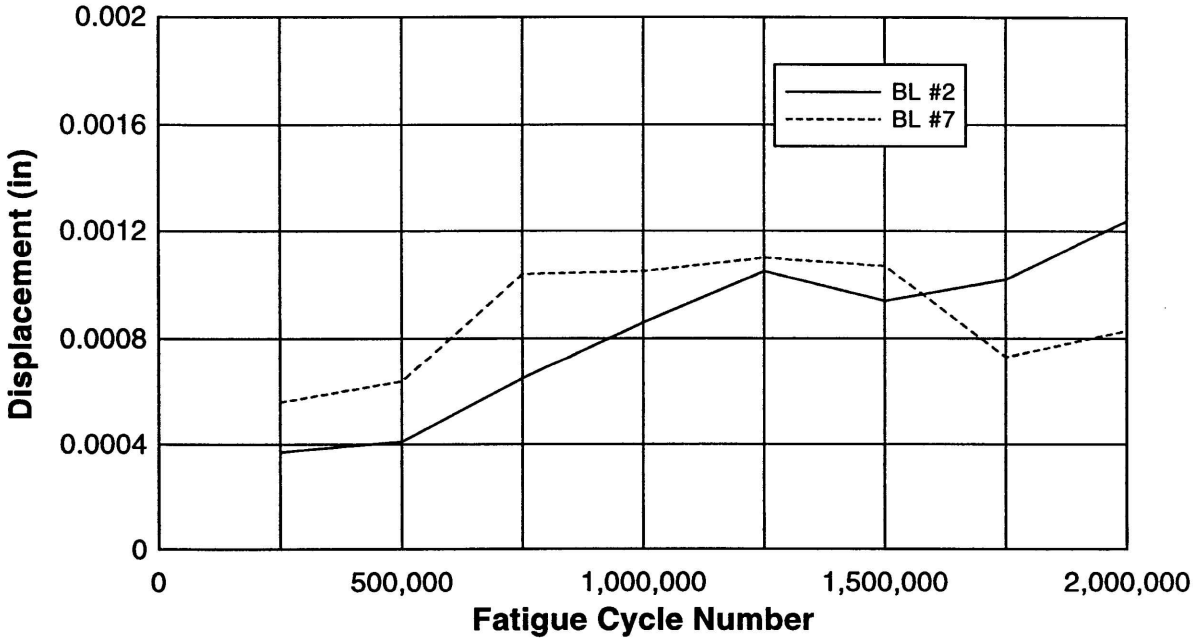


Fig. 31g – Relative displacement between steel grid and concrete slab at 41.6 kips at each static test interval during fatigue test.

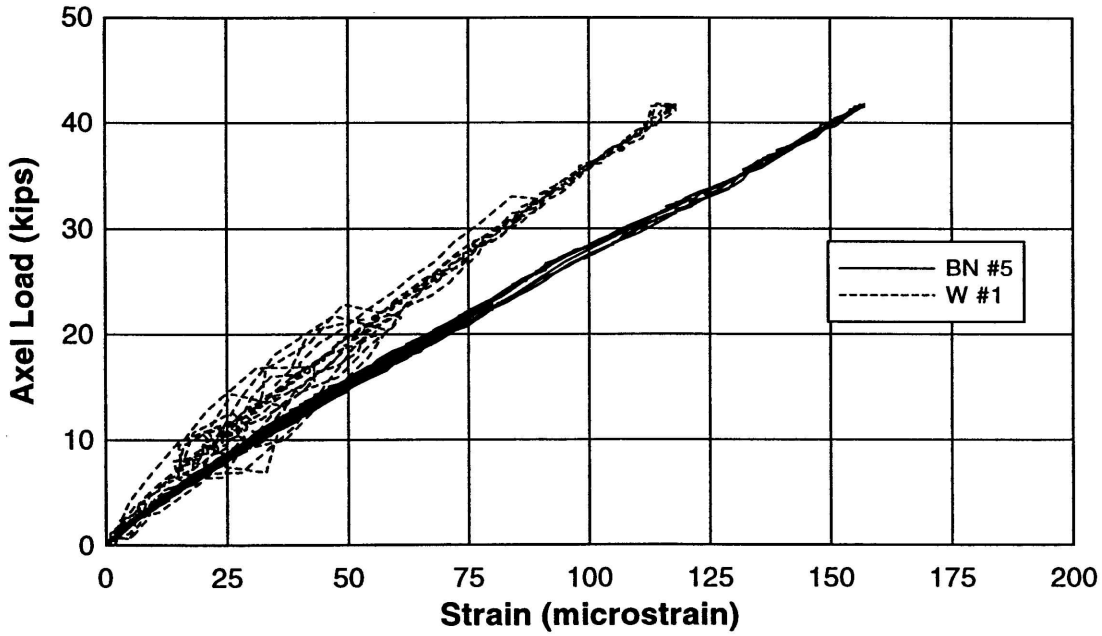


Fig. 32 – Typical main bar web and flange strains.

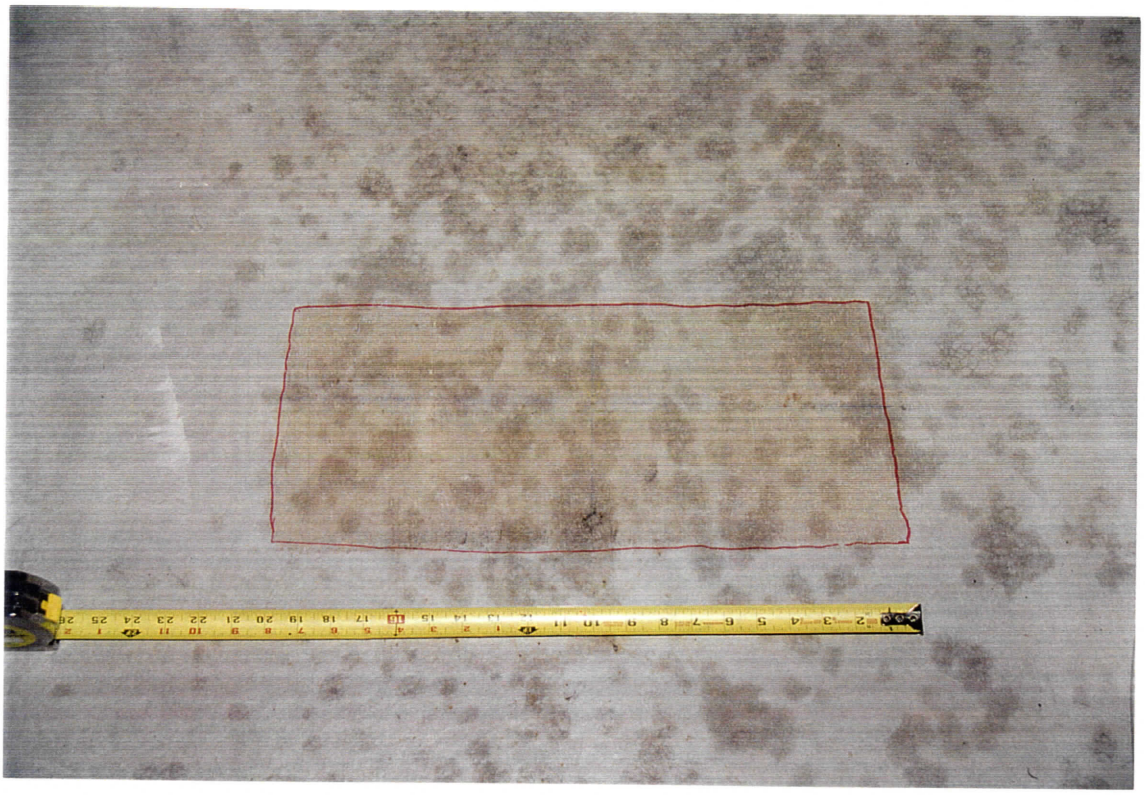

Fig. 33 - Markings on concrete slab under south span load patch.

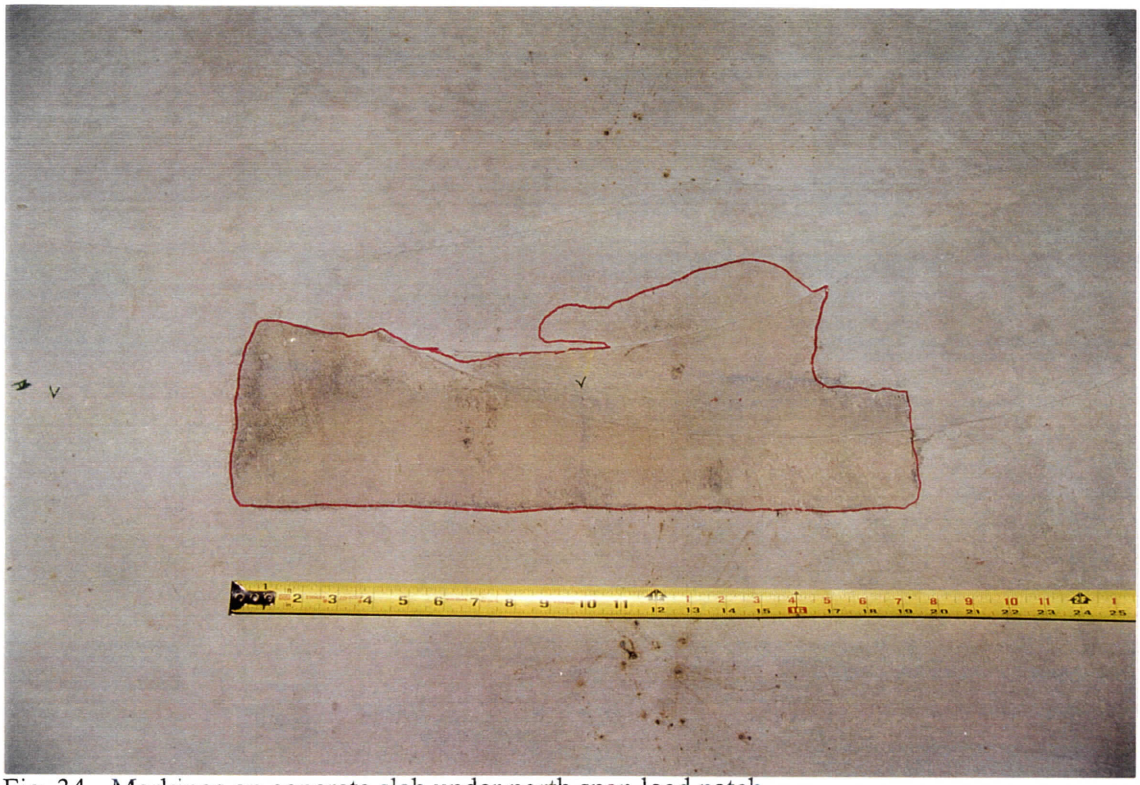

Fig. 34 - Markings on concrete slab under north span load patch.

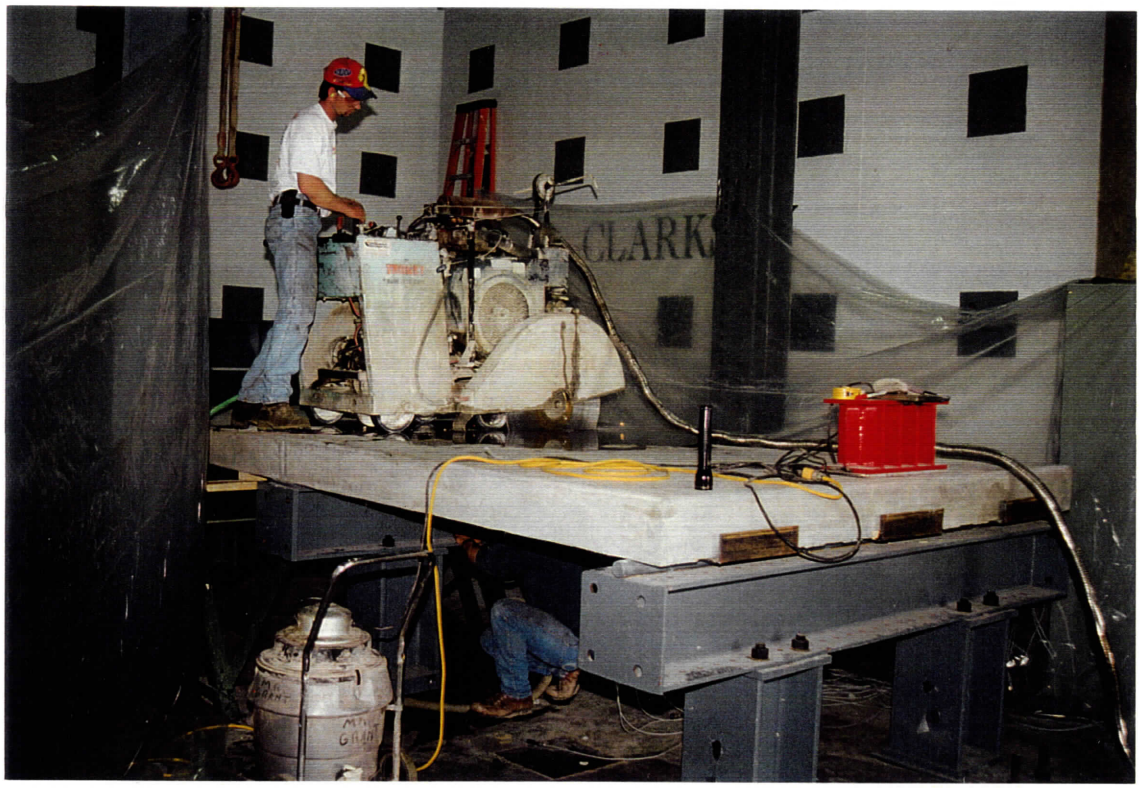

Fig. 35 – Contractor cutting north span of deck after fatigue tests.

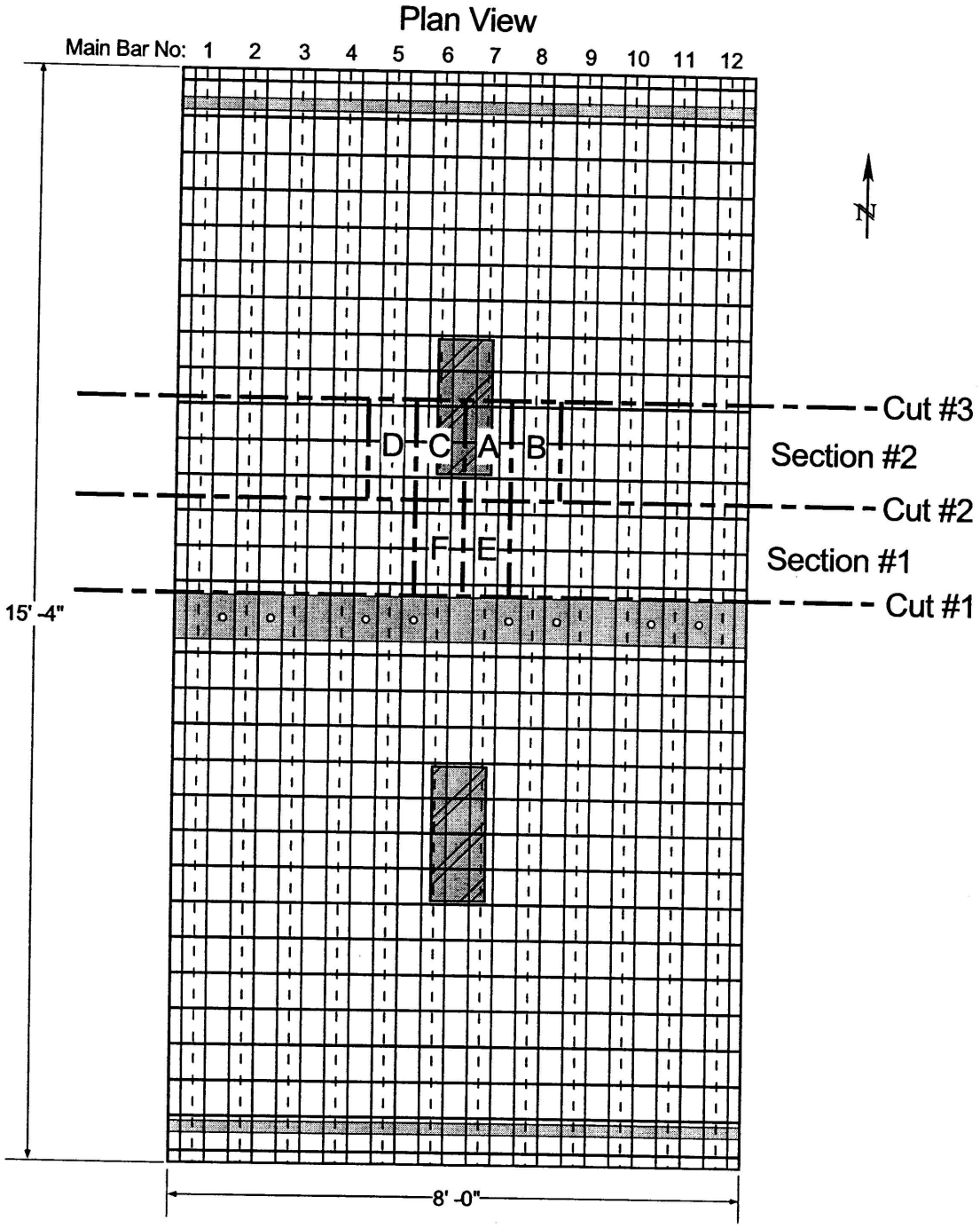


Fig. 36 - Plan view of cuts made on north span of deck.

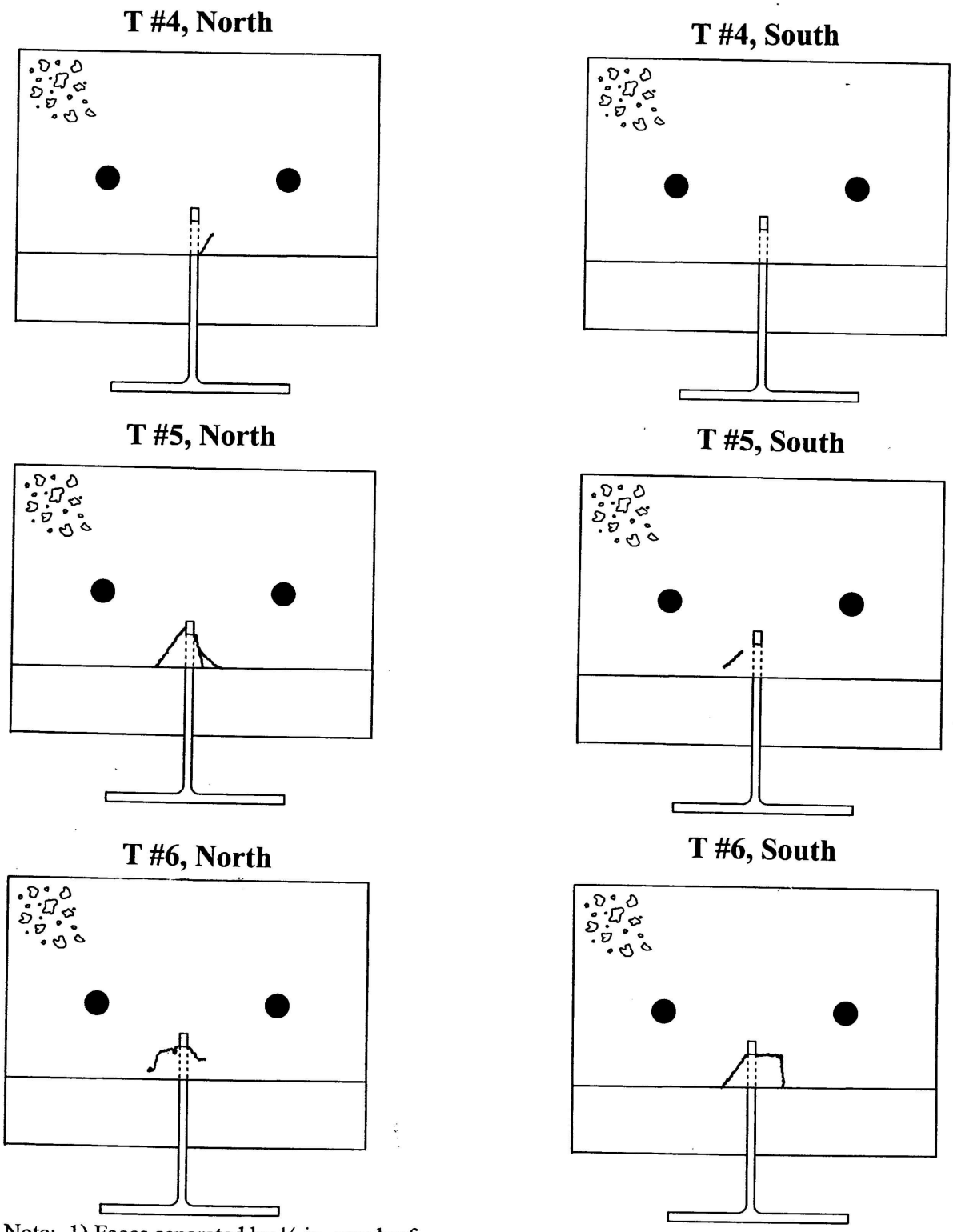


Note: 1) Faces separated by ¼ in. saw kerf.
2) Crack widths are hairline
3) No cracks seen at other cuts

Fig. 37a – Cracks observed near shear holes along cut #3.

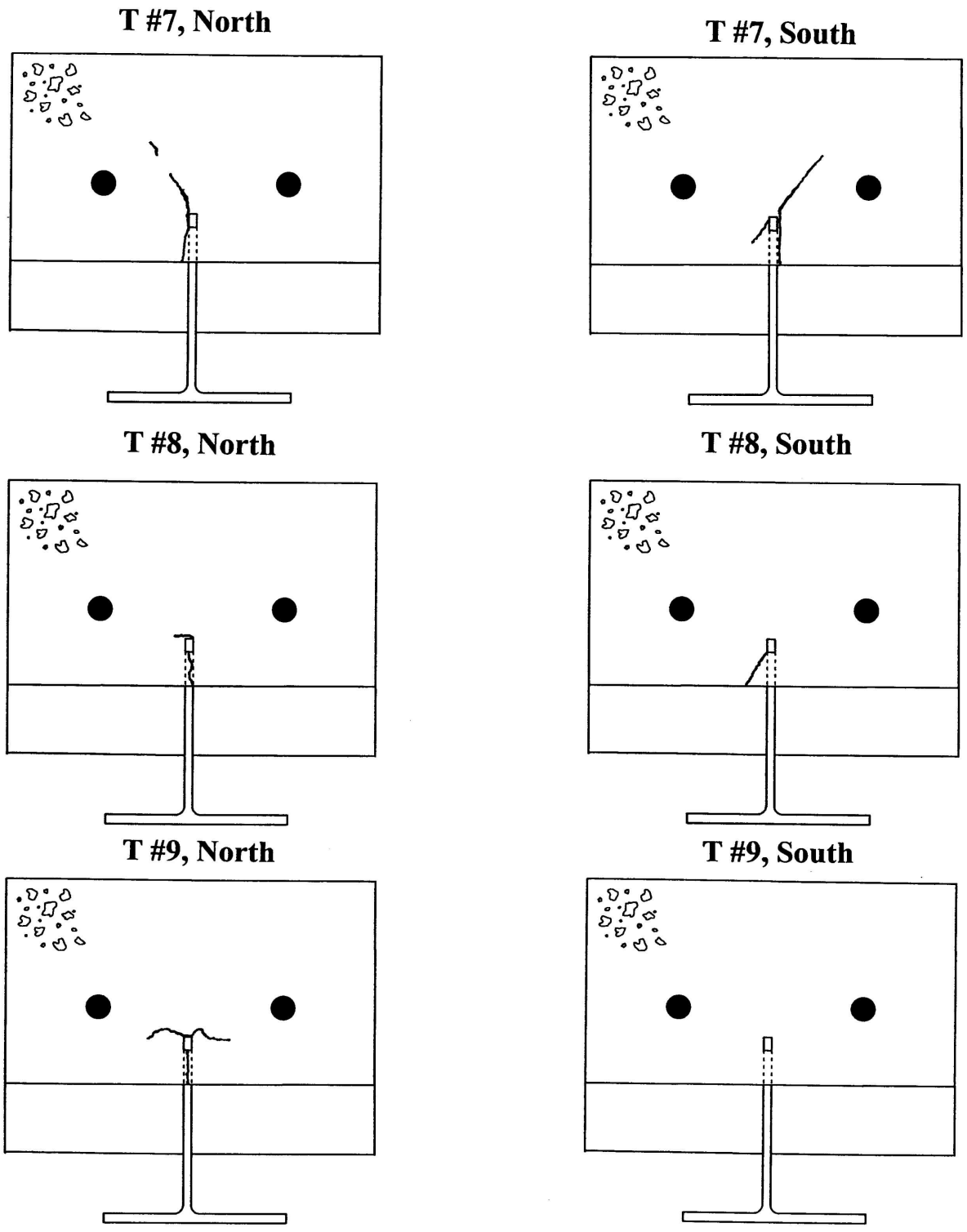


Note: 1) Faces separated by ¼ in. saw kerf.
2) Crack widths are hairline
3) No cracks seen at other cuts

Fig. 37b – Cracks observed near shear holes along cut #3.

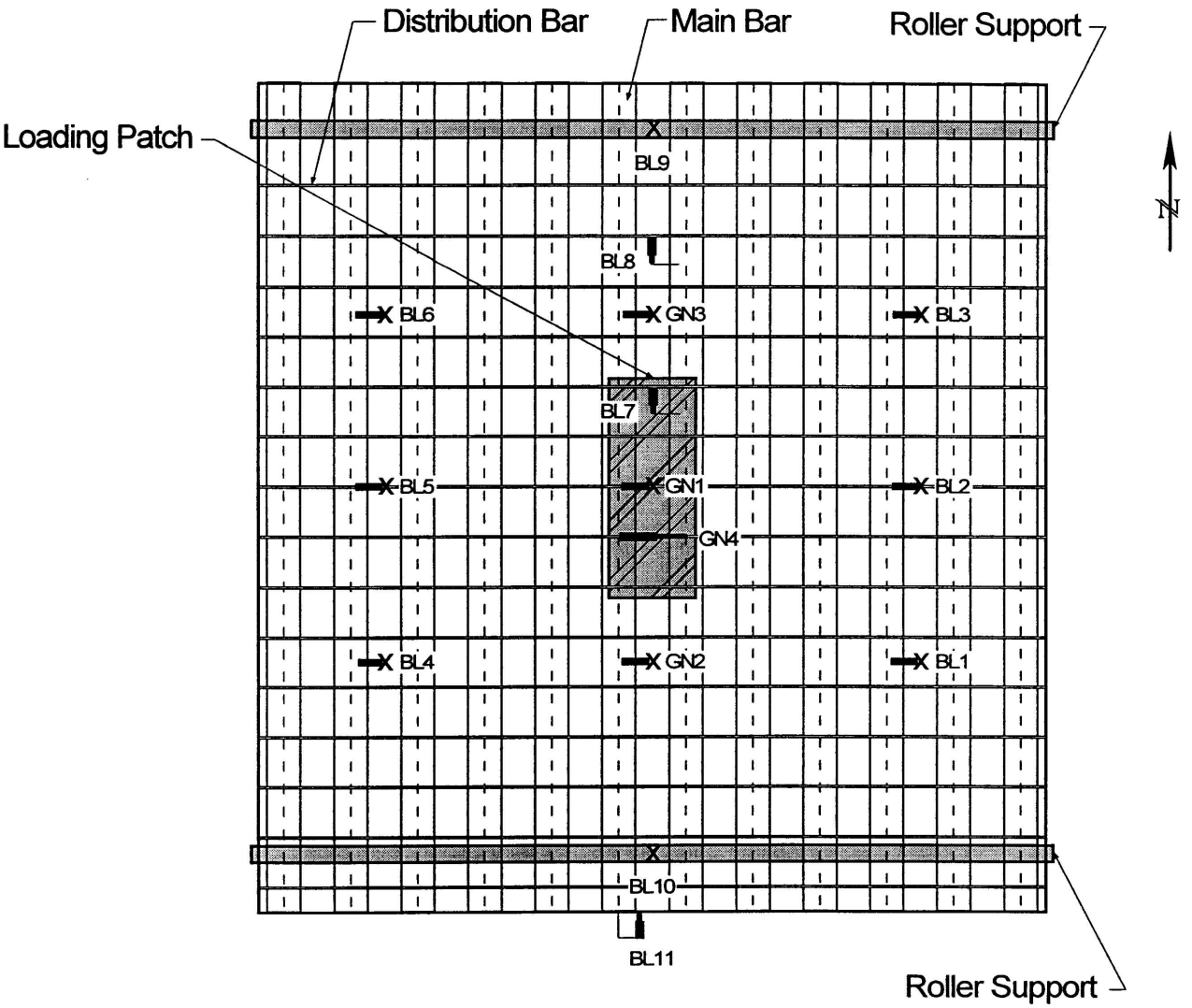


Legend

- Displacement transducer. Rectangle indicates connection to T-section.
- Displacement transducer. Measures deformation of support.
- Displacement transducer. Measures relative deformation between T-section webs.
- Slip gage. Bonded to underside of concrete and measures relative deformation from adjacent T-section flange.

Fig. 38 - Displacement transducer locations for static test of south span.

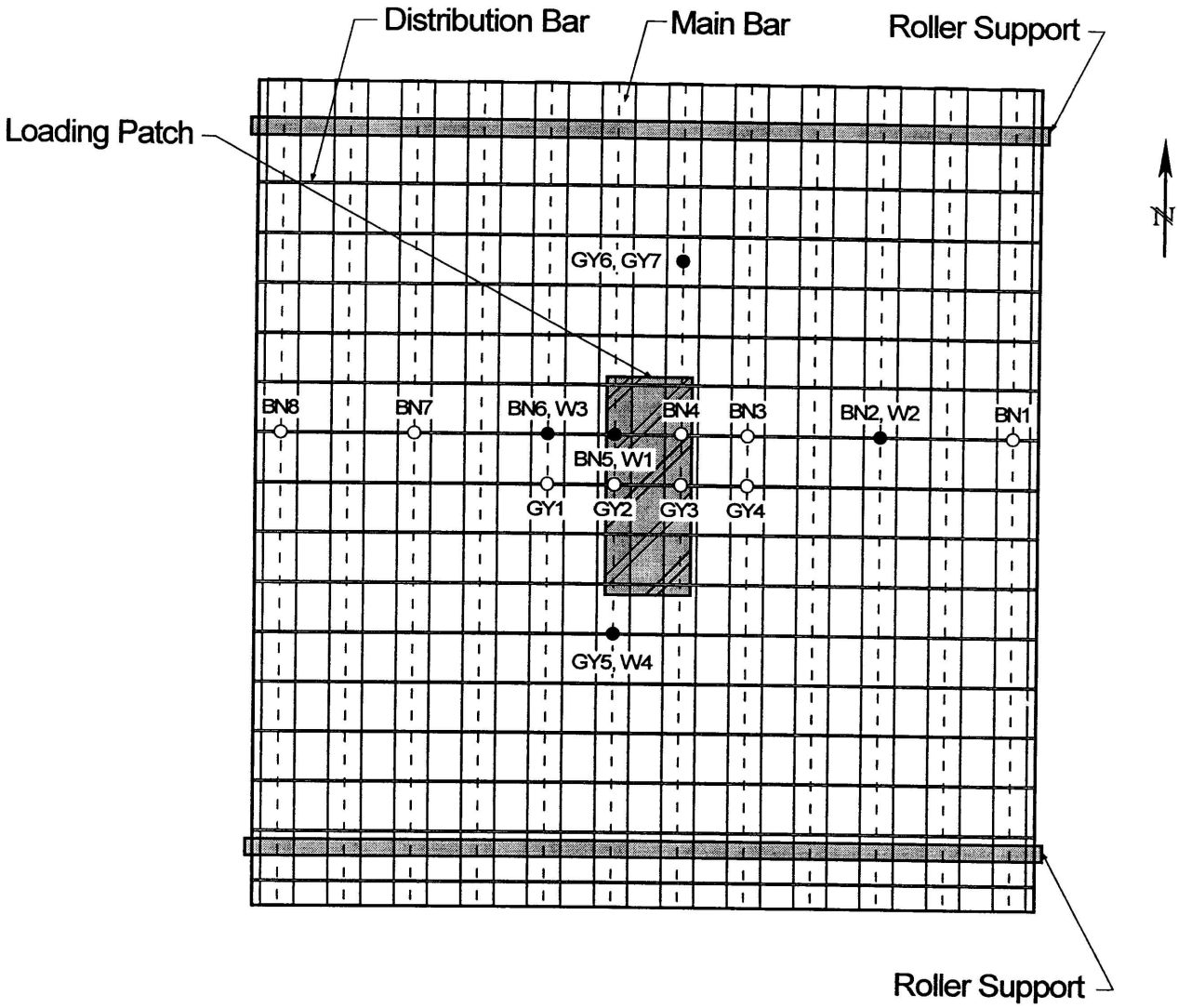


Legend

- Strain gages on T-section flange and web. GY5, 6 and BN2, 5, 6 on flange. W1, 2, 3, 4 and GY7 on web.

- ○ Single strain gage on flange of T-section.

Fig. 39 - Strain gage locations on steel grid for static test of south span.

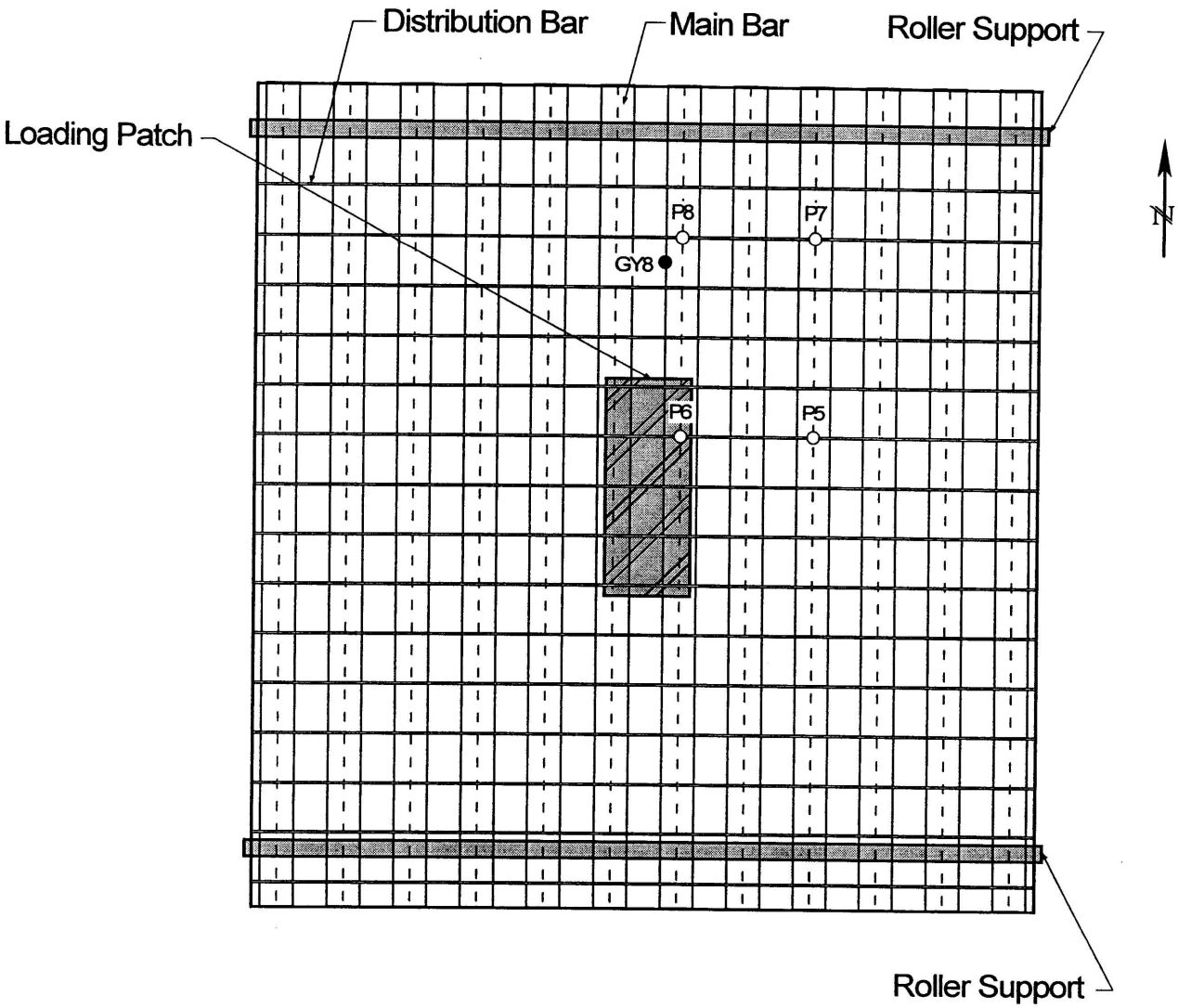


Fig. 40 - Strain gage locations on reinforcing steel for static test of south span.

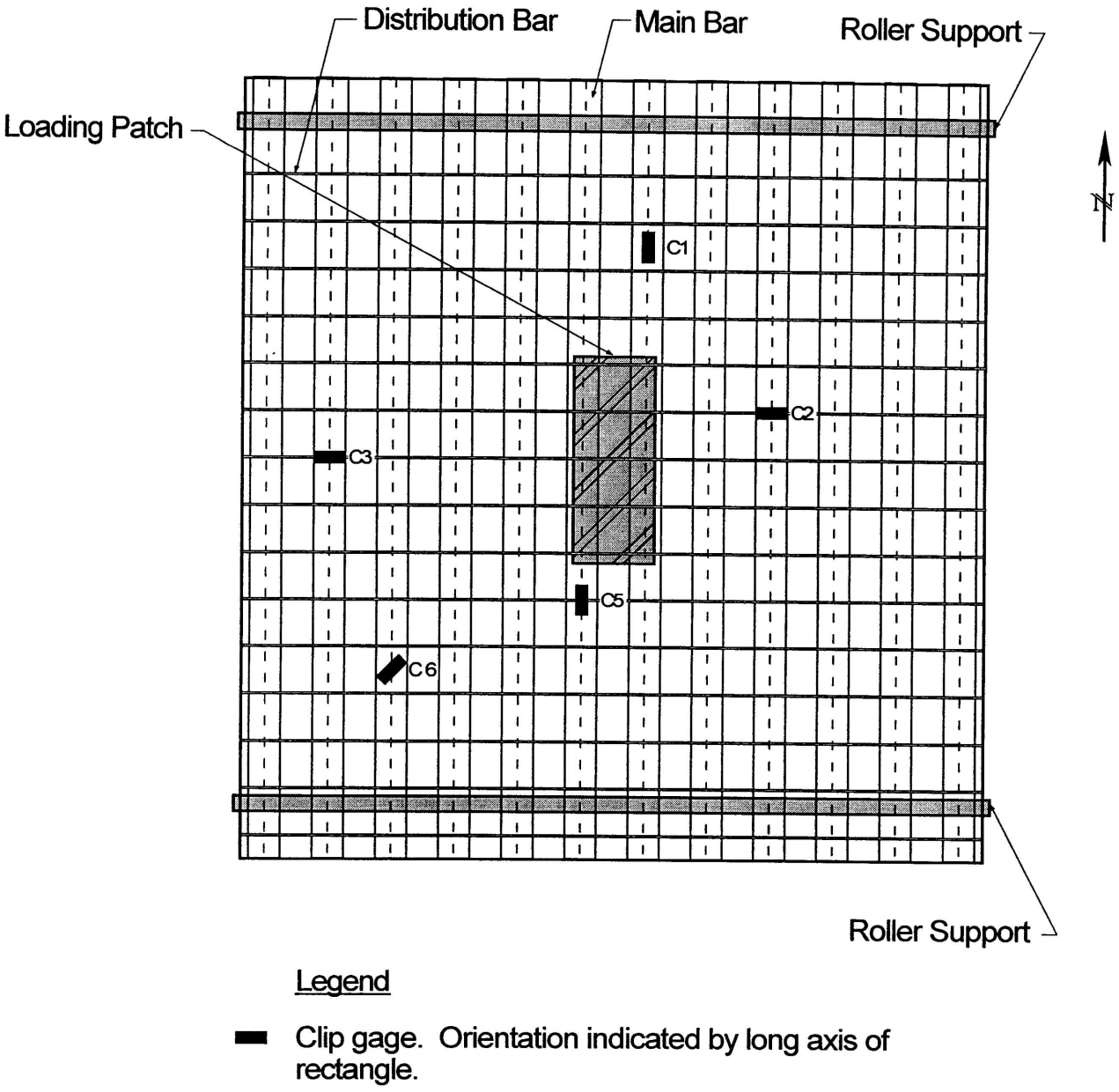


Fig. 41 - Clip gage locations for static test of south span.

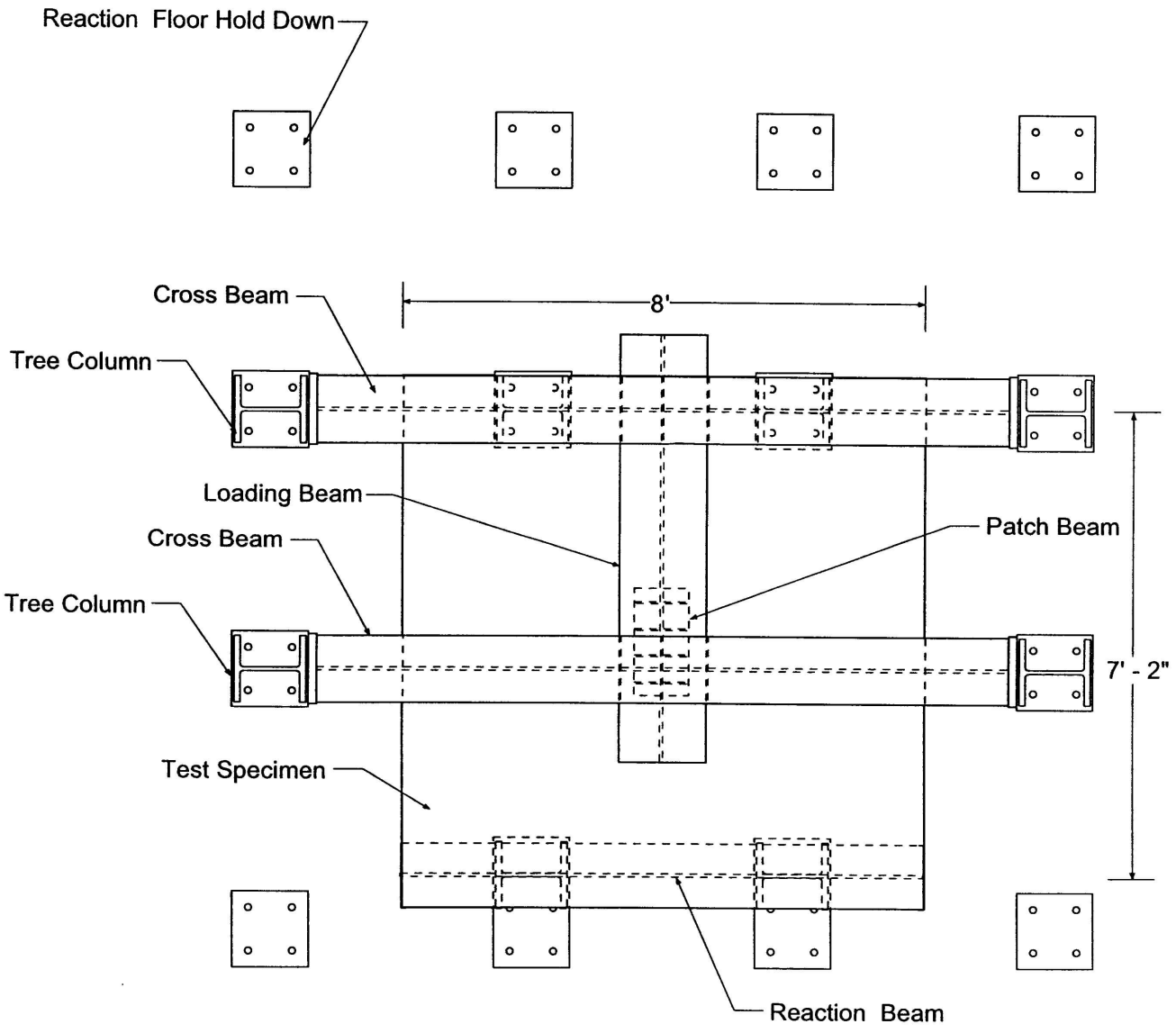


Fig. 42 - Plan view of test set-up for static test of south span.

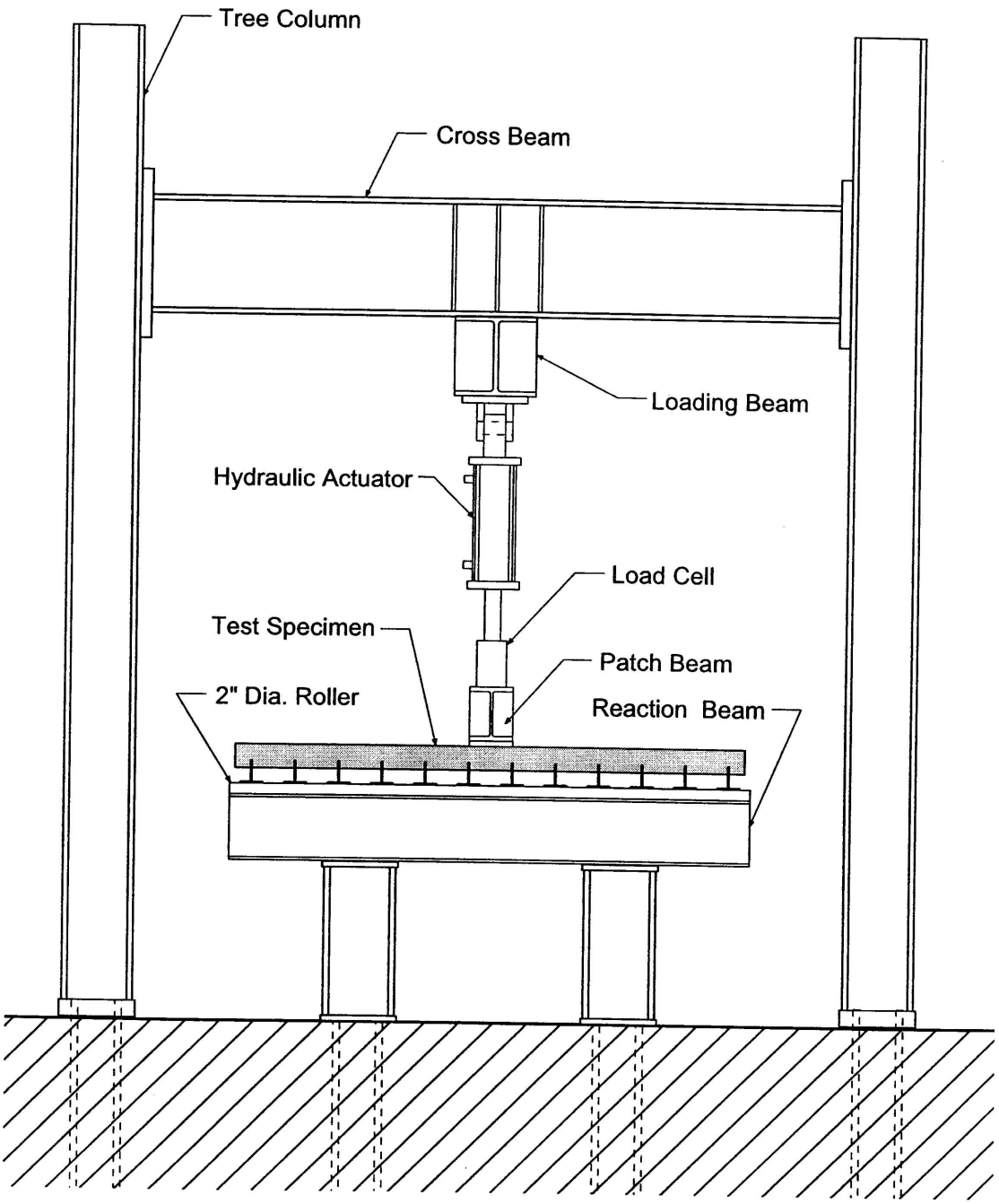


Fig. 43 - Elevation view of test set-up for static test of south span.

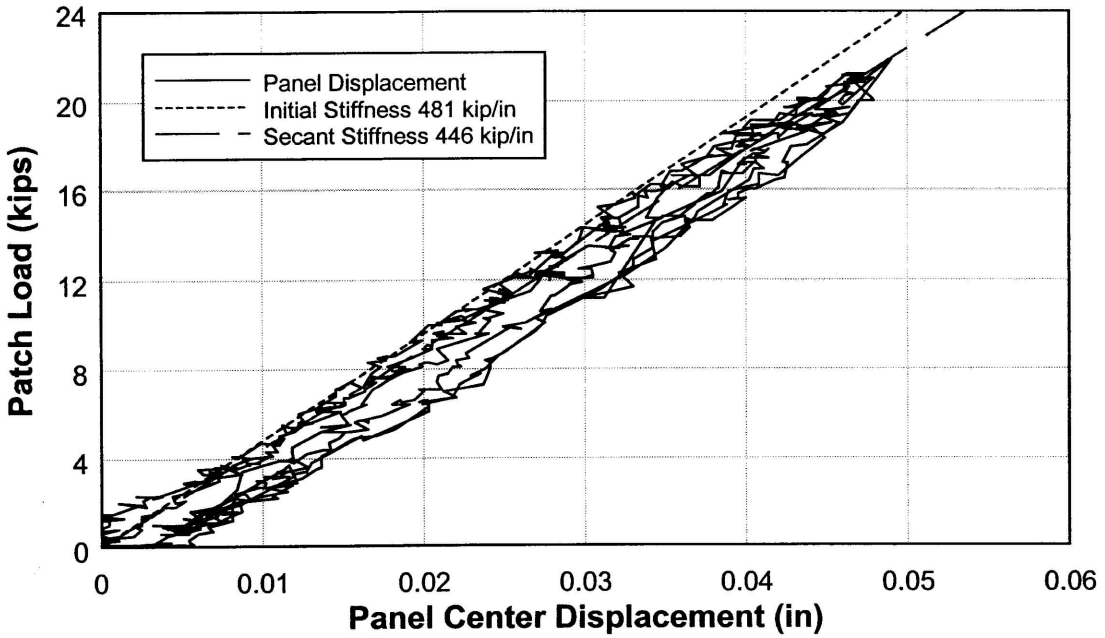


Fig. 44 - Load-displacement response at center of panel with load patch oriented perpendicular to main bars in service load range.

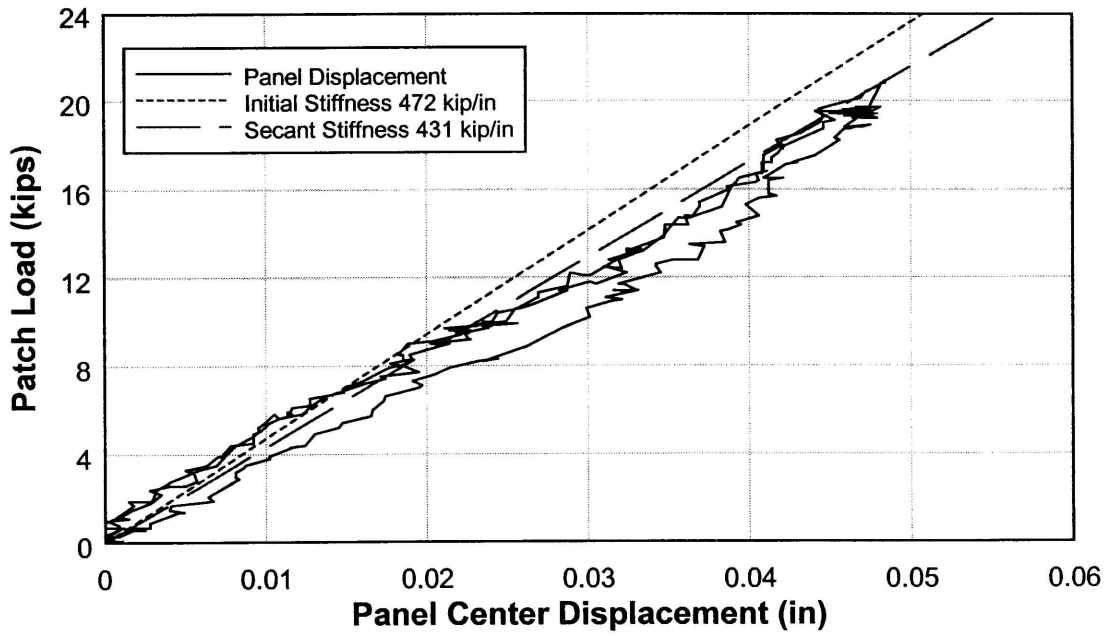


Fig. 45 - Load-displacement response at center of panel with load patch oriented parallel to main bars in service load range.

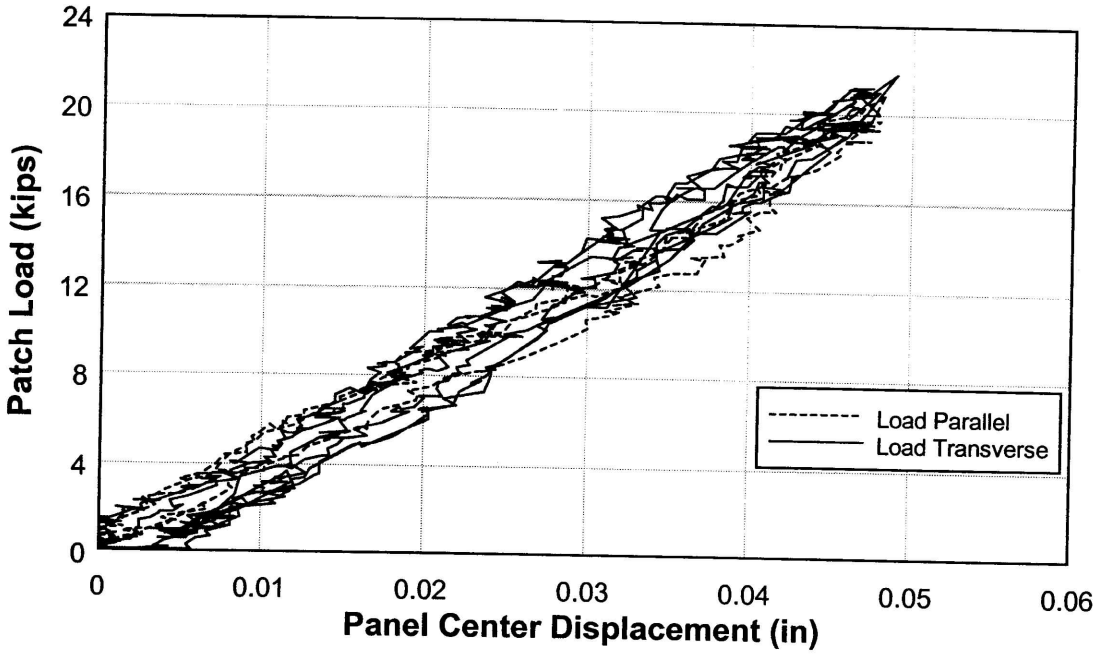


Fig. 46 - Load-displacement response at center of panel for two different load patch orientations in service load range.

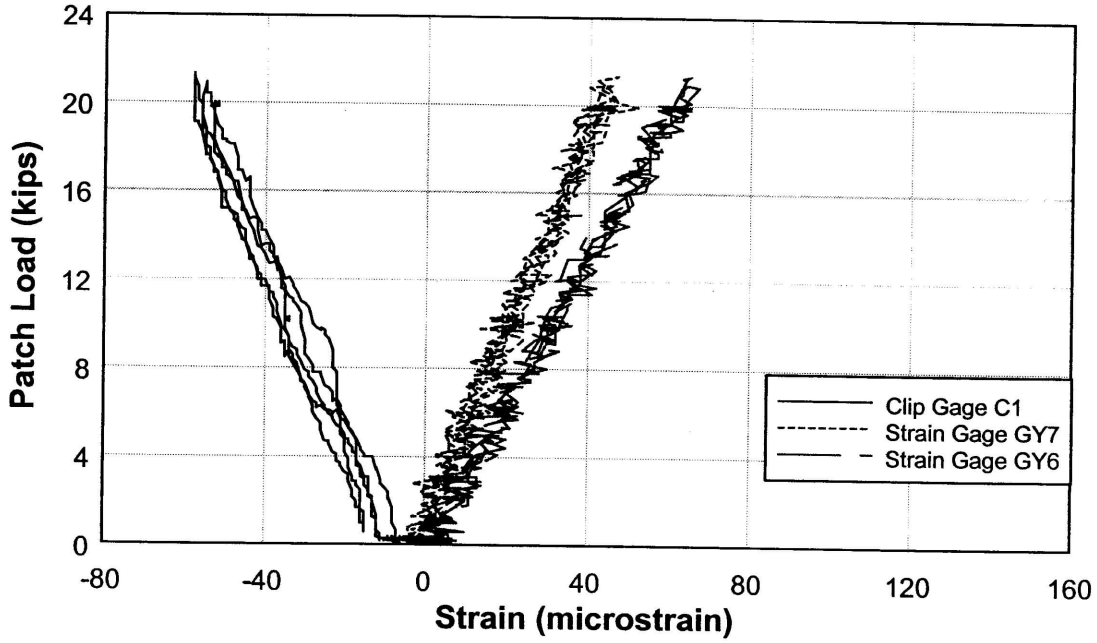


Fig. 47 - Measured strains across deck section at location C1 in service load range.

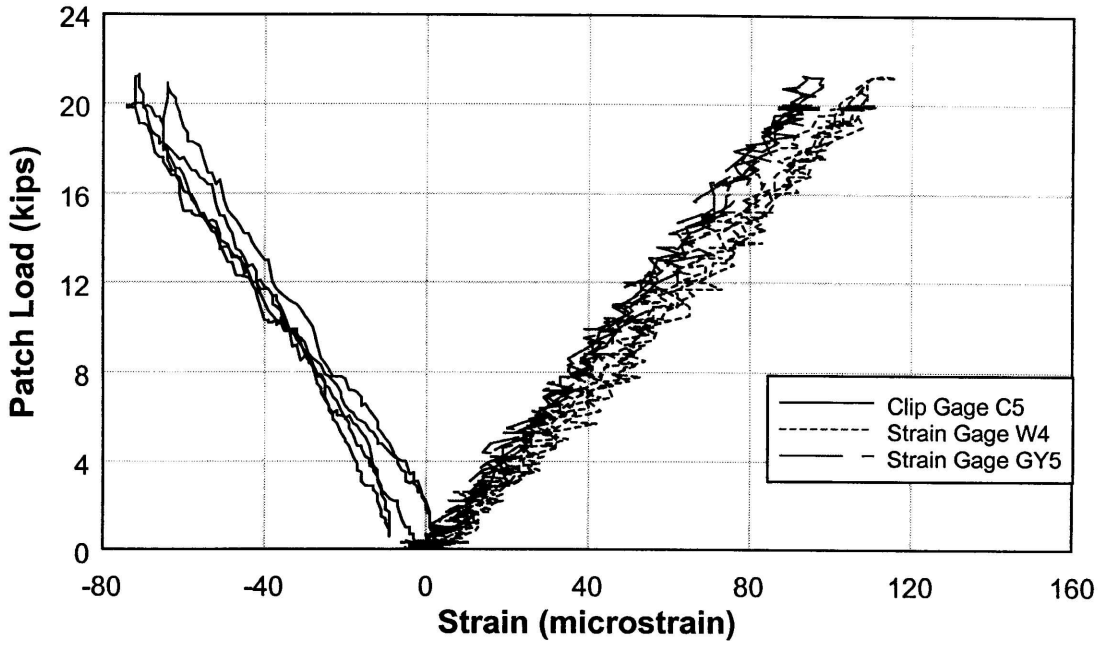


Fig. 48 - Measured strains across deck section at location C5 in service load range.

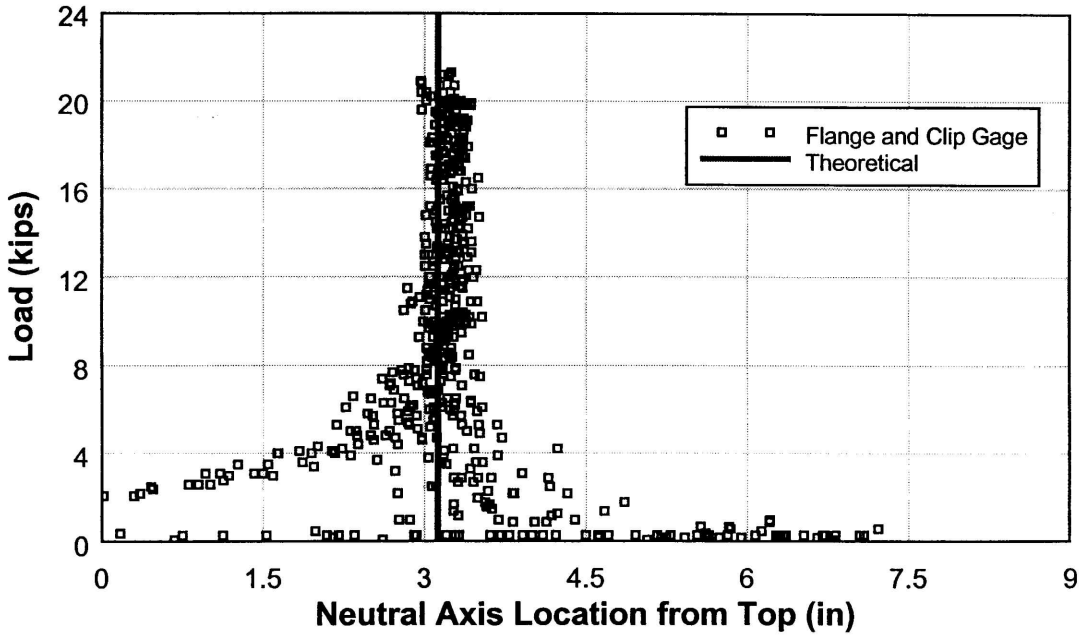


Fig. 49 - Computed and theoretical neutral axis location using concrete and flange strain at location C5 in service load range.

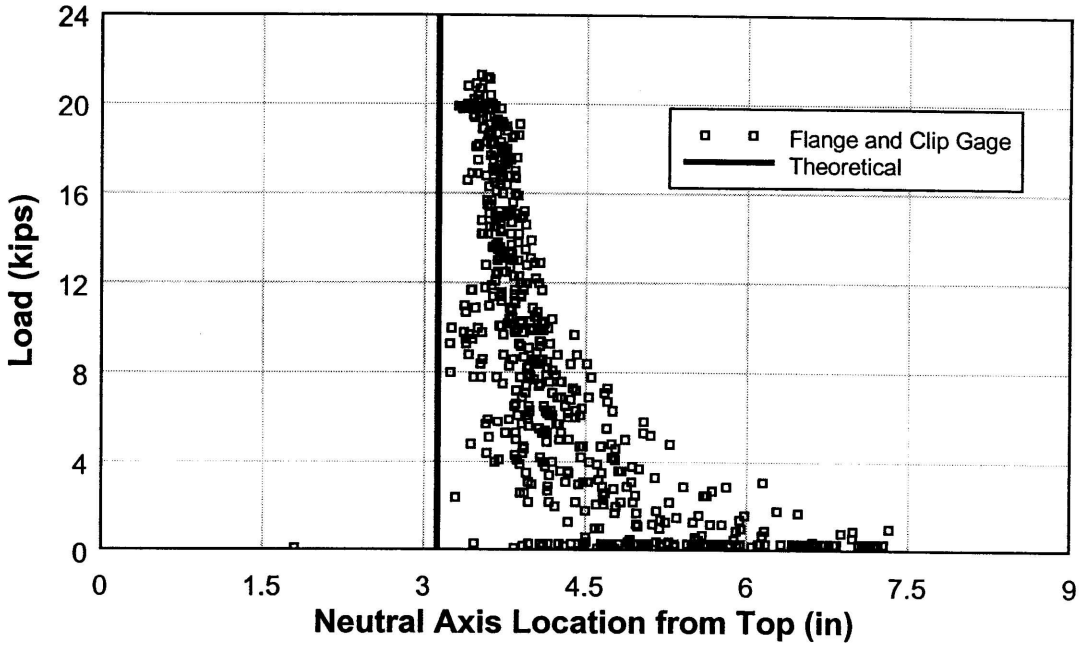


Fig. 50 - Computed and theoretical neutral axis location using concrete and flange strain at location C1 in service load range.

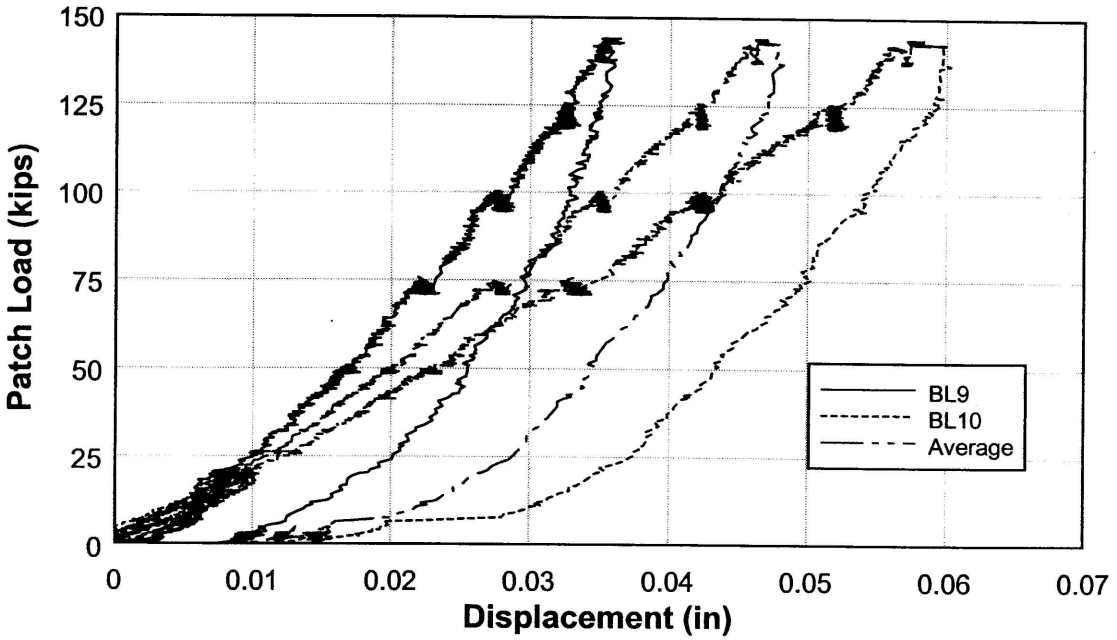


Fig. 51 - Measured support displacements at midpoint across deck.

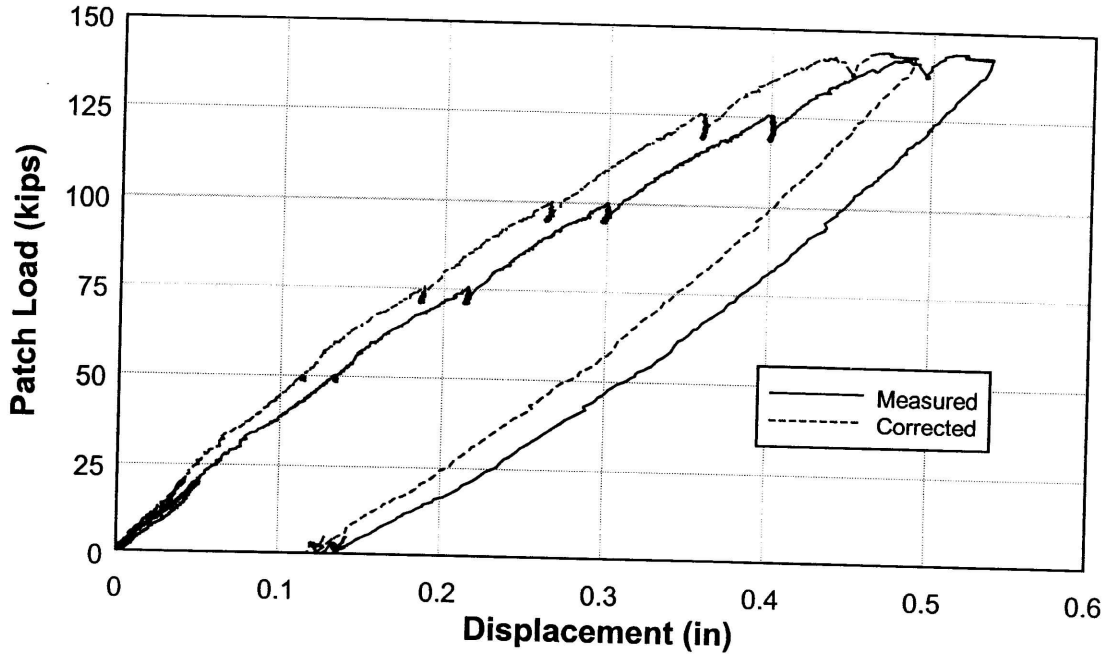


Fig. 52 - Total and relative load-displacement response at center of panel.

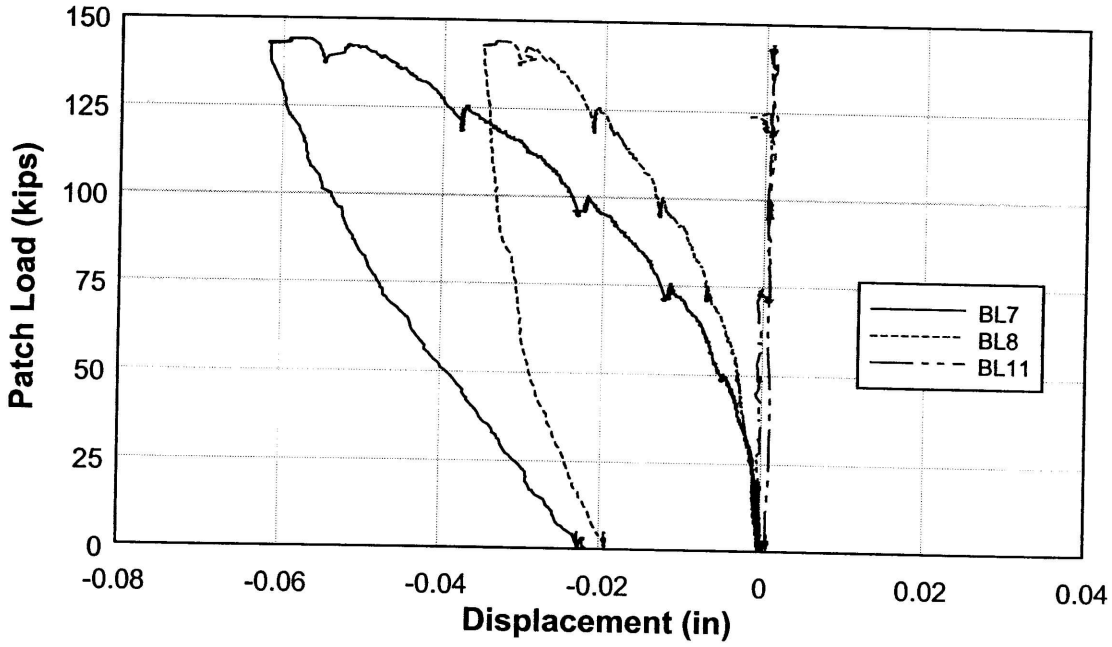


Fig. 53 - Relative displacement between bottom of concrete slab and adjacent main bar.

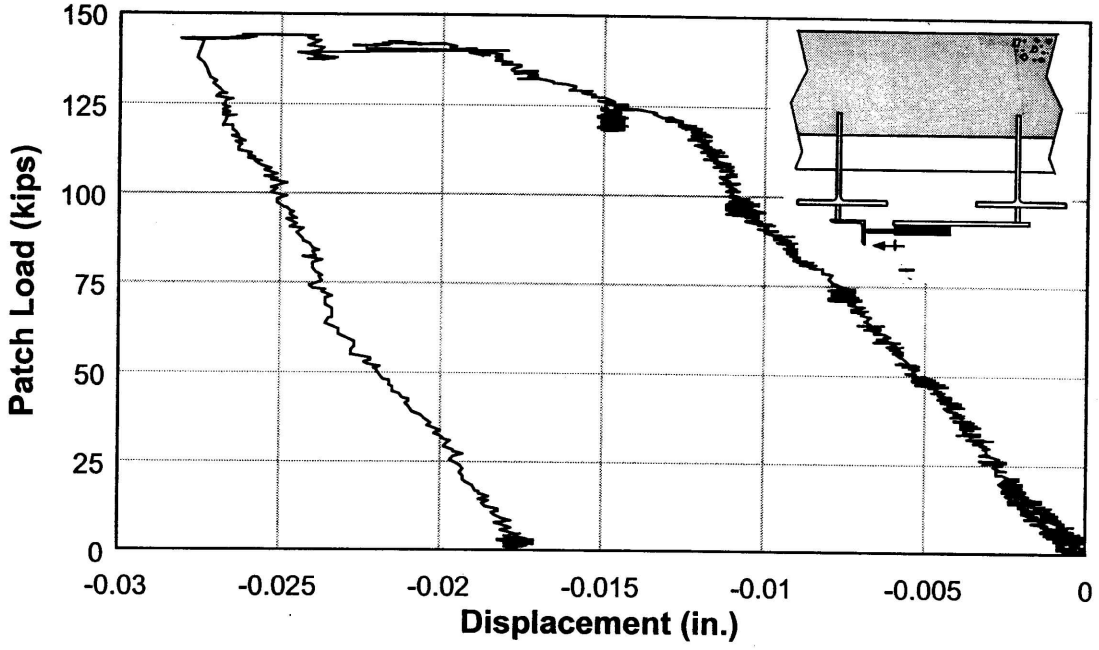


Fig. 54 - Lateral displacement between main bars #6 and 7.

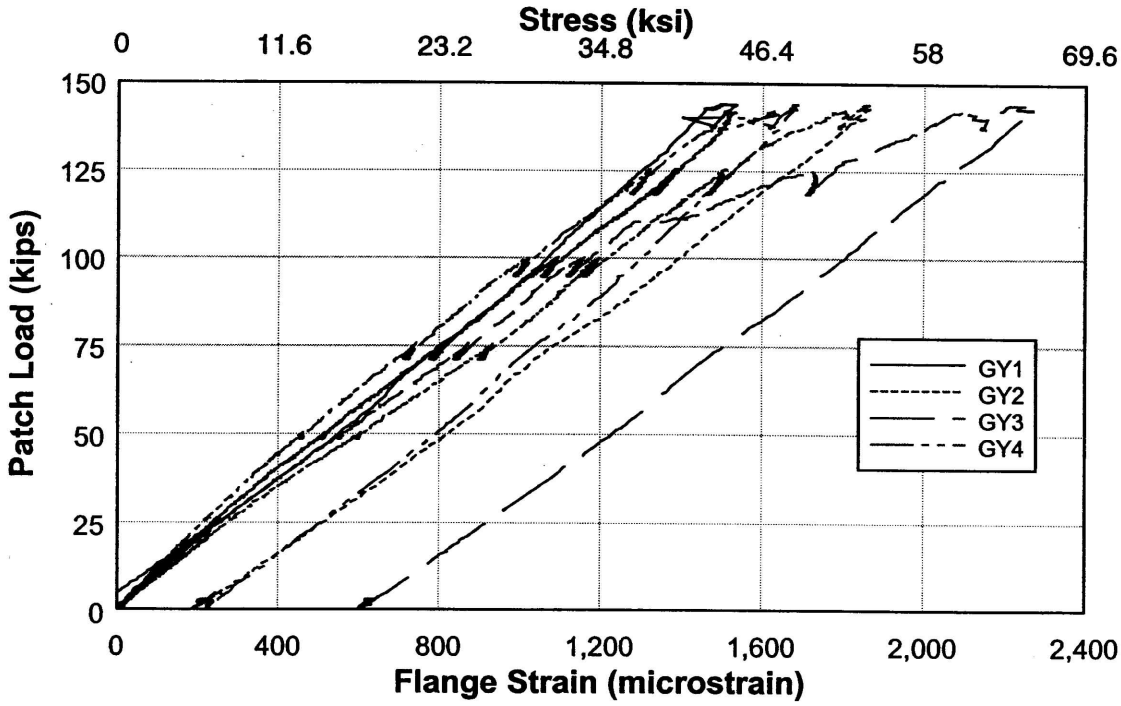


Fig. 55 - Main bar flange strain and stress.

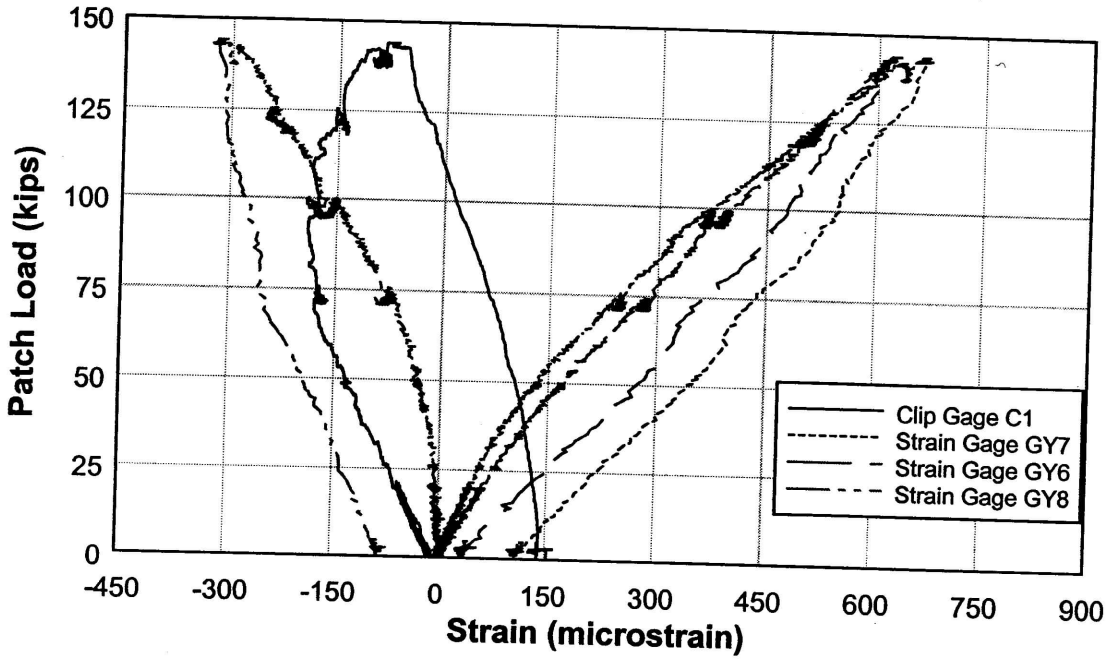


Fig. 56 - Measured strains across deck section at location C1.

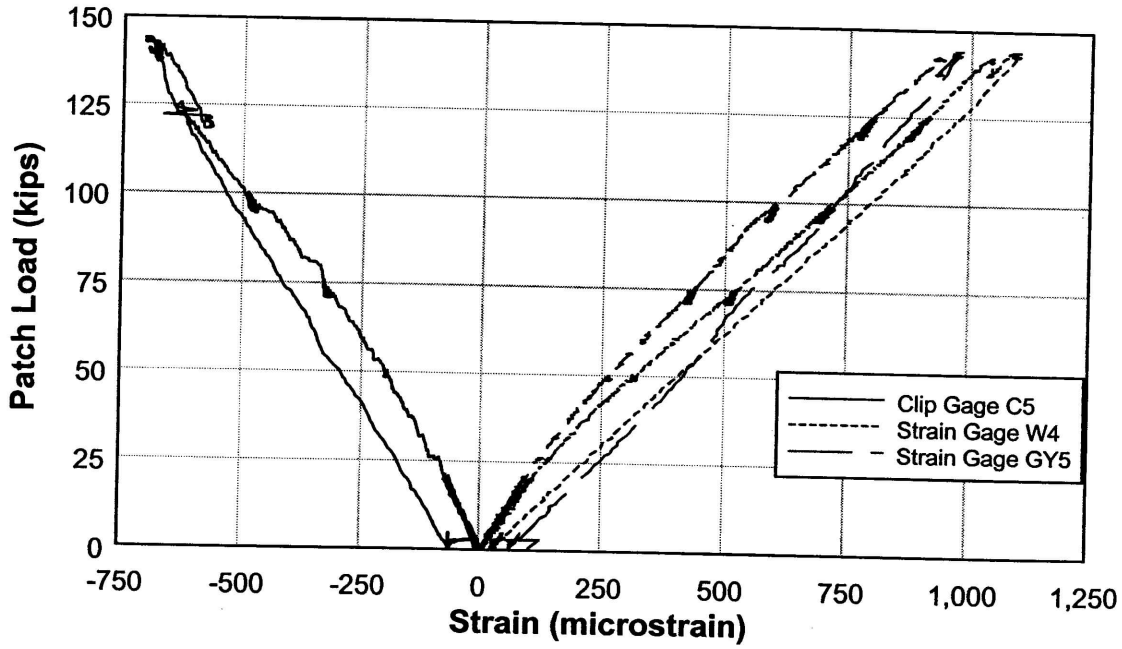


Fig. 57 - Measured strains across deck section at location C5.

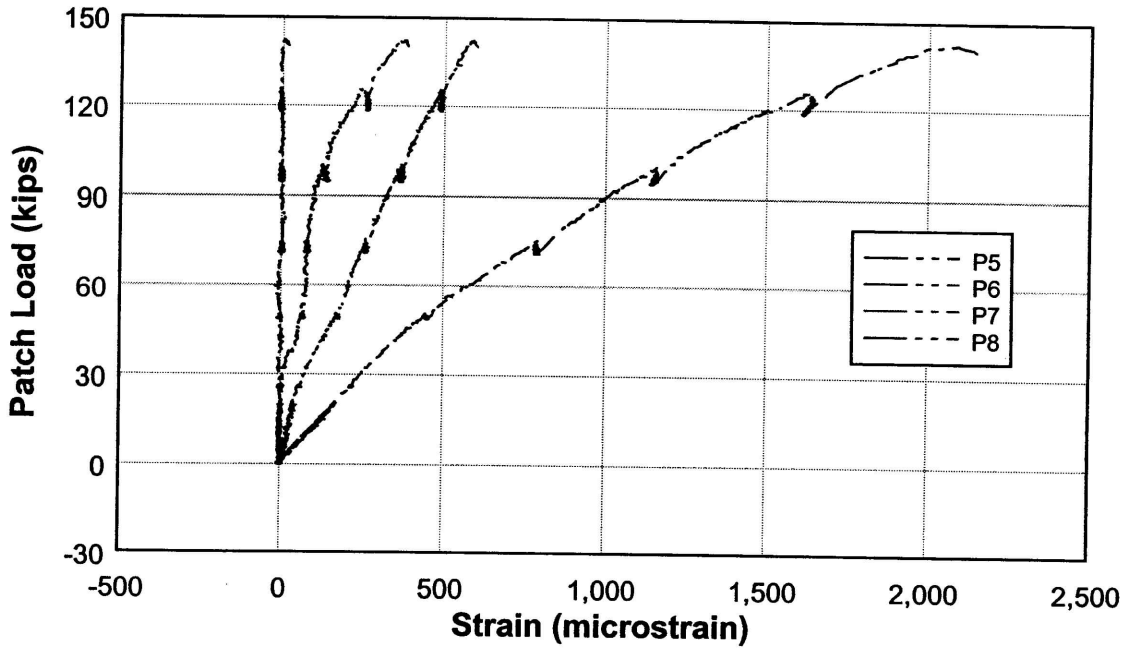


Fig. 58 - Measured strains in all #3 reinforcing bars.

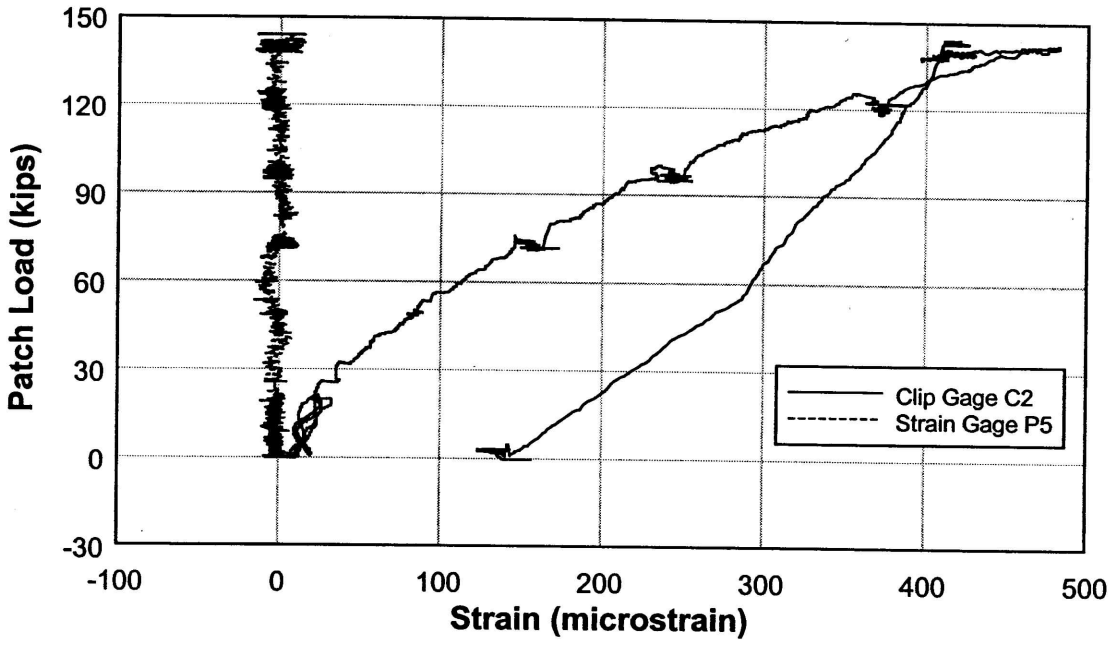


Fig. 59 - Concrete and #3 reinforcing bar strain at location C2.

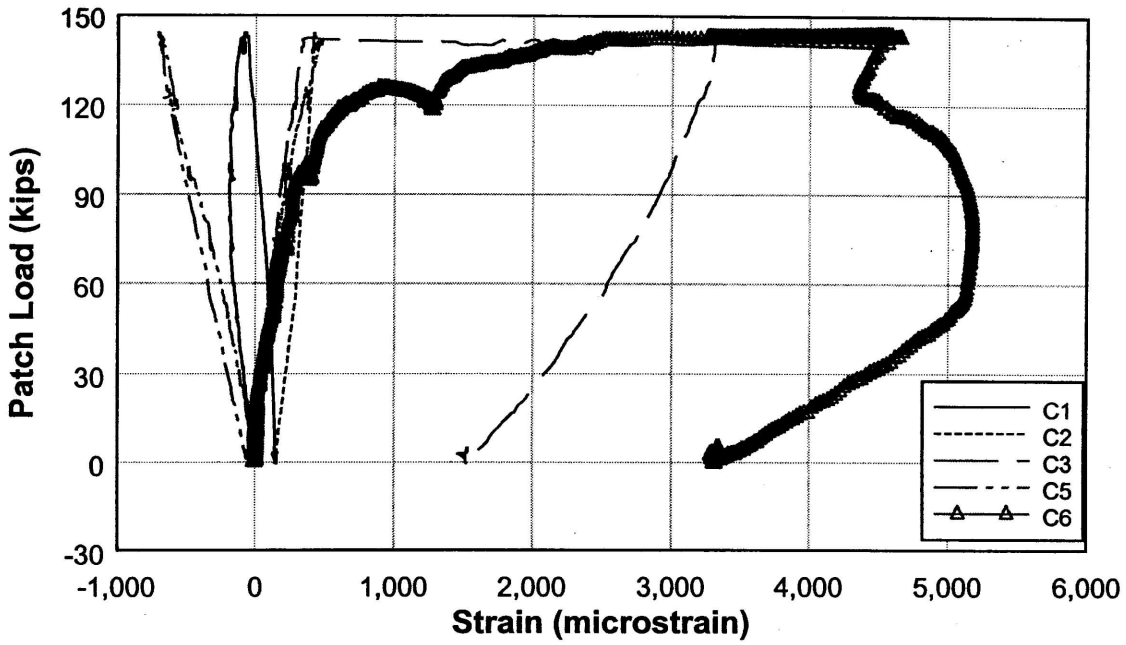


Fig. 60 - Measured concrete strains at all clip gage locations.

# Appendix A

## Concrete Mix Specification

## (Compressive strengths are shown in Table 1)

2.03 The Class DP Portland Cement concrete shall have a minimum 28 day compressive strength of 5000 psi and shall conform to Subsection 555-2 of the Standard Specifications and proportion according to the mix criteria below.

Use a Water-Reducing and Retarding Admixture meeting the requirements of Subsection 711-08 of the Standard Specifications to delay setting until after final concrete placement and finishing, and produce the desired slump without exceeding the maximum watereementitious material ratio.

**MIX CRITERIA**

| | |
|---|---|
| Cement (lbs./c.y.) | 536 |
| Fly ash (lbs./c.y.) | 145 |
| Microsilica (lbs./c.y.) | 44 |
| Sand - % of total aggregate (solid volume) | 45.8 |
| Maximum water/cementitious material ratio (725 lbs. total) | 0.40 |
| Desired air (%)<br>Allowable air (%) | 7.5<br>6.0 - 9.0 |
| Desired slump (inches)<br>Allowable slump (inches) | 3<br>2½ - 4 |
| Aggregate gradation | CA 1 |

**NOTE:** Criteria given for design information is based on a fine aggregate fineness modulus of 2.80. Determine the mixture proportions by using actual fineness modulus and bulk specific gravities (saturated surface dry for aggregate). Compute proportions according to Department written instructions.

Supply either a densified powder or slurry form of microsilica admixture whose brand name appears on the New York State Department of Transportation Material Bureau Approved List. Use only one brand for any structural element. Provide written certification from the Supplier that the microsilica meets the requirements of the Materials Bureau. Include the following data: fineness, silica content, total chloride ion content, solids content for slurries, and moisture content for densified powders.

Agitate the slurry as necessary to prevent separation. Remove and replace slurry that reaches a temperature less than 32°F., at no cost to the New York State Thruway Authority.

The Regional Materials Engineer will take a ½ - 1 quart microsilica sample directly from the storage container, for each days placement, for testing by the Department.

If densified powder is used - weigh cumulatively in the following order: cement, fly ash and microsilica. Base the batching tolerance of ±½% on the total weight of cementitious material, for each material draw weight.

If microsilica slurry is used - use proportioning equipment approved by the Regional Materials Engineer. Add through an existing automation system or a two stop, off-line automated, batching system meeting the following requirements:

Delivery accuracy - ±1% (by volume)
Program quantity - gallons (nearest tenth)
Batching tolerance - ±2.0% (by volume)
System interlocks
Print requirements:

a. Date and time
b. Truck number (or alternate method relating microsilica to batch ticket)
c. Delivered quantity (gallons, nearest tenth)

Locate the control box/printer for a two stop, off-line batching system at the batch plant operator's work station unless otherwise approved by the Regional Materials Engineer.

Calibrate in accordance with procedures approved by the Regional Materials Engineer. Recalibrate the entire system if part or all of the off-line system is moved.

# Appendix B

# Instrumentation Tables

Table B1 - Sensor identification and description for fatigue test.

Expansion Board No. 0

| Absolute Channel No. | Expansion Board ID | Sequential Channel No. | Channel Name | Conversion Factor | Channel Description |
|---|---|---|---|---|---|
| 0 | 0 | 1 | L1 | -10 kips /Volt | Load Cell, Excitation Voltage=5 V |
| 1 | 1 | 2 | BL5 | -0.8 in /Volt | Displacement Transducer, Excitation Voltage=5 V |
| 2 | 2 | 3 | BL6 | -0.6 in /Volt | Displacement Transducer, Excitation Voltage=5 V |
| 3 | 3 | 4 | BL7 | 0.1 in /Volt | Displacement Transducer, Excitation Voltage=5 V |
| 4 | 4 | 5 | C1 | -5601 με /Volt | Clip Gage #1, Excitation Voltage=5 V |
| 5 | 5 | 6 | C2 | -5639 με /Volt | Clip Gage #2, Excitation Voltage=5 V |
| 6 | 6 | 7 | C3 | -5763 με /Volt | Clip Gage #3, Excitation Voltage=5 V |
| 7 | 7 | 8 | C4 | -5904 με /Volt | Clip Gage #4, Excitation Voltage=5 V |
| 8 | 8 | 9 | P1 | 479.6 με /Volt | Strain Gage on #5 Reinforcing Steel, Excitation Voltage=4 V |
| 9 | 9 | 10 | P2 | 479.6 με /Volt | Strain Gage on #5 Reinforcing Steel, Excitation Voltage=4 V |
| 10 | 10 | 11 | P3 | 479.6 με /Volt | Strain Gage on #5 Reinforcing Steel, Excitation Voltage=4 V |
| 11 | 11 | 12 | P4 | 479.6 με /Volt | Strain Gage on #5 Reinforcing Steel, Excitation Voltage=4 V |
| 12 | 12 | 13 | P5 | 479.6 με /Volt | Strain Gage on #3 Reinforcing Steel, Excitation Voltage=4 V |
| 13 | 13 | 14 | P6 | 479.6 με /Volt | Strain Gage on #3 Reinforcing Steel, Excitation Voltage=4 V |
| 14 | 14 | 15 | P7 | 479.6 με /Volt | Strain Gage on #3 Reinforcing Steel, Excitation Voltage=4 V |
| 15 | 15 | 16 | P8 | 479.6 με /Volt | Strain Gage on #3 Reinforcing Steel, Excitation Voltage=4 V |

Expansion Board No. 1

| Absolute Channel No. | Expansion Board ID | Sequential Channel No. | Channel Name | Conversion Factor | Channel Description |
|---|---|---|---|---|---|
| 16 | 0 | 17 | O1 | -479.6 με /Volt | Strain Gage Main Bar Bottom Flange, Excitation Voltage=4 V |
| 17 | 1 | 18 | O2 | -479.6 με /Volt | Strain Gage Main Bar Web, Excitation Voltage=4 V |
| 18 | 2 | 19 | O3 | -479.6 με /Volt | Strain Gage on #5 Reinforcing Steel, Excitation Voltage=4 V |
| 19 | 3 | 20 | O4 | -479.6 με /Volt | Strain Gage Main Bar Bottom Flange, Excitation Voltage=4 V |
| 20 | 4 | 21 | O5 | -479.6 με /Volt | Strain Gage Main Bar Web, Excitation Voltage=4 V |
| 21 | 5 | 22 | O6 | -479.6 με /Volt | Strain Gage on #5 Reinforcing Steel, Excitation Voltage=4 V |
| 22 | 6 | 23 | O7 | -479.6 με /Volt | Strain Gage on #3 Reinforcing Steel, Excitation Voltage=4 V |
| 23 | 7 | 24 | O8 | -479.6 με /Volt | Strain Gage on #3 Reinforcing Steel, Excitation Voltage=4 V |
| 24 | 8 | 25 | BN1 | 479.6 με /Volt | Strain Gage Main Bar Bottom Flange, Excitation Voltage=4 V |
| 25 | 9 | 26 | BN2 | 479.6 με /Volt | Strain Gage Main Bar Bottom Flange, Excitation Voltage=4 V |
| 26 | 10 | 27 | BN3 | 479.6 με /Volt | Strain Gage Main Bar Bottom Flange, Excitation Voltage=4 V |
| 27 | 11 | 28 | BN4 | 479.6 με /Volt | Strain Gage Main Bar Bottom Flange, Excitation Voltage=4 V |
| 28 | 12 | 29 | BN5 | 479.6 με /Volt | Strain Gage Main Bar Bottom Flange, Excitation Voltage=4 V |
| 29 | 13 | 30 | BN6 | 479.6 με /Volt | Strain Gage Main Bar Bottom Flange, Excitation Voltage=4 V |
| 30 | 14 | 31 | BN7 | 479.6 με /Volt | Strain Gage Main Bar Bottom Flange, Excitation Voltage=4 V |
| 31 | 15 | 32 | BN8 | 479.6 με /Volt | Strain Gage Main Bar Bottom Flange, Excitation Voltage=4 V |

| Expansion Board No. | | 2 | | | |
|---|---|---|---|---|---|
| Absolute Channel No. | Expansion Board ID | Sequential Channel No. | Channel Name | Conversion Factor | Channel Description |
| 32 | 0 | 33 | GY8 | 479.6 με /Volt | Strain Gage Main Bar Bottom Flange, Excitation Voltage=4 V |
| 33 | 1 | 34 | GY7 | 479.6 με /Volt | Strain Gage Main Bar Bottom Flange, Excitation Voltage=4 V |
| 34 | 2 | 35 | GY6 | 479.6 με /Volt | Strain Gage Main Bar Bottom Flange, Excitation Voltage=4 V |
| 35 | 3 | 36 | GY5 | 479.6 με /Volt | Strain Gage Main Bar Bottom Flange, Excitation Voltage=4 V |
| 36 | 4 | 37 | GY4 | 479.6 με /Volt | Strain Gage Main Bar Bottom Flange, Excitation Voltage=4 V |
| 37 | 5 | 38 | GY3 | 479.6 με /Volt | Strain Gage Main Bar Bottom Flange, Excitation Voltage=4 V |
| 38 | 6 | 39 | GY2 | 479.6 με /Volt | Strain Gage Main Bar Bottom Flange, Excitation Voltage=4 V |
| 39 | 7 | 40 | GY1 | 479.6 με /Volt | Strain Gage Main Bar Bottom Flange, Excitation Voltage=4 V |
| 40 | 8 | 41 | GN1 | -1 in /Volt | String Pot, Excitation Voltage=5 V |
| 41 | 9 | 42 | GN2 | -2 in /Volt | String Pot, Excitation Voltage=5 V |
| 42 | 10 | 43 | GN3 | -1 in /Volt | String Pot, Excitation Voltage=5 V |
| 43 | 11 | 44 | GN4 | -2 in /Volt | String Pot, Excitation Voltage=5 V |
| 44 | 12 | 45 | BL1 | -0.6 in /Volt | Displacement Transducer, Excitation Voltage=5 V |
| 45 | 13 | 46 | BL2 | 0.1 in /Volt | Displacement Transducer, Excitation Voltage=5 V |
| 46 | 14 | 47 | BL3 | -0.6 in /Volt | Displacement Transducer, Excitation Voltage=5 V |
| 47 | 15 | 48 | BL4 | -0.6 in /Volt | Displacement Transducer, Excitation Voltage=5 V |

Table B2 - Sensor identification and description for fatigue test.

Table B3 - Sensor identification and description for final static test.

Expansion Board No. 0

| Absolute Channel No. | Expansion Board ID | Sequential Channel No. | Channel Name | Conversion Factor | Channel Description |
|---|---|---|---|---|---|
| 0 | 0 | 1 | BL5 | -0.8 in /Volt | Displacement Transducer, Excitation Voltage=5 V |
| 1 | 1 | 2 | BL6 | -0.6 in /Volt | Displacement Transducer, Excitation Voltage=5 V |
| 2 | 2 | 3 | BL7 | 0.1 in /Volt | Displacement Transducer, Excitation Voltage=5 V |
| 3 | 3 | 4 | BL8 | 0.1 in /Volt | Displacement Transducer, Excitation Voltage=5 V |
| 4 | 4 | 5 | BL9 | 0.3 in /Volt | Displacement Transducer, Excitation Voltage=5 V |
| 5 | 5 | 6 | BL10 | 0.3 in /Volt | Displacement Transducer, Excitation Voltage=5 V |
| 6 | 6 | 7 | BL11 | 0.3 in /Volt | Displacement Transducer, Excitation Voltage=5 V |
| 7 | 7 | 8 | OPEN | X | OPEN |
| 8 | 8 | 9 | OPEN | X | OPEN |
| 9 | 9 | 10 | OPEN | X | OPEN |
| 10 | 10 | 11 | OPEN | X | OPEN |
| 11 | 11 | 12 | OPEN | X | OPEN |
| 12 | 12 | 13 | P5 | 4796.2 με /Volt | Strain Gage on #3 Reinforcing Steel, Excitation Voltage=4 V |
| 13 | 13 | 14 | P6 | 4796.2 με /Volt | Strain Gage on #3 Reinforcing Steel, Excitation Voltage=4 V |
| 14 | 14 | 15 | P7 | 4796.2 με /Volt | Strain Gage on #3 Reinforcing Steel, Excitation Voltage=4 V |
| 15 | 15 | 16 | P8 | 4796.2 με /Volt | Strain Gage on #3 Reinforcing Steel, Excitation Voltage=4 V |

Expansion Board No. 1

| Absolute Channel No. | Expansion Board ID | Sequential Channel No. | Channel Name | Conversion Factor | Channel Description |
|---|---|---|---|---|---|
| 16 | 0 | 17 | OPEN | X | OPEN |
| 17 | 1 | 18 | OPEN | X | OPEN |
| 18 | 2 | 19 | OPEN | X | OPEN |
| 19 | 3 | 20 | OPEN | X | OPEN |
| 20 | 4 | 21 | OPEN | X | OPEN |
| 21 | 5 | 22 | OPEN | X | OPEN |
| 22 | 6 | 23 | OPEN | X | OPEN |
| 23 | 7 | 24 | OPEN | X | OPEN |
| 24 | 8 | 25 | BN1 | 4796.2 με /Volt | Strain Gage Main Bar Bottom Flange, Excitation Voltage=4 V |
| 25 | 9 | 26 | BN2 | 4796.2 με /Volt | Strain Gage Main Bar Bottom Flange, Excitation Voltage=4 V |
| 26 | 10 | 27 | BN3 | 4796.2 με /Volt | Strain Gage Main Bar Bottom Flange, Excitation Voltage=4 V |
| 27 | 11 | 28 | BN4 | 4796.2 με /Volt | Strain Gage Main Bar Bottom Flange, Excitation Voltage=4 V |
| 28 | 12 | 29 | BN5 | 4796.2 με /Volt | Strain Gage Main Bar Bottom Flange, Excitation Voltage=4 V |
| 29 | 13 | 30 | BN6 | 4796.2 με /Volt | Strain Gage Main Bar Bottom Flange, Excitation Voltage=4 V |
| 30 | 14 | 31 | BN7 | 4796.2 με /Volt | Strain Gage Main Bar Bottom Flange, Excitation Voltage=4 V |
| 31 | 15 | 32 | BN8 | 4796.2 με /Volt | Strain Gage Main Bar Bottom Flange, Excitation Voltage=4 V |

Table B4 - Sensor identification and description for final static test.

Expansion Board No. 2

| Absolute Channel No. | Expansion Board ID | Sequential Channel No. | Channel Name | Conversion Factor | Channel Description |
|---|---|---|---|---|---|
| 32 | 0 | 33 | GY8 | 4796.2 με /Volt | Strain Gage on #3 Reinforcing Steel, Excitation Voltage=4 V |
| 33 | 1 | 34 | GY7 | 4796.2 με /Volt | Strain Gage Main Bar Web, Excitation Voltage=4 V |
| 34 | 2 | 35 | GY6 | 4796.2 με /Volt | Strain Gage Main Bar Bottom Flange, Excitation Voltage=4 V |
| 35 | 3 | 36 | GY5 | 4796.2 με /Volt | Strain Gage Main Bar Bottom Flange, Excitation Voltage=4 V |
| 36 | 4 | 37 | GY4 | 4796.2 με /Volt | Strain Gage Main Bar Bottom Flange, Excitation Voltage=4 V |
| 37 | 5 | 38 | GY3 | 4796.2 με /Volt | Strain Gage Main Bar Bottom Flange, Excitation Voltage=4 V |
| 38 | 6 | 39 | GY2 | 4796.2 με /Volt | Strain Gage Main Bar Bottom Flange, Excitation Voltage=4 V |
| 39 | 7 | 40 | GY1 | 4796.2 με /Volt | Strain Gage Main Bar Bottom Flange, Excitation Voltage=4 V |
| 40 | 8 | 41 | W1 | 4796.2 με /Volt | Strain Gage Main Bar Web, Excitation Voltage=4 V |
| 41 | 9 | 42 | W2 | 4796.2 με /Volt | Strain Gage Main Bar Web, Excitation Voltage=4 V |
| 42 | 10 | 43 | W3 | 4796.2 με /Volt | Strain Gage Main Bar Web, Excitation Voltage=4 V |
| 43 | 11 | 44 | W4 | 4796.2 με /Volt | Strain Gage Main Bar Web, Excitation Voltage=4 V |
| 44 | 12 | 45 | OPEN | X | OPEN |
| 45 | 13 | 46 | OPEN | X | OPEN |
| 46 | 14 | 47 | OPEN | X | OPEN |
| 47 | 15 | 48 | OPEN | X | OPEN |

Expansion Board No. 3

| Absolute Channel No. | Multiplexer ID | My Channel No. | Channel Name | Conversion Factor | Channel Description |
|---|---|---|---|---|---|
| 48 | 0 | 49 | GN1 | -1 in /Volt | String Pot, Excitation Voltage=5 V |
| 49 | 1 | 50 | GN2 | -1 in /Volt | String Pot, Excitation Voltage=5 V |
| 50 | 2 | 51 | GN3 | -2 in /Volt | String Pot, Excitation Voltage=5 V |
| 51 | 3 | 52 | GN4 | 0.3 in /Volt | Displacement Transducer, Excitation Voltage=5 V |
| 52 | 4 | 53 | BL1 | -0.6 in /Volt | Displacement Transducer, Excitation Voltage=5 V |
| 53 | 5 | 54 | BL2 | -0.8 in /Volt | Displacement Transducer, Excitation Voltage=5 V |
| 54 | 6 | 55 | BL3 | -0.6 in /Volt | Displacement Transducer, Excitation Voltage=5 V |
| 55 | 7 | 56 | BL4 | -0.6 in /Volt | Displacement Transducer, Excitation Voltage=5 V |
| 56 | 8 | 57 | L1 | -36.088 kips /Volt | Load Cell, Excitation Voltage=5 V |
| 57 | 9 | 58 | C1 | 5601.613 με /Volt | Clip Gage #1, Excitation Voltage=4 V |
| 58 | 10 | 59 | C2 | 5639.14 με /Volt | Clip Gage #2, Excitation Voltage=4 V |
| 59 | 11 | 60 | C3 | 5763.157 με /Volt | Clip Gage #3, Excitation Voltage=4 V |
| 60 | 12 | 61 | C4 | 5809.239 με /Volt | Clip Gage #4, Excitation Voltage=4 V |
| 61 | 13 | 62 | C5 | 5446.623 με /Volt | Clip Gage #5, Excitation Voltage=4 V |
| 62 | 14 | 63 | OPEN | X | OPEN |
| 63 | 15 | 64 | OPEN | X | OPEN |

# Appendix C

# Crack Patterns on Concrete Surface

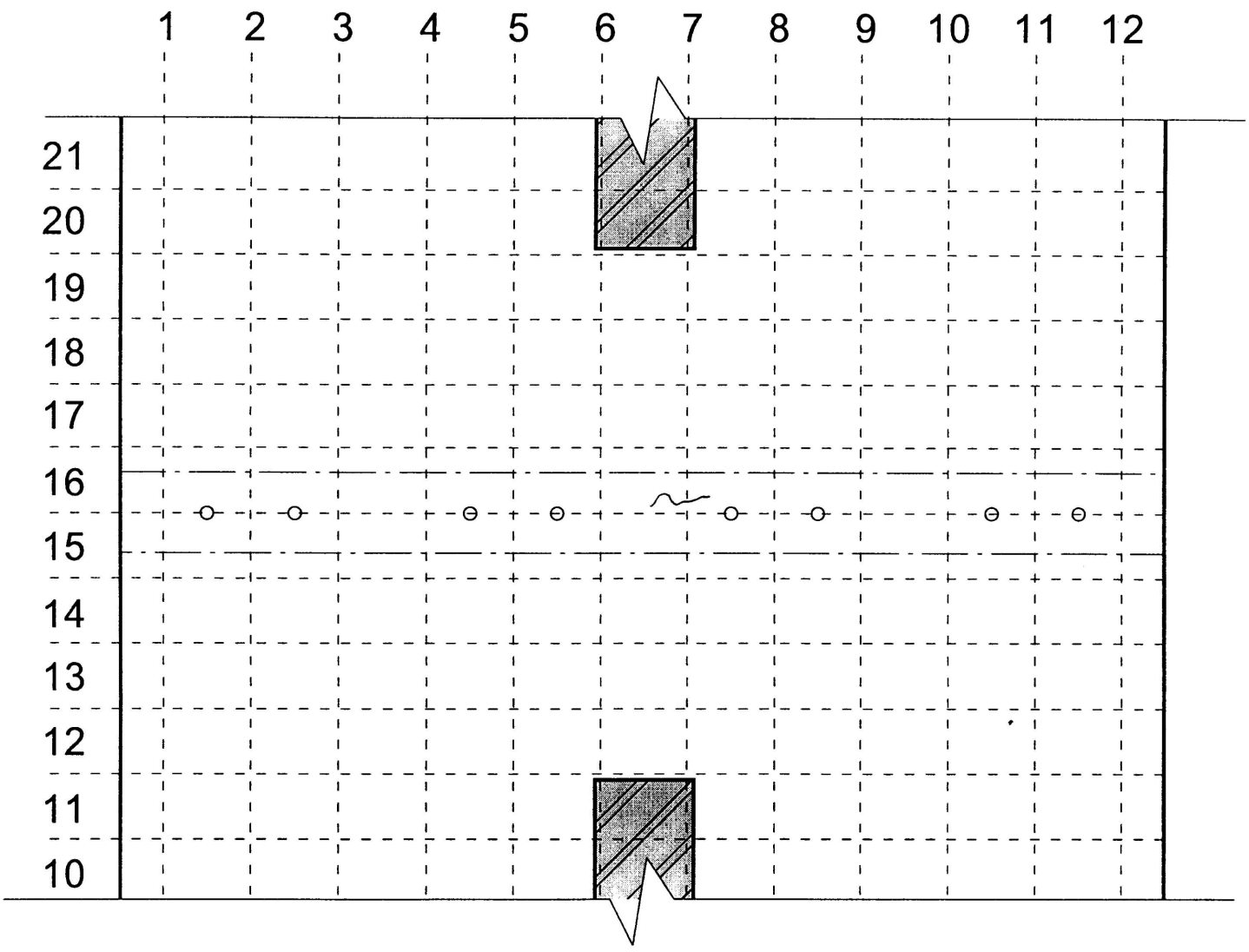


Fig. C1 – Cumulative crack pattern on concrete surface at 20 kips.

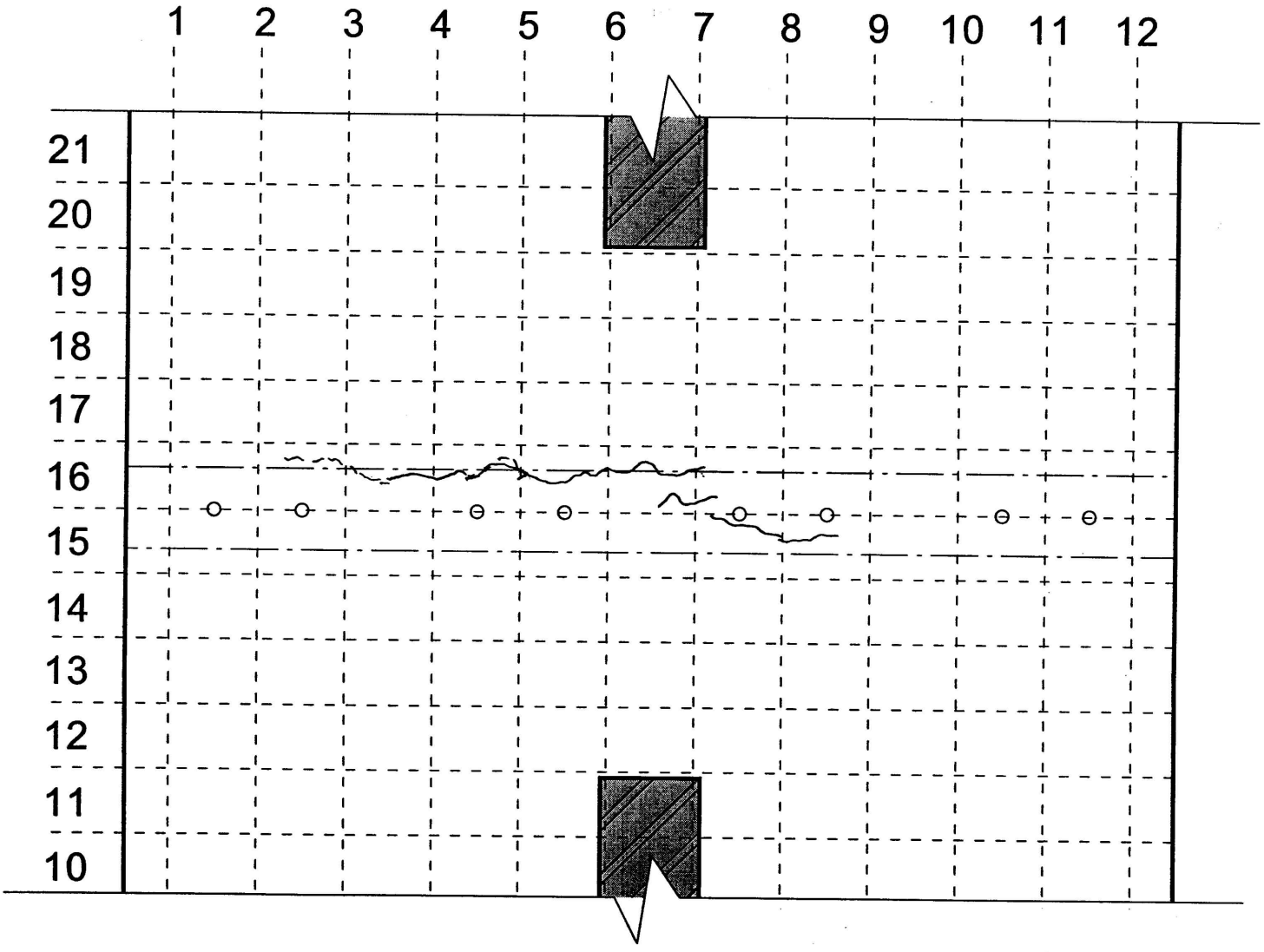


Fig. C2 – Cumulative crack pattern on concrete surface at 25 kips.

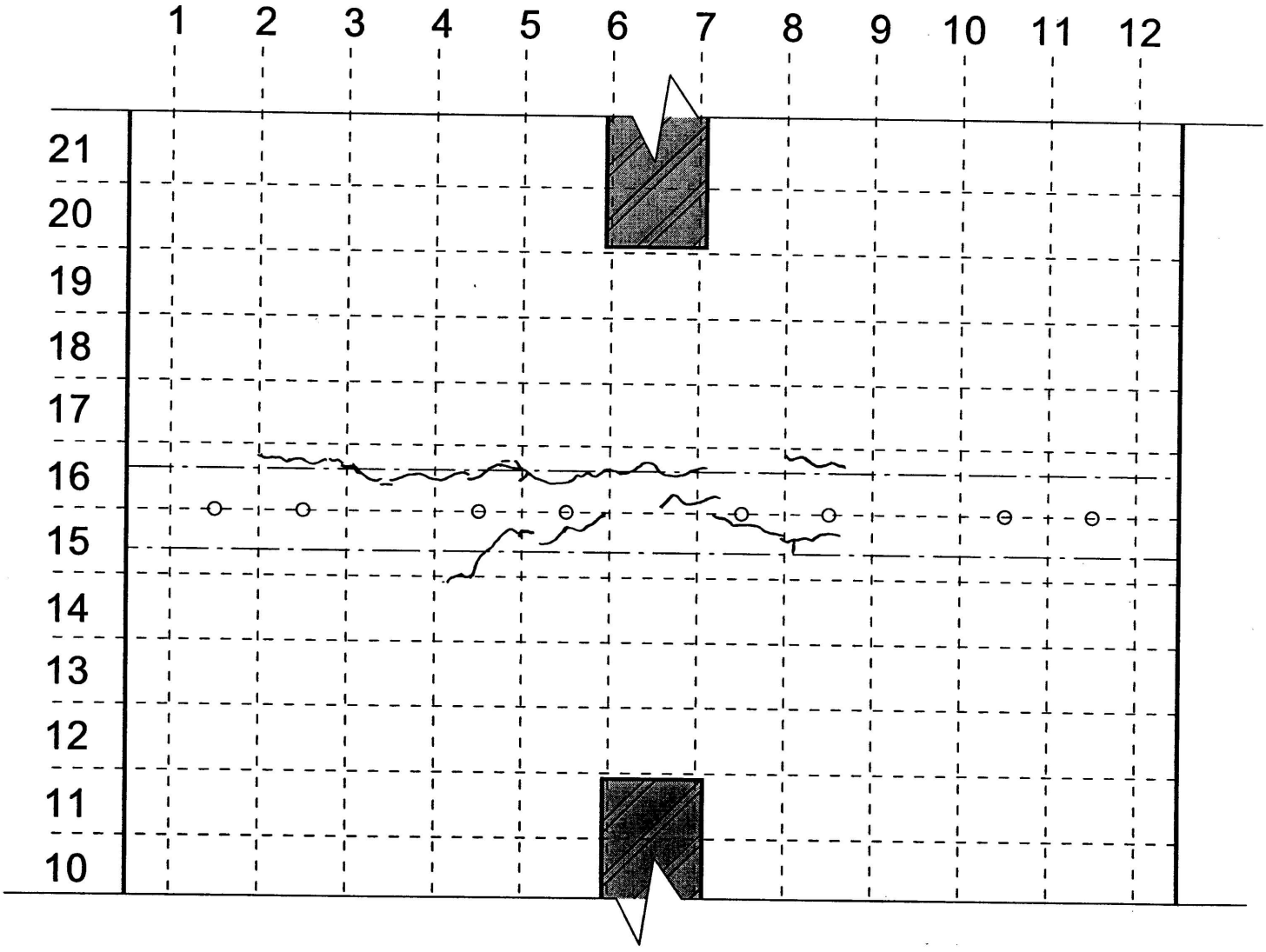


Fig. C3 – Cumulative crack pattern on concrete surface at 30 kips.

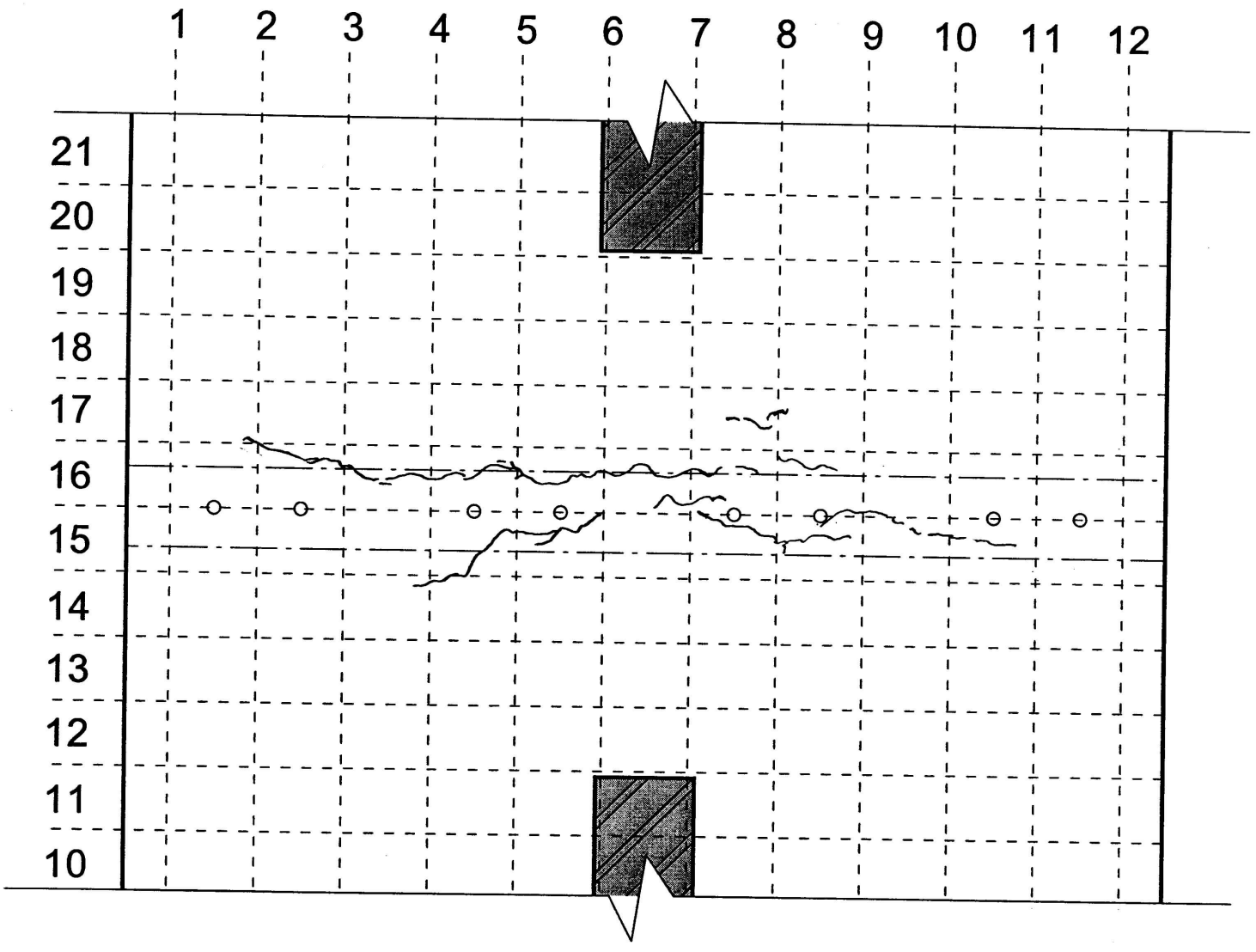


Fig. C4 – Cumulative crack pattern on concrete surface at 35 kips.

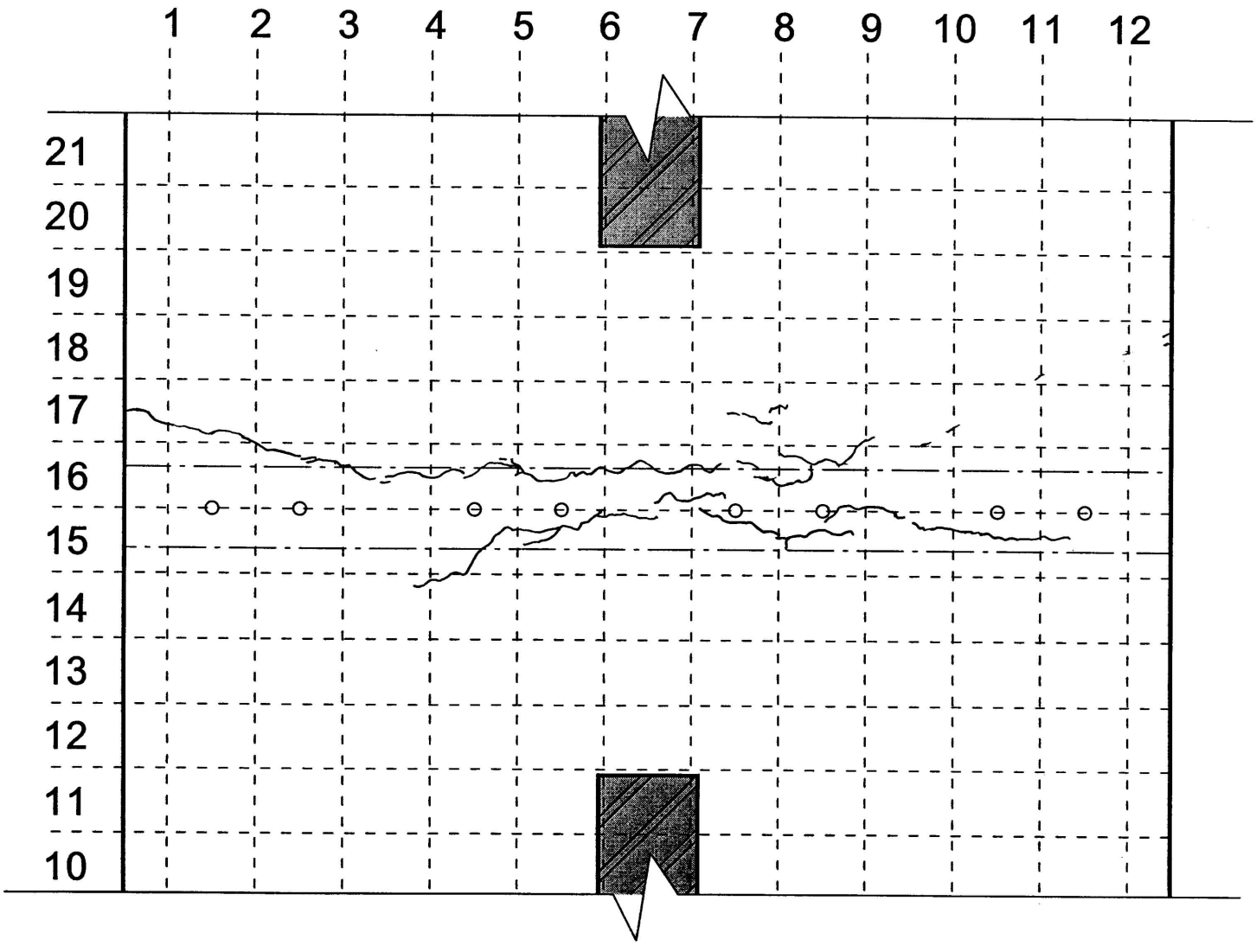


Fig. C5 – Cumulative crack pattern on concrete surface at 41.6 kips.

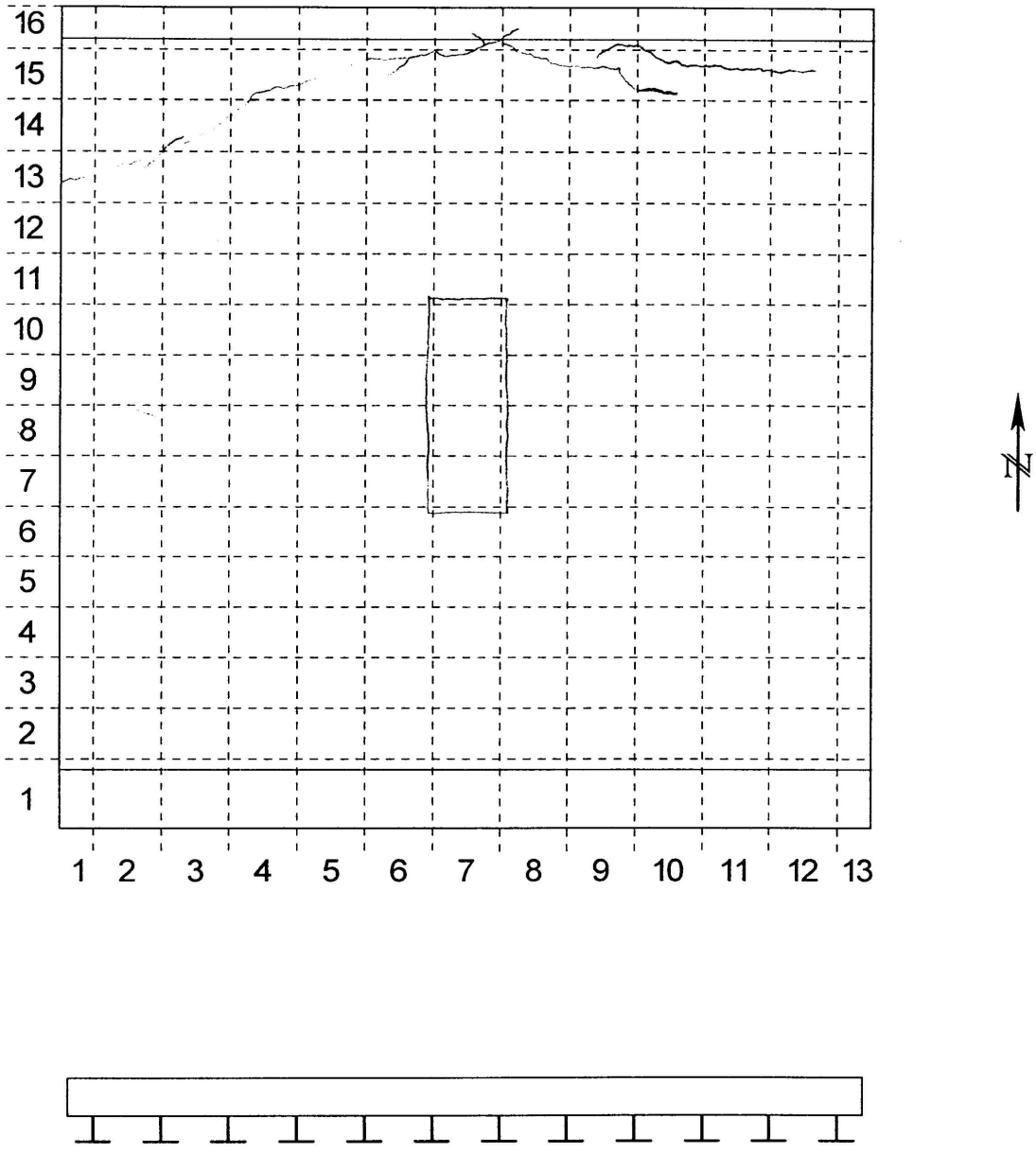


Fig. C6 – Crack pattern on concrete surface at start of simple span test.

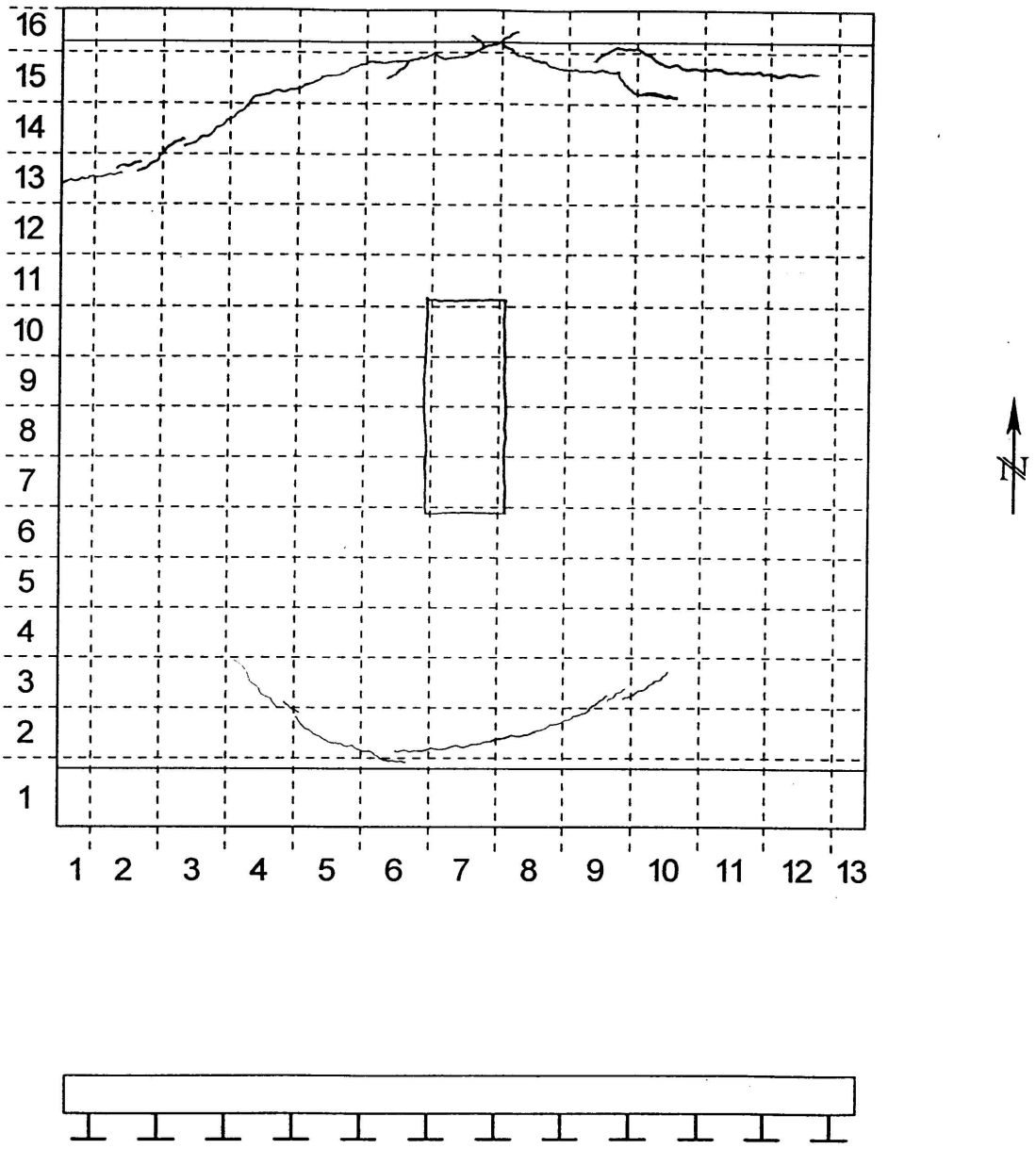


Fig. C7 – Cumulative crack pattern on concrete surface at 125 kips for simple span test.

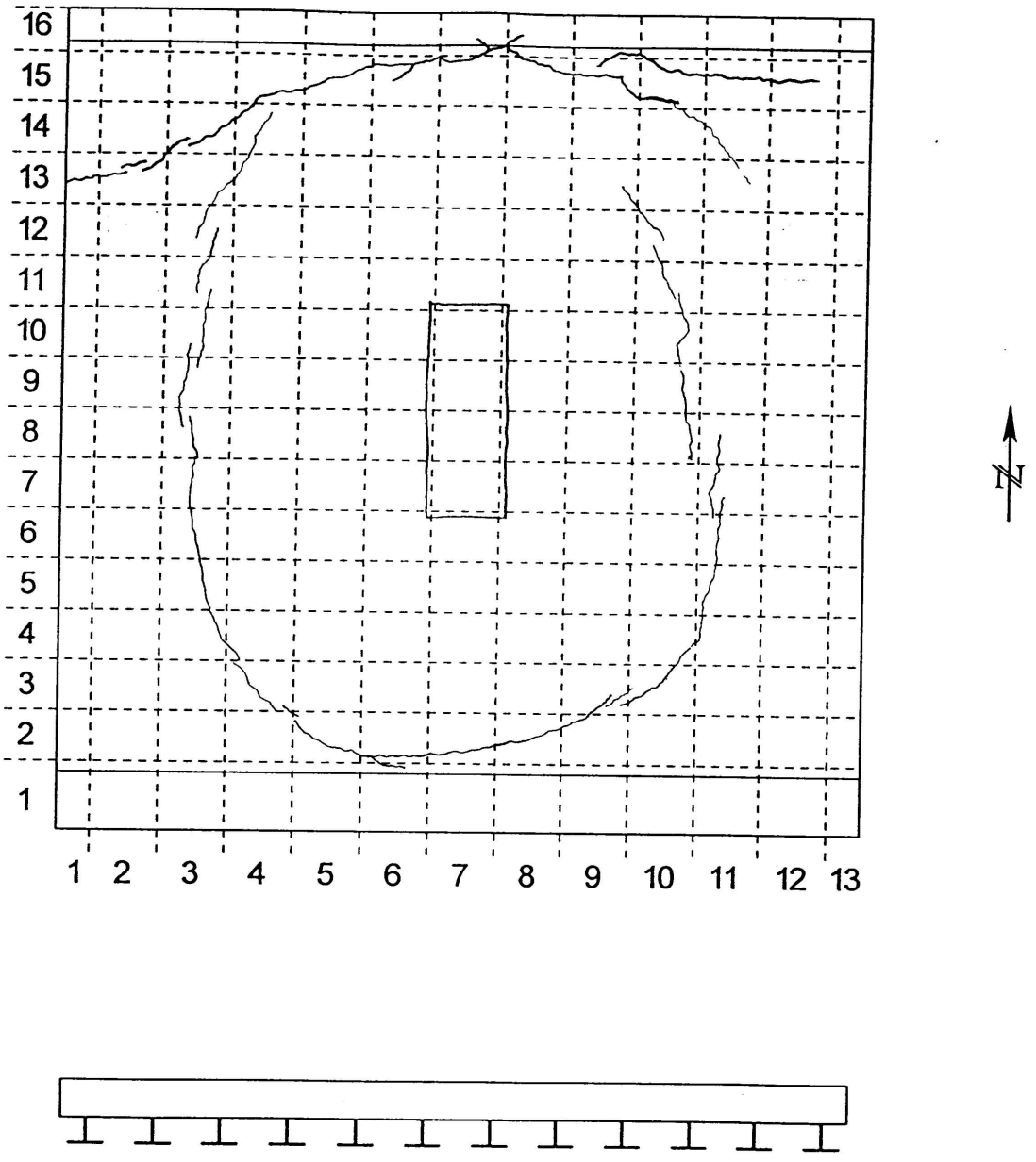


Fig. C8 – Cumulative crack pattern on concrete surface at 143 kips for simple span test.